A Morphological Investigation of Polymer Blends of Two Engineering Thermoplastics with a Liquid Crystalline Copolyester

by

Kent Gordon Blizard

Thesis submitted to the Graduate Faculty of the Virginia Polytechnic Institute and State University in partial fulfillment of the requirements for the degree of

MASTER OF SCIENCE
in
Chemical Engineering

APPROVED:

Dr. D.G. Baird

Dr. G.L. Wilkes

Dr. W.L. Conger

February, 1986
Blacksburg, Virginia

Attention Patron:

Page ii omitted from numbering

Attention Patron:

Page iii omitted from numbering

ACKNOWLEDGMENTS

The author wishes to express his sincere appreciation to his advisor, Professor Donald G. Baird, for his criticism, advice, and support in the course of this study. He would also like to thank his advisory committee, Professors Garth Wilkes and William Conger, for their interest and suggestions.

Thanks also go to , , , , and ( ) for their help in the laboratory and their guidance in writing this thesis. Finally, the author would like to thank his brother, , for the excellent drawings he did, often at all hours of the night.

TABLE OF CONTENTS

LIST OF FIGURES

LIST OF TABLES

1. INTRODUCTION

The field of polymer science and technology has expanded greatly over the past three decades. Advances have occurred in the chemical synthesis of polymers and in the structures obtained from an endless variety of monomers. Recently, though, the alteration of properties by means of physically blending two or more polymers has been of increasing importance; not always are the time and expense of generating new chemical compounds warrented when problems with mechanical, thermal, or rheological properties can be successfully tackled from a physical perspective.

When examining the properties of a specific "polyblend", several salient considerations must be addressed. The properties of the blend are determined to a large extent by the relationship between the different polymeric phases present. This structure, or morphology, is in turn a function of the thermodynamics and kinetics, as well as the composition and processing history of the system. Miscibility, used here interchangeably with

the term compatibility, can best be understood from a thermodynamic viewpoint, and in part accounts for the state of dispersion in the blend. Interfacial forces determine the degree of physical adhesion between the components. Kinetics plays a role in determining the rate at which the components can interdiffuse and thus whether this process is negligibly slow.

Two phase blends can have numerous morphologies. One component may be dispersed in a matrix of the other; in this instance the matrix properties tend to dominate. A parallel arrangement, such as fibrils, in which both components significantly affect the properties, may occur. Alternatively, the two components may form an interlocking structure in which the phases are physically interpenetrating. To what extent viscous and elastic properties, as well as mechanical properties such as tensile and flexural moduli and impact strength, are critically determined by the morphology has been researched by several investigators over the last decade. Much remains to be done, however, as the systems studied have been limited and quantitative data are difficult to obtain. Qualitative results, although arguably of limited value, provide an important guidepost to further research in the field as well as some useful information on the system being studied. Correlations of structure

with processing conditions and composition vary widely and no general theory has been completely acceptable for all blends studied.

This present work considers two blends not previously studied: nylon 6,6 with a copolymer of 60% p-hydroxybenzoic acid with poly(ethylene terephthalate) and polycarbonate also with the same liquid crystal polymer, 60% PHB/PET. The physical modification of these two common engineering thermoplastics with a liquid crystal polymer (LCP) is correlated through changes in mechanical and rheological properties with changing processing history and composition, and hence, changing morphology. The research has been undertaken in an attempt to answer the following questions:

i. What influence do the viscosity ratio of the components, the stress level during processing, the total shear experienced by the material, and the composition of each blend have on the formation of continuous phases of both liquid crystal polymer and thermoplastic in the mixtures? Can these effects be quantitatively correlated?

ii. Does the morphology of the blend affect the rheology, especially the viscosity? Do any positive or negative deviations with composition reflect a changing

morphology?

iii. Are the blends stable thermally and under shear? Does annealing the extrudate alter the structure? Can a fibrous structure even be formed in the absence of extensional forces?

iv. What mechanical property enhancement is exhibited by the blends? Are these changes in tensile and flexural moduli and impact strength dependent on morphology?

This work was organized into five chapters. Following the introduction, Chapter 2 reviews work done related to the project under investigation that might be helpful in understanding and interpreting the results. Chapter 3 describes the experimental techniques and procedures used in studying the present polyblends together with some problems that were encountered with the materials and the instruments employed. Chapter 4 lists the results of the measurements and discusses the questions outlined above and tries to answer them, while drawing also from the results of other investigators. Finally, Chapter 5 includes a summary of the conclusions as well as some recommendations for further research that should be done to more fully understand the behavior of these particular blends.

In completing this introduction, it should be

reiterated that the importance of understanding the relationship between the rheology, processing history, and the morphology stems from the industrial necessity of consistently achieving blends with the desired properties; the conditions required to obtain this goal should be known as exactly as possible. Modifying thermoplastics by blending them with a liquid crystal polymer is simply one way to obtain a polymer with enhanced mechanical properties at a reasonable cost.

2. LITERATURE REVIEW

Polymer structure and its relationship to processing history, rheological properties, and thermodynamics will be reviewed in this chapter. The first section is concerned with the thermodynamics of blends and briefly describes some concepts fundamental to the understanding of phase dispersion. Next, interfacial phenomena and adhesion between polymers are discussed. In section 2.3 the structure of specific blend systems is surveyed extensively, with an emphasis on work of scope similar to that of the present. In particular, morphological correlations used by other investigators will be scrutinized. In section 2.4 the rheology of polymer blends is discussed. Finally, in section 2.5 the theory of laminar mixing, especially as it applies to the single screw geometry, is developed; its importance in determining the extrudate's morphology is also considered.

2.1. Thermodynamics of Polymeric Blends

The large molecular weights of most polymers provide the unique limit to their miscibility. The entropy of mixing dS_{mix} in the Gibbs free energy expression

$$dG_{mix} = dH_{mix} - TdS_{mix}$$

will be very small due to the relatively small number of moles of each polymer in the blend as a result of their high molecular weights. A necessary condition for the miscibility of two or more components in a blend is a negative free energy of mixing. As the heat of mixing is generally quite large, at least for relatively nonpolar systems, the entropy term, though favoring a single phase system, usually does not offset dH_{mix}.

Although a negative Gibbs free energy is necessary, it is not a sufficient condition for compatibility. Scott [1] extended the solution theory of Flory-Huggins [2,3,4,5] to mixtures of polymers and obtained for the Gibbs free energy the following:

$$dG_{mix} = (RTV/V_r)[(\varphi_A/x_A)\ln\varphi_A + (\varphi_B/x_B)\ln\varphi_B + \chi_{AB}\,\varphi_A\varphi_B]$$

where V is the total volume, V_r is a reference volume, taken as close to the molar volume of the smallest polymer repeat unit as possible, φ_A and φ_B are the volume fractions of each polymer, x_A and x_B are the degrees of polymerization with respect to V_r, and χ_{AB} is related to the interaction enthalpy of the repeat units. Scott found the critical conditions in such a system to be

$$(\chi_{AB})_{cr} = \tfrac{1}{2}[1/x_A^{\frac{1}{2}} + 1/x_B^{\frac{1}{2}}]^2$$

$$(\varphi_A)_{cr} = x_B^{\frac{1}{2}}/[x_A^{\frac{1}{2}} + x_B^{\frac{1}{2}}]$$

$$(\varphi_B)_{cr} = x_A^{\frac{1}{2}}/[x_A^{\frac{1}{2}} + x_B^{\frac{1}{2}}]$$

Scott noted that for appreciable degrees of polymerization, $(\chi_{AB})_{cr}$ would be very small. The interaction parameter is often written in terms of Hildebrand [6,7] solubility parameters:

$$\chi_{AB} = (V_r/RT)(\delta_A - \delta_B)^2$$

where δ_A and δ_B are the solubility parameters for polymers A and B, respectively.

Numerous schemes have been devised to predict compatibility of two polymers. One of the simplest methods,

and in addition a reasonably accurate one, is estimating the solubility parameters from calculated molar attraction constants, such as those of Hoy [8]. Each group or feature of the repeat unit is given a molar attraction value, F_i, which are then summed:

$$\delta = \rho \Sigma F_i / M$$

where ρ is the density of the polymer at the temperature of interest and M is the molecular weight of the repeat group. From the solubility parameters, one can then obtain the interaction parameter, χ_{AB}. If one uses 25°C and a value for V_r of 100 cm^3/mol, the interaction parameter may be taken as approximately

$$\chi_{AB} \approx (\delta_A - \delta_B)^2/6$$

as shown by Krause[9]. Using a convenient approximation for x_A as $M_A/100$, she obtained for two polymers of the same degree of polymerization $(\chi_{AB})_{cr}$ and thus the critical difference of solubility parameters that must not be exceeded if complete miscibility is required.

It should be borne in mind that these calculations are only approximate, but are generally of sufficient accuracy for most demands. If any doubt remains, the

compatibility should of course be checked experimentally, using differential calorimetry, electron microscopy, or dynamic mechanical measurements. One physical property that is frequently checked is the glass transition temperature; if more than one distinct T_g exists, multiple phases are present.

2.2 Interfacial Phenomena in Polymer Blends

Since most polymers blends are not miscible because of the thermodynamic arguments discussed above, interfacial energies affect the morphology, dispersion, and adhesion of a blend, and ultimately its mechanical properties. Thus, the prediction of interfacial tension and from that the adhesion is useful in determining whether the blend properties will be enhanced in relation to the homopolymers. This section will present one useful method in reaching this goal.

Accurate values of surface tension of polymers are generally not available because of the experimental difficulties involved; hence reliance on calculated values is necessary [10]. One method makes use of solubility parameters. Wu has shown [11] that the surface tension may be related to the solubility parameter and the density by

$$\gamma = 0.2575\ \delta^2 \rho^{-1/3}$$

Its accuracy is to within a few dynes/cm.

Several theories may be used to predict the interfacial tension [12-18]. The theory of fractional

polarity of Wu is selected here because of its simplicity and accuracy. The Harmonic-Mean equation has given good results for polymers[15]:

$$\gamma_{12} = \gamma_1 + \gamma_2 - \frac{4\gamma_1^d \gamma_2^d}{\gamma_1^d + \gamma_2^d} - \frac{4\gamma_1^p \gamma_2^p}{\gamma_1^p + \gamma_2^p}$$

where the surface tension of phase j is given by

$$\gamma_j = \gamma_j^d + \gamma_j^p$$

where the superscripts d and p refer to the nonpolar, or dispersion, and the polar components, respectively. If x_j^p is defined as the polarity of phase j,

$$x_j^p = 1 - x_j^d = \gamma_j^p / \gamma_j$$

then one may then relate the polarity of each phase to the solubility parameters:

$$x^p = (\delta_p/\delta)^2$$

where δ_p is the polar component of δ [15].

Typical values of interfacial tensions are reproduced

in Table 2.1. These values range from less than unity for polymers of similar polarity to more than ten dynes/cm for mixtures of widely differing polarity.

From the interfacial tension, one then needs to calculate the adhesion in some manner. One theory that has been useful for polymers is the wetting-contact theory of adhesion [11,19-23], which states that van der Waals forces alone are sufficient to give good adhesion if the two surfaces are in good contact. Although the topic is controversial, this theory is sufficient for the present purpose. The spreading coefficient has been proposed by Wu [11] to be the critical parameter in wetting the surfaces:

$$\lambda_{12} = \gamma_2 - \gamma_1 - \gamma_{12}$$

Where λ_{12} is the spreading coefficient of phase one on phase two. From the Harmonic-Mean equation, the spreading coefficient can thus be obtained. A negative value indicates poor adhesion, whereas a large positive one reflects good contact between the surfaces. Values of some polymer pairs are shown in Table 2.2.

Knowing some quantitative measure of the adhesion between the components of a polymer blend, what have we proven? The mechanical strength of the adhesive bond

TABLE 2.1

Values of Interfacial Tension Between Polymers

Polymer pairs	Interfacial Tension (dyn/cm)		
	100°C	140°C	180°C
L-PE - PMMA	10.4	9.7	9.0
PS - PMMA	2.2	1.6	1.1
PS - PVA	3.9	3.7	3.5
PCP - PDMS	6.7	6.5	6.3
PMMA - PnBMA	2.4	2.0	1.5
PVA - PnBMA	4.6	4.2	3.8

from [10]. L-PE = linear polyethylene, PS = polystyrene, PMMA = poly(methyl methacrylate), PVA = poly(vinyl acetate), PCP = polychloroprene, PDMS = poly(dimethylsiloxane), PnBMA = poly(n-butyl methacrylate).

TABLE 2.2

Spreading Coefficient and Adhesion
Between Some Polymer Pairs

Polymer pairs	Lambda (ergs/cm^2)	Adhesion
L-PE - PMMA	-6.5	Poor
PS - PMMA	-1.6	Poor
PS - PVA	-0.2	Fair
PVA - PnBMA	+1.6	Fair
PMMA - PnBMA	+6.0	Good
PCP - PDMS	+12.0	Good

from [10].

consists of several contributions; the extent of contact, the size of defects, interfacial chemical bonding, and interdiffusion all play more or less important parts in determining bond strength. In order to avoid adhesive fracture at low stresses, the sum of these contributions should be as large as possible.

2.3 The Morphology of Polymer Blends

Recent investigations have spanned a multitude of blend systems, from the polyolefins to polystryene to rubbers such as ehtylene-propylene diene and butadiene. Nor have the polyacrylates, polyacetates, nylons, and polycarbonates been neglected. This section reviews some of the numerous studies undertaken in order to better comprehend the various structures and dispersions that one can generate. Although by no means exhaustive, this section covers the spectrum of recent blend research.

The morphology of polyolefin blends has been characterized by numerous researchers [24-32,48,49,66]. Starita [24] processed an atactic polystyrene/linear polyethylene blend in a normal stress extruder and analyzed the extrudate with scanning electron microscopy (SEM) after solvent leaching the samples. He concluded that blending conditions and rheological properties determined whether both phases were continuous. He also noticed the phenomenon of encapsulation, which occurred when the minor component had a much higher viscosity than the matrix. In this case, the dispersion was coarse. At the other extreme, a fine dispersion resulted when the minor component was less viscous than the major one. If

the viscosities were nearly equal, a fine dispersion resulted, independent of which component was the minor phase. Starita also concluded that the elastic properties were important in determining the state of dispersion.

C.D. Han and coworkers [25] extruded PP/PS blends with a single screw, with and without a static mixer, and with a twin screw extruder. Fibrils of polystyrene were formed in the single screw, but with a static mixer and in the twin screw, particles of PS resulted. Micrographs were examined after leaching the polypropylene from the sample. Although both produced a particulate phase, the dispersions of polystyrene were not identical for the corotating twin screw and the static mixer.

More closely related to this study is the work done by Vinogradov and coworkers [26,27] on linear PE/PS blends. By extruding through a capillary 20%-40% crystallizable polyethylene blended with polystyrene, they noticed the formation of ultrafine fibers of a few micrometers diameter [26]. Factors considered in the fibrillation of the blend were the composition, surface tension, fineness of the fiber-forming component, the viscosity ratio of the two phases, and the stress level, τ. The morphological examination was carried out using Soxhlet extraction, and electron and optical microscopy

coupled with microtoming. The researchers concluded that the method of preparation and the composition, within the limits studied, were not critical to fiber formation. The authors plotted S, the viscosity ratio of PE to PS, against the stress level, τ, on a log-log plot, shown in Figure 2.1. The approximate range of fiber formation was determined and a critical stress level, τ_{cr} was calculated, above which fibers of "unlimited length" were formed. The equation of τ_{cr} was estimated to be:

$$\tau_{cr} = 8x10^4(S)^{0.7} \quad Pa$$

They also noticed a limiting stress level, τ_{lim}, above which no fibers were observed because of high elastic turbulence. Vinogradov noted that near τ_{lim} the surface and shape of the extrudate were distorted. The log of the limiting stress was determined to be 5.0 ±.1 Pa. A broad area of imperfect fiber formation below τ_{cr} was seen; this structure is characterized by fibers of limited length and variable cross section over that length.

A similar correlation was performed by Vinogradov for the deformation of PE/PS blends in a rotary viscometer [27]. In a pure shear field, a narrower range of fiber formation than found in the extensional flow in the capillaries was found, as is shown in Figure 2.2.

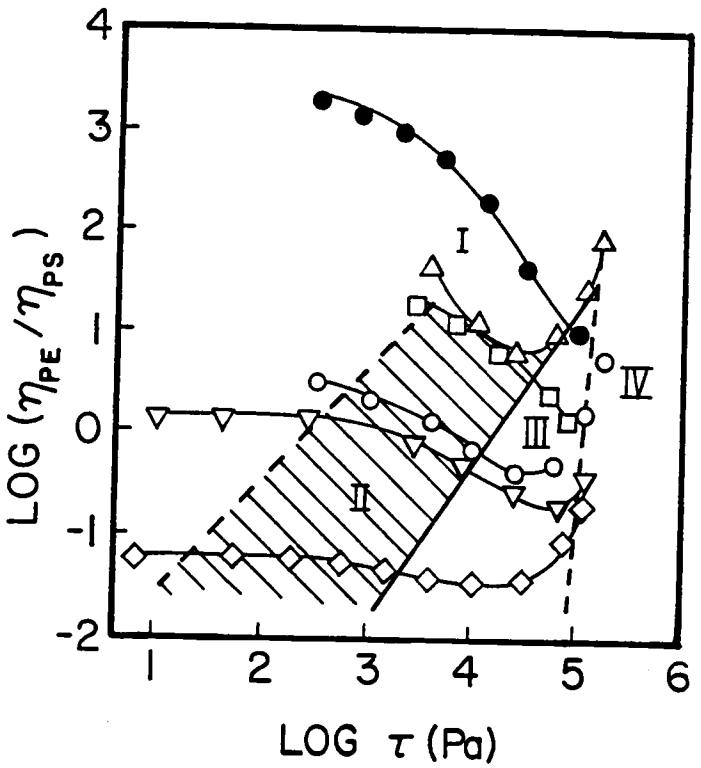

Figure 2.1. Viscosity ratio versus shear stress for PE in PS blends. Region I, no fibers; II, imperfect fibers; III, perfect PE fibers; IV, disintegrated fibers. From [26].

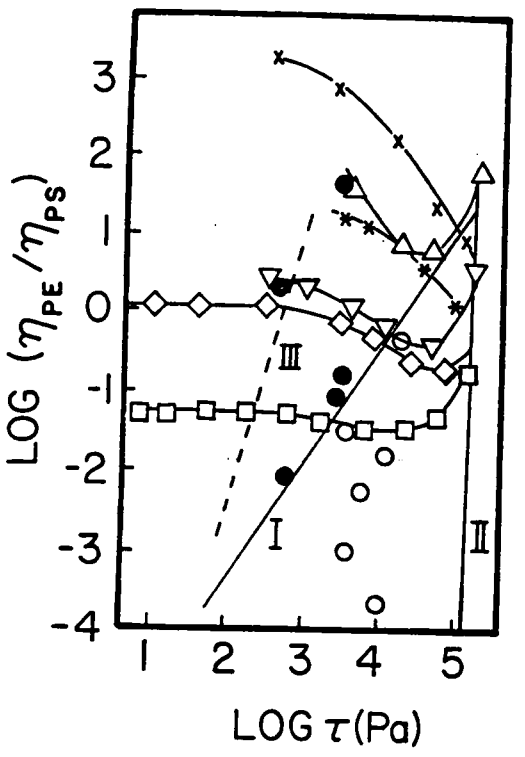

Figure 2.2. Viscosity ratio versus τ for PE/PS mixtures. Open circles represent fibril formation in a rotary viscometer, closed circles show no fibril formation. Other symbols from capillary results (Fig. 2.1). From [27].

Vinogradov concluded that the decisive factor was the viscosity ratio, S, and that the elasticities only had minimal, if any, effect on fibrillation, since S varied by several orders of magnitude and the elasticity ratio varied by no more than one decade. Furthermore, he concluded that the fibers formed in the capillary because of the coalescence and extension that occurred at the inlet due to the unstable converging flow.

Dispersions of rubbers in polyolefins have been studied by several investigators [28-31]. The results all tend to agree that finer, more oriented dispersions can occur if the minor component has a lower viscosity than the matrix. Danesi and Porter [28] and Wu-jing Ho [29] note the occurrence of phase inversion, which takes place at as small a content of rubber as 30%. At this point, the samples showed abrupt changes in mechanical properties. Markin [30] noticed that a better dispersion resulted in a higher tensile modulus, but also in a lower impact strength, although his data on PP/ABS blends were qualitative. Ho [29] concluded that the adhesion between the phases, in addition to their size and distribution, was critical to obtaining good physical properties in mixtures of PP/EPDM. Along with Markin, he noticed that the polypropylene tended to migrate to the outer edge of injection-molded samples, resulting in a skin-core

morphology. Danesi and Porter [28] also concluded that the mechanical characterization reflected different states of orientation of the disperse phase.

In his often cited work, Van Oene [32] used two dimensionless correlating parameters in characterizing the morphology of the polymer blends of PS, PE, PMMA, and Surlyn ionomer: the viscosity ratio mentioned before, and from the theory of hydrodynamic stability [35], k, the ratio of interfacial tension to the product of stress and a characteristic length, typically the radius of the droplet or fiber:

$$k = \gamma / \tau a$$

Interfacial tension, important for large values of k, is only of the order of unity for drops smaller than one micrometer in diameter. Since the normal stress function depends only on the magnitude of the shear stress, which varies only with radial position, he considered droplets and fibers to be in the same morphological class, distinct from a lamellar or stratified structure; this conclusion was reached from the fact that a cross section of an extrudate from a capillary is identical for both fibers and droplets, but different for a lamellar structure. The extrudates were stable with respect to re-

extrusion, which only helped homogenize the sample, and did not alter the morphology.

Blends of two rubbers have also been investigated. Avgeropoulos, et al [33] examined the structure of ethylene-propylene diene/butadiene blends. He correlated the morphology as a function of torque ratio and the composition on a Brabender Plasticorder, shown in Figure 2.3. The torque ratio can be related directly to the viscosity ratio of the components. The mean domain diameter is seen to be about an order of magnitude smaller for torque ratios near one. Co-continuous phases were obtained only for a composition consisting of equal amounts of each rubber in cases where their viscosities were similar.

Tsebrenko, Rezanova, and Vinogradov [34] also studied the fibrillation of poly(oxymethylene) blended with a copolymer of ethylene and vinyl acetate. About 20% POM was optimal for counting and sizing the fibers. For a viscosity ratio of POM to CEVAc that approached 4.3, only imperfect fibers were formed. Contrastingly, for a viscosity ratio of about one, perfect fibers occurred in converging flow. Table 2.3 statistically characterizes the fibers. No fibers were formed if the viscosity ratio was greater than 10. The level of shear stress also determines the fineness of the fibers. At the lower

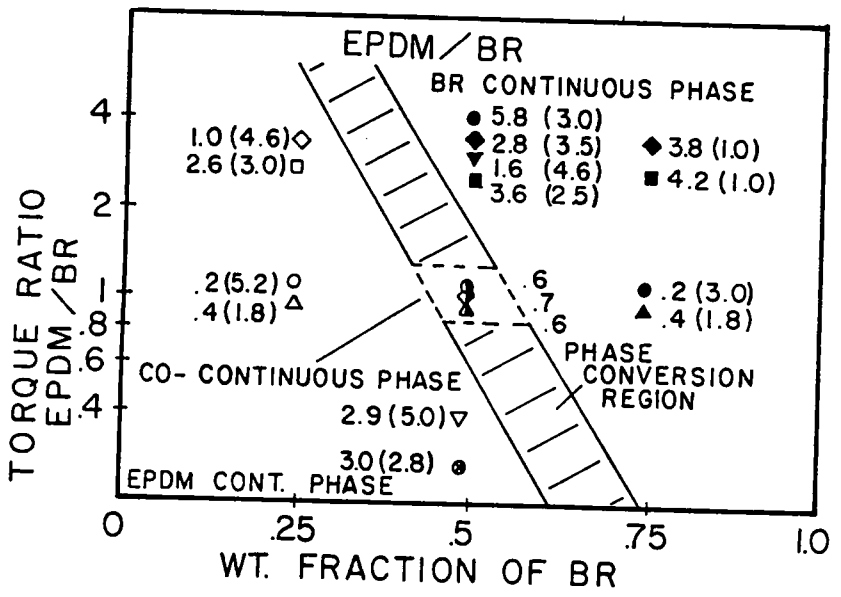

Figure 2.3. Morphology changes as a function of torque ratio and composition. Numbers represent domain diameter in μm and length to diameter ratio in parentheses. Shadad symbols indicate EPDM as dispersed phase, open symbol BR. From [33].

TABLE 2.3

Effect of the Viscosity Ratio POM/CEVAc
on the Characteristics of POM Blends

POM/PEVAc	Mean Fiber Dia. (μm)	σ (μm)	# fibers
0.31	5.3	2.54	6150
0.91	4.2	1.85	1320
1.05	5.5	3.59	6800
1.7	6.2	3.55	4300
4.1	7.3	5.84	4400

from [34].

levels of stress, the fibers were fewer in number and had a larger diameter. Vinogradov also mentions the theory of hydrodynamic stability [35] to discuss the importance of the ratios S and k in predicting the effect of viscosity and interfacial tension, although the theory is strictly true for Newtonian liquids only.

Majnusz has reported on work done with blends of polycarbonates and aromatic copolyesters [36]. Although polycarbonates form miscible blends with most polyesters [37-40], when the polyester is crystallizable, no such homologous blend is formed unless the polycarbonate in the solid is present in great excess [36]. As little as 10% of aromatic copolyester added to polycarbonate has yielded a significant increase in mechanical strength.

A recent paper by Siegmann [80] discusses research done on blends of an amorphous polyamide with a liquid crystalline copolyester. Fracture and etched surfaces of the blends were examined by electron microscopy and wide angle X-ray. The authors found a droplet in matrix structure for blends with less than 25% LCP, and a fibrous structure for polyblends with a higher fraction of the liquid crystal. Enhanced tensile and elastic moduli were noted with the addition of as little as 5% LCP. The injection-molded bars employed for the mechanical tests showed a skin-core morphology in which

the core was far less oriented than the outer layers.

This section has considered the development and influences on the morphology of some polyblends studied in the literature. The next section of this review will analyze the rheology of various blends reported on in the technical literature.

2.4 The Rheology of Polymer Blends

Rheological data on incompatible polymer blends have shown peculiarities that have rendered their characterization difficult, if not impossible, in terms of the models proposed. Viscosity maxima and minima occur at intermediate compositions; sometimes both are seen for the same blend. Utracki and Kamal [41] and Van Oene [42] have recently reviewed the melt rheology of polymer blends and classified the behavior into three categories: positive deviation blends, in which the viscosity or other rheological function is greater than the mean between the two homopolymers, negative deviation blends in which the reverse is true, and blends that exhibit both characteristics. Polymers that show positive deviation are listed in Table 2.4. The system POM/CPA [43] is shown in Figure 2.4 in which the maximum occurs at about 60% CPA. The effects of reextrusion can also be seen. Since B, the die swell ratio, is related the the recoverable shear strain, S [44]:

$$S^2 = 2(B^6 - 1)$$

where

$$S = N_1/2\sigma_{12}$$

TABLE 2.4

Positive Deviation Blends

Polymers	Temperature (°C)
PE/Ethylene vinyl acetate	160-200
POM/copolyamide	190
PS/PMMA	200
LDPE/PA-6	240
HDPE/PP	200
PE/PMMA	160

from [41].

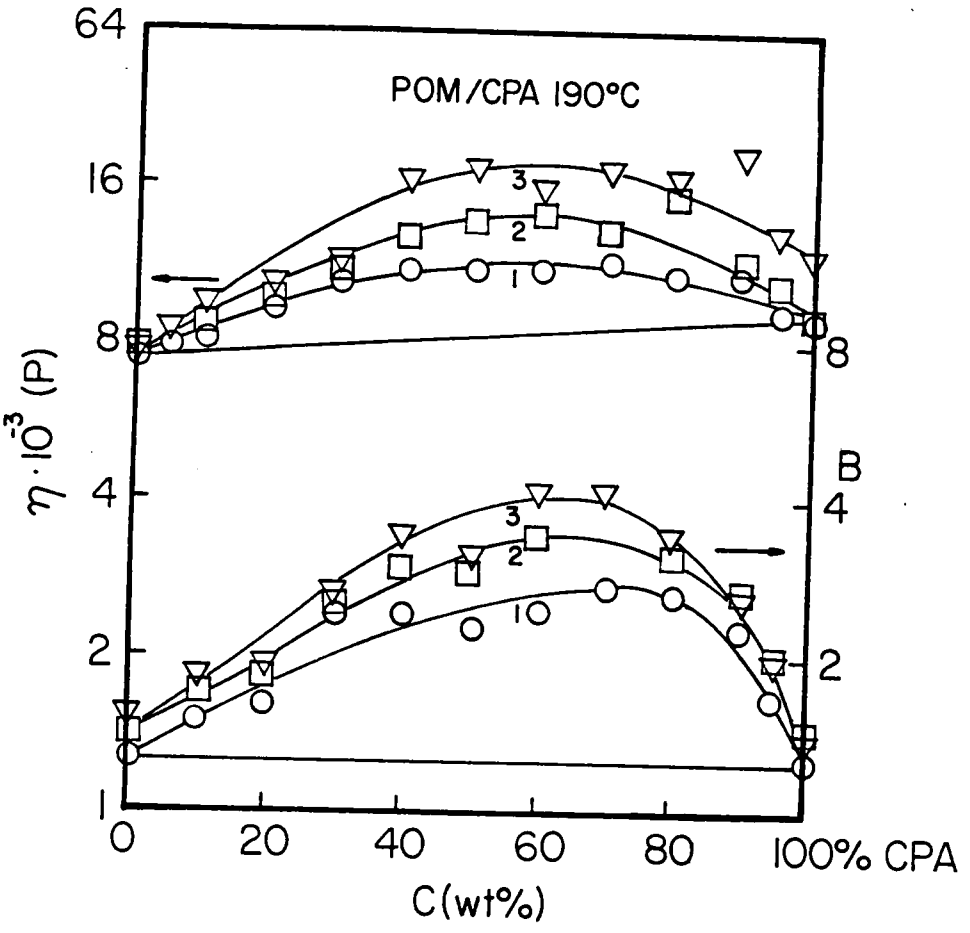

Figure 2.4. Viscosity and die swell of POM/copolyamide blend as a function of concentration. Number of times the sample was extruded is indicated. From [43].

the strong positive deviation in the die swell indicates a larger normal stress than would be observed for the homopolymers.

Results for negative deviation blends are shown in Table 2.5. The deviations from additive behavior vary broadly; one of the largest deviations is shown in Figure 2.5 [45]. The minima for NDB's frequently occur near a 70% concentration of one polymer. The effect is enhanced for low shear rates and fine, uniform dispersions.

The positive-negative deviation behavior group is more curious still; no generalization can be made, but a summary of these systems is shown in Table 2.6. One example is the system shown in Figure 2.6 of polybutadiene/cis-polyisoprene [46]. The authors believe that the S-shape of the composition-viscosity curve is the result of phase inversions.

As with morphology, the rheology of polyblends has been a subject of much recent investigation. Some examples will now be discussed. Han [25] has examined the system PS/PP and determined the viscosity and first normal stress difference as a function of composition at constant shear stress and also at constant shear rate; he prefers the former in correlating the data because in the absence of slip, it is continuous at the interfacial boundary, whereas the deformation may not be a continuous

TABLE 2.5

Negative Deviation Blends

Polymers	Temperature (°C)
iPP/EPR	200
PE/EPDM	190
PC/PMMA	250
PS/LDPE	200
PET/PA-6	275
iPP/HDPE	180-210
PS/PC	180-260

from [41].

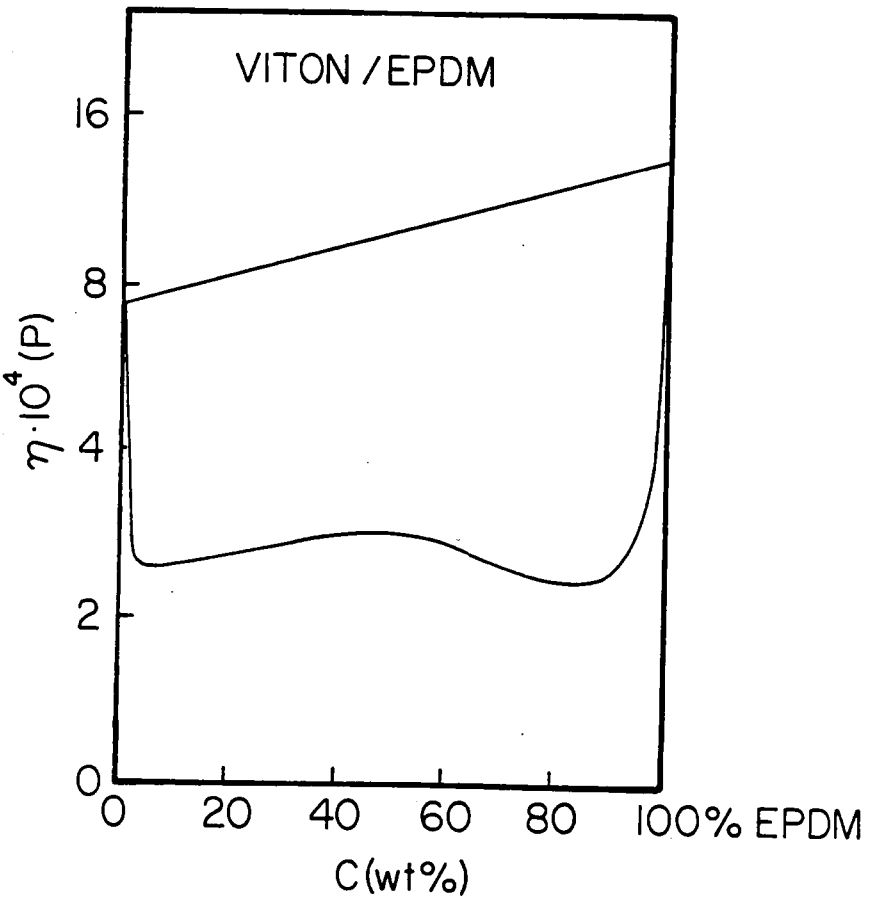

Figure 2.5. Viscosity as a function of concentration for a VITON/EPDM blend. From [45].

TABLE 2.6

Positive-Negative Deviation Blends

Polymers	Temperature (°C)
PS/HDPE	200-240
PS/PBD	-
PBD/PIP	-
POM/PE	140-200
POM/HDPE	140-200
iPP/PE	140-270

from [41].

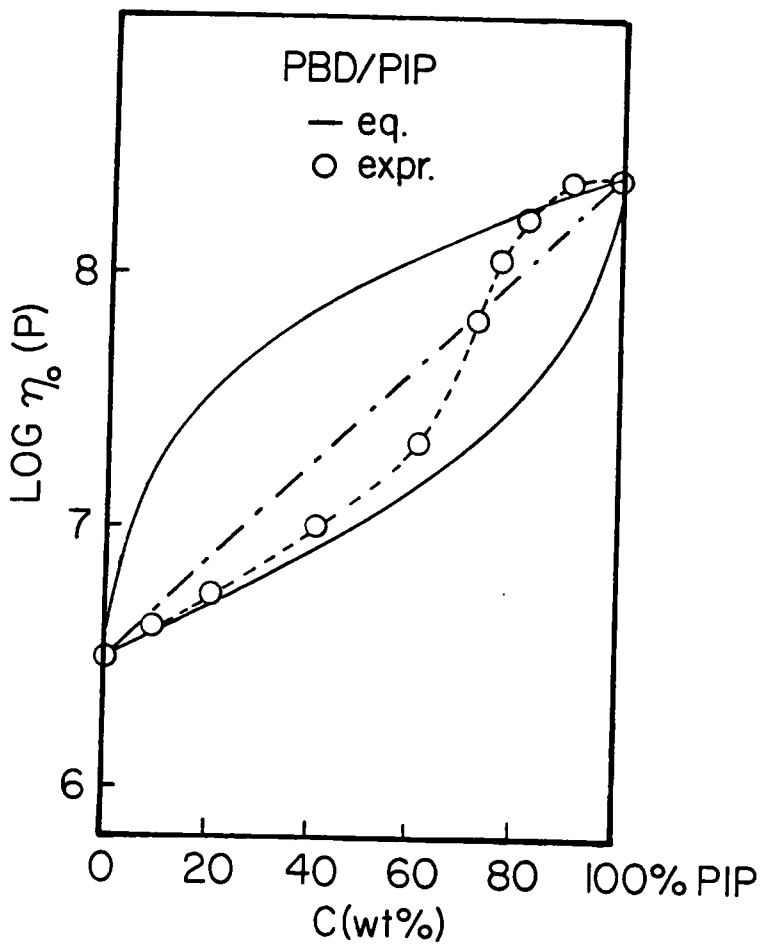

Figure 2.6. Viscosity of PBD/PIP blends as a function of concentration. From [46].

function. Figure 2.7 shows the negative deviation of the viscosity at 200°C when processed with a twin screw extruder.

Blends of polyethylene and poly(methyl methacrylate) were analyzed by Martinez and Williams [48] on a Weissenberg rheogoniometer. Dynamic oscillatory and steady shear data were obtained at composition intervals of 10%. The dynamic results are shown in Figure 2.8. It can be seen that a maximum in the dynamic viscosity occurs at 90% PMMA, although the minimum is found at pure polyethylene. Steady shear data, Figure 2.9, show the same maximum in viscosity; the gap between $\varphi = 0.5$ and $\varphi = 0.6$ indicates a phase inversion. Reduced on a composition-viscosity diagram at varying shear rates (Figure 2.10), one can see the positive deviation for blends whose dominant phase is PMMA.

Various researchers have attempted to systematize the rheological data in absence of an acceptable general theory [49]. No one empirical correlation has been generally applicable, and often these approximations have resulted in substantial errors. Several of the most well known blending rules will be presented here. An equation that has been used for polyolefin blends is the log-additivity rule [50]:

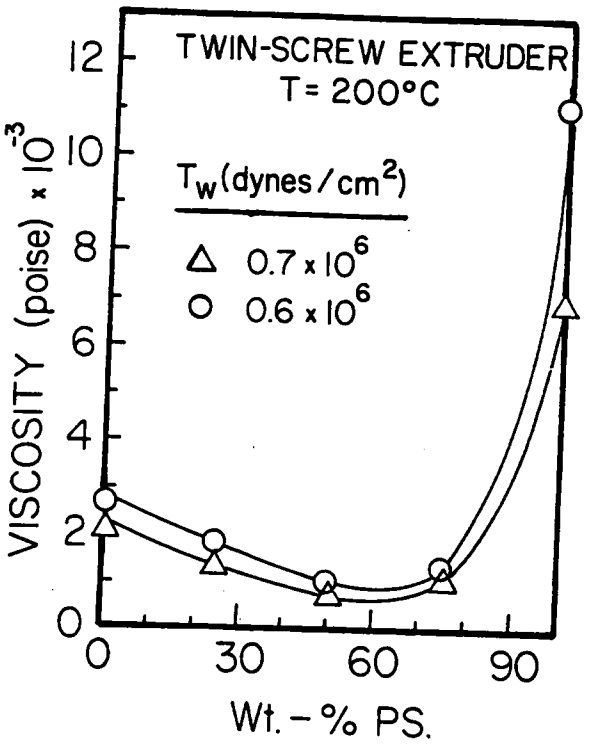

Figure 2.7. Viscosity versus blending ratio for PS/PP blends prepared with a twin screw extruder. From [25].

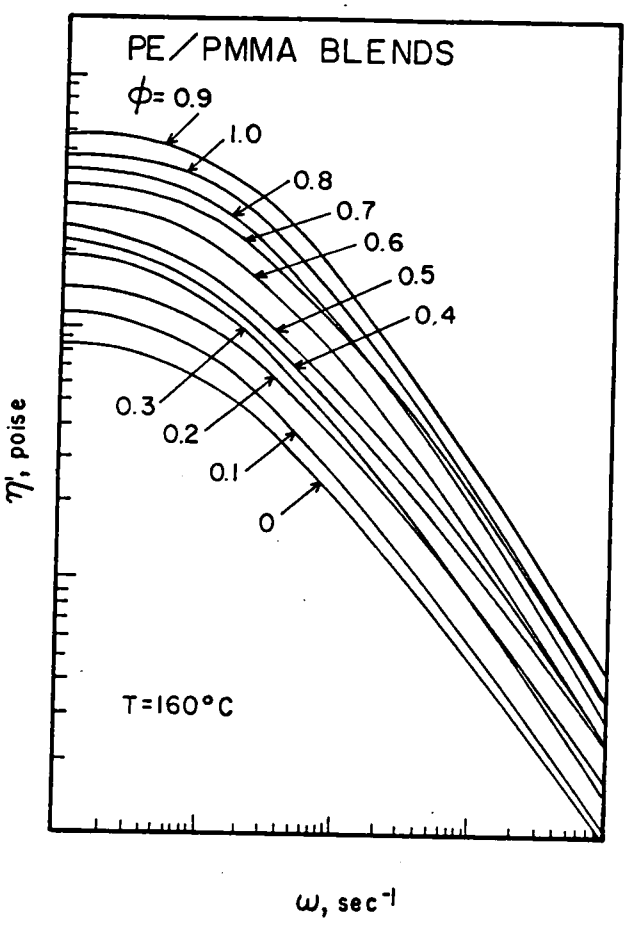

Figure 2.8. Smoothed curves for dynamic viscosity of PE/PMMA blends, for all volume fractions. From [48].

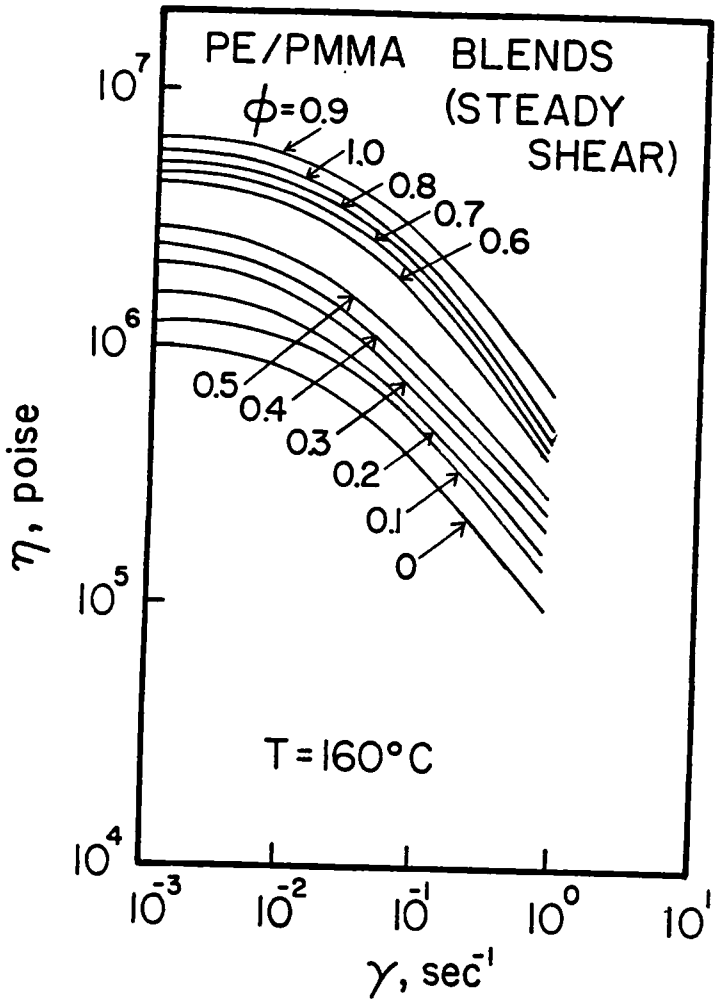

Figure 2.9. Smoothed curves for non-Newtonian viscosity for PE/PMMA blends. From [48].

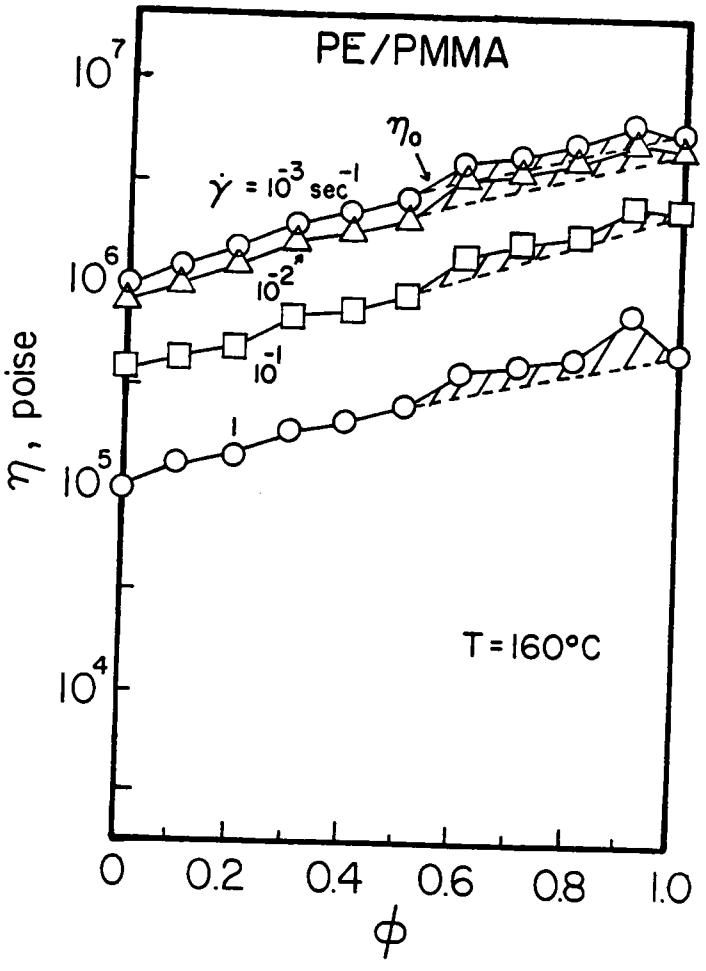

Figure 2.10. Dependence of viscosity on composition for several shear rates for PE/PMMA blends. From [48].

$$\log\eta = \varphi_1 \log\eta_1 + \varphi_2 \log\eta_2$$

where is the viscosity and φ_1 and φ_2 are the weight fractions of the components. Heitmuller [51] presented an equation based on the steady multi-layered stratified flow in a capillary:

$$1/\eta = w_1/\eta_1 + w_2/\eta_2$$

where w represents the volume or weight fraction. Hayashida et al. [52] presented a similar equation, except for the interchange of the subscripts on the weight or volume fractions:

$$1/\eta = w_2/\eta_1 + w_1/\eta_2$$

Carley [53] discussed the McAllister three body model, quoting an Arrhenius-type model for blends:

$$\ln\mu = x_1 \ln\mu_1 + x_2 \ln\mu_2$$

where μ is the Newtonian viscosity and x_i denotes the mole fraction of the respective component.

Carley [53] has studied PMMA mixed with nylon 12 and

found negative as well as positive deviation, depending on whether the shear rate is low or high. Figure 2.11 shows the inadequacies of similar blending rules for this system; the complex three-body model of McAllister [54], which requires the determination of two interactive viscosities, is much more useful in this instance.

Another polyblend that has been studied is similar to the nylon system under investigation. Utracki and Kamal [41,47] worked with a blend of poly(ethylene terephthalate) and nylon 6,6 in capillary and rotational rheometers. This system also shows negative deviation behavior at low concentrations of nylon 6,6, with a minimum at 10%, shown in Figure 2.12. The viscosity-shear rate curve at this composition is shown in Figure 2.13. The open circles represent Instron Capillary Rheometer data and the solid circles data from the Rheometrics Mechanical Spectrometer. The agreement is only fair because of suspected wall slippage in the capillary, noticeable especially at 280°C. It should be noted that the data were corrected for sample degradation, which was a problem because of the long times required to obtain the measurements. By plotting the decrement of viscosity with time, the apparent overall activation energy of the degradation process was estimated, and the subsequent data corrected for this.

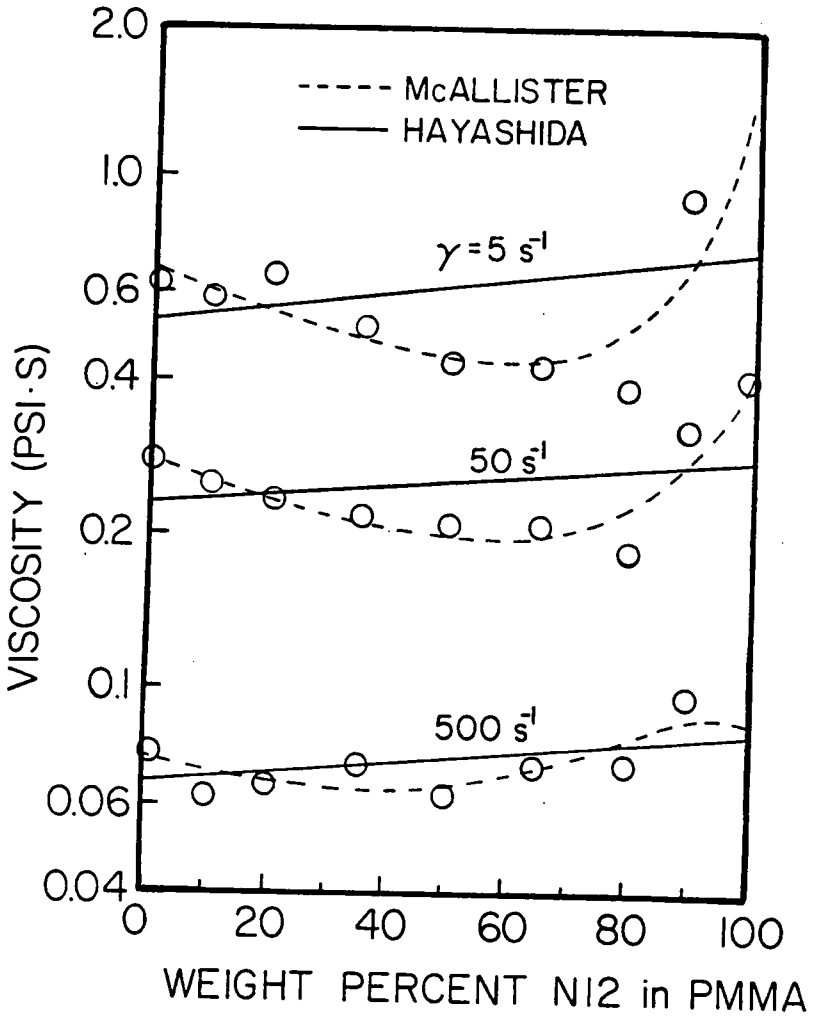

Figure 2.11. Viscosity dependence on compostion for the N12/PMMA system. From [53].

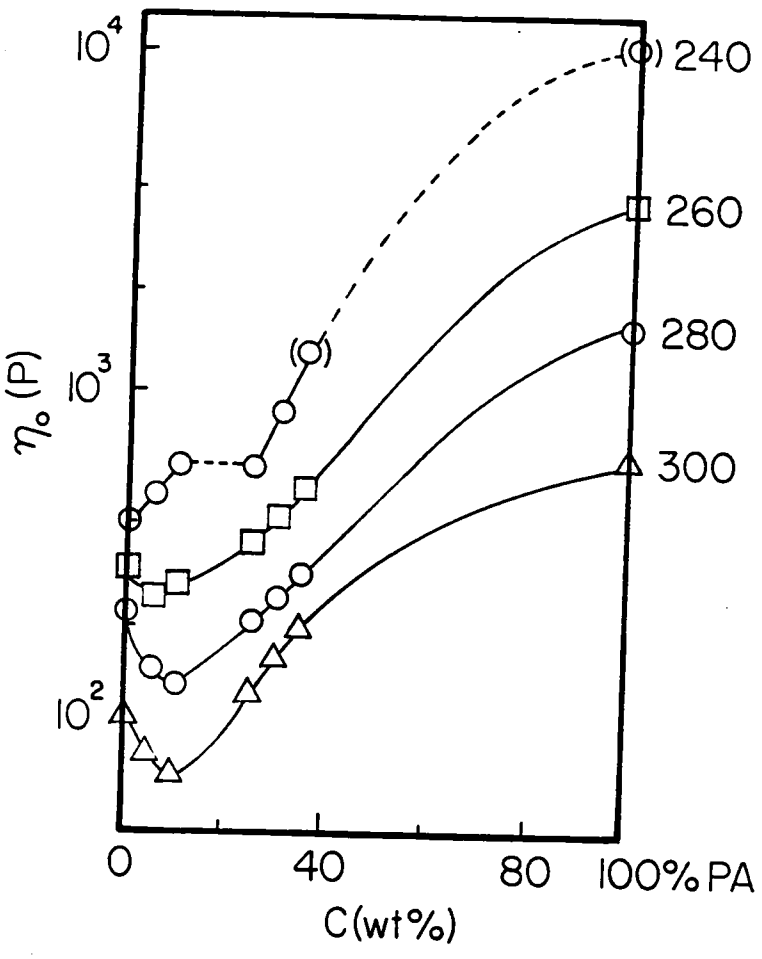

Figure 2.12. Compositional dependence of zero shear viscosity at four temperatures for PET/PA 6,6 blends. From [41].

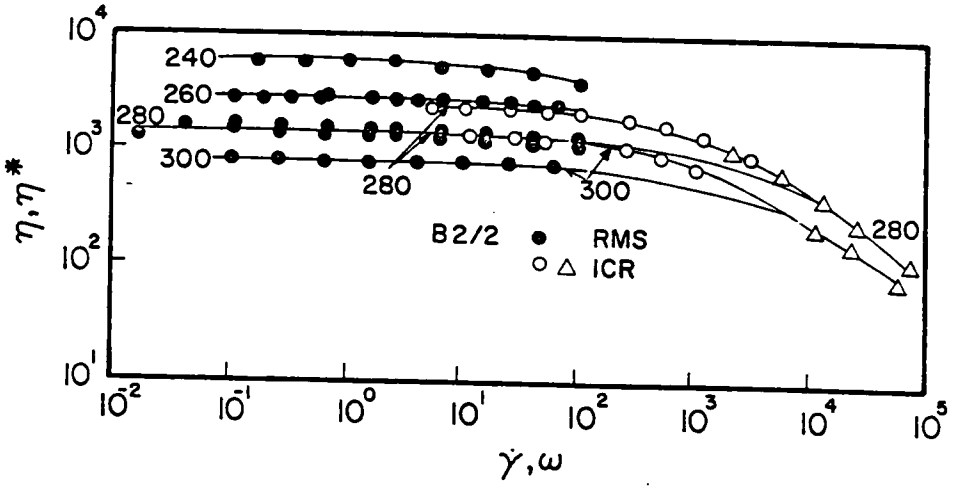

Figure 2.13. Viscosity of 10% PA 6,6 in PET at four temperatures for both RMS and ICR measurements. From [41].

A final polyblend that also exhibits negative deviation behavior was the polyamide - liquid crystal blend studied by Siegmann [80]. Figure 2.14 shows that at only 5% LCP the blend viscosity reaches a minimum for all shear rates studied in a capillary rheometer. The authors decline to speculate as to what causes this behavior.

This section has summarized some of the research that has taken place in the rheological characterization of polymer blends. Next we will consider the mixing of viscous liquids and its application to the specific processing history of the blends of thermoplastics and LCP that have been studied here.

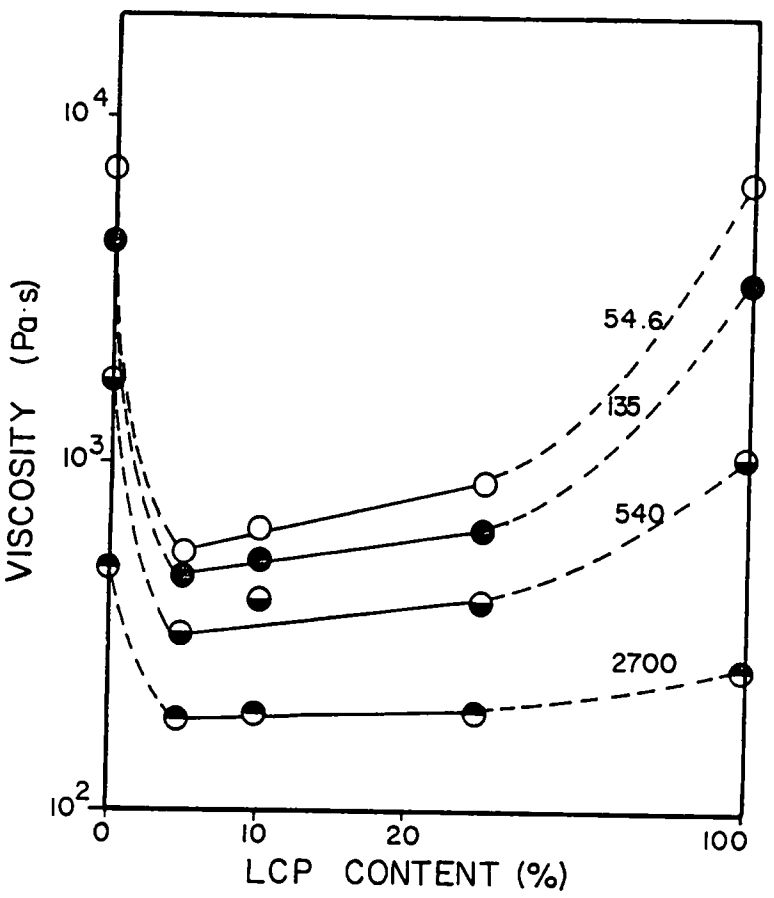

Figure 2.14. Composition dependence of LCP/PA blends as a function of shear rate at 260°C. From [80].

2.5 Mixing Theory

The mixing of very viscous liquids is an important unit operation in the polymer processing industry, and numerous authors have dealt with it, either from a theoretical and statistical viewpoint, or in relation to its practical application in various geometries. This section will review laminar and distributive mixing in terms of a striation thickness and then develop the theories that have been used for a single screw configuration.

Because of the very large viscosities present in polymeric systems, diffusion does not play an important role in the mixing process [67]. The deformation of a liquid drop was first analyzed by Taylor in his classic work [68]. He considered the ratio of phase viscosities, surface tension, and drop radius to be important in the deformation of a highly viscous Newtonian liquid. Taylor also found that upon bursting, the drop would break up into a hundred or so smaller drops of varying sizes.

The mixing process may be divided into two parts: laminar mixing, the increase in interfacial area due to a reduction of striation thickness, and dispersive mixing, or the break up of droplets to form numerous smaller

ones. The striation thickness is defined as the total volume of the component divided by one half the interfacial surface area [69]:

$$s = V/(A/2)$$

For uniformly spaced, equal sized alternating regions, s becomes the linear distance of one repetitive unit. Tadmor amd Gogos [67] developed an expression for large deformations for the ratio of new to original surface area:

$$A/A_0 = |\cos \alpha x|$$

where cos α_x is a direction cosine describing the initial orientation of the particle. Therefore, accepting the increase in interfacial area to be a measure of the mixing of the system, one concludes strain is the critical value in quantitively characterizing the mixing process.

Mohr, Saxton, and Jepson [70] extended the concept of striation thickness to include the effect of viscosity:

$$s/s_0 = 1/(\gamma\varphi_d)\cdot\mu_d/\mu_c$$

where s/s_0 represents the reduction of striation

thickness and the discrete phase viscosity, μ_d, is larger than the continuous phase viscosity, μ_c, and γ is the net shear applied. This development assumed that the boundary was wetted by the major component and that the interfacial tension was negligible.

Two recent reviews of laminar mixing have summarized the theories to date [71,72]. Hold [71] argues that the pressure difference across the interface and the viscosity difference, as well as interfacial tension, and normal forces, do not play a dominant role in mixing. The deciding factors are the total shear strain and the magnitude of the shear stress. Strasser and Erwin [73] point out that although mixing is a simple function of strain, strain is not always a simple function of stress, and hence fluid mechanics depend on the mixing process when the components have different constitutive relationships. If the stress is continuous at the interface, the higher viscosity component will have a lower strain and therefore mixing will be limited, as shown in Figure 2.15.

The theory of mixing has been extended to the single screw geometry [72,74-78]. Mohr, Saxton, and Jepson [62] calculated the amount of shear in terms of particle position (i.e. channel depth) in the channel; the shear was found to be a function of screw length, channel

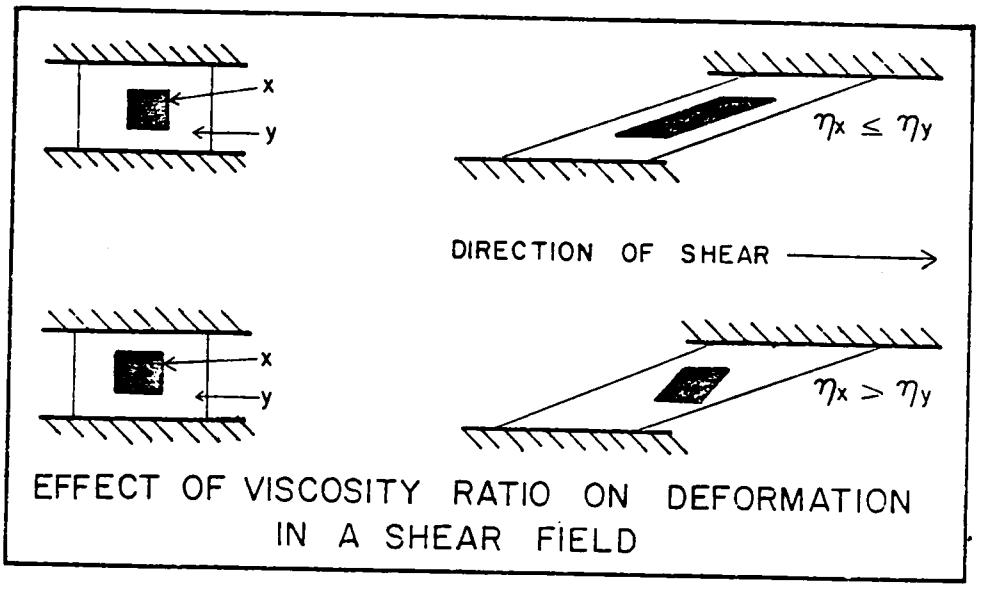

Figure 2.15. The effect of viscosity ratio of the minor to major component on the deformation in a simple shear field.

depth, and the pressure to drag flow ratio. Pure drag flow occurs under conditions of open discharge; at closed discharge the pressure flow is the only component of the velocity profile, as shown in Figure 2.16. For a Newtonian fluid, the pressure and drag flows can be shown to be additive. In most developments the screw channel is "unwound" and modeled as a rectangular channel in which curvature is neglected. Such a configuration described by Pinto and Tadmor [76] is shown in Figure 2.17. V_b is the barrel velocity relative to the "stationary" screw root and θ is the helix angle, the angle that the moving barrel makes relative to the down channel direction. They have calculated a residence time distribution (RTD) for a Newtonian fluid flowing in a single screw extruder:

$$f(t)dt = 9/2\ V_b\ \sin\theta\ \cos\theta\ (1 + \varphi)/L$$

where L is the screw length and φ is the pressure to drag flow ratio.

The residence time itself is not directly related to the degree of mixing a particle will experience since particles at different initial locations will be exposed to different amounts of total strain. In order to correct for this phenomenon, the Weighted Average Total

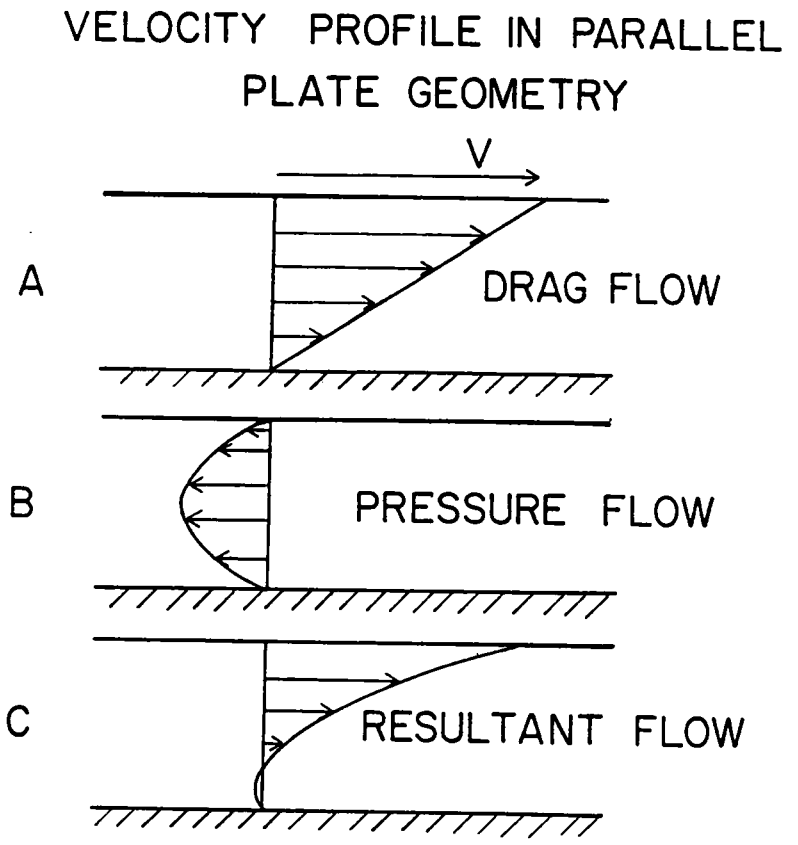

Figure 2.16. The velocity profile for a Newtonian fluid in parallel plate geometry. From [74].

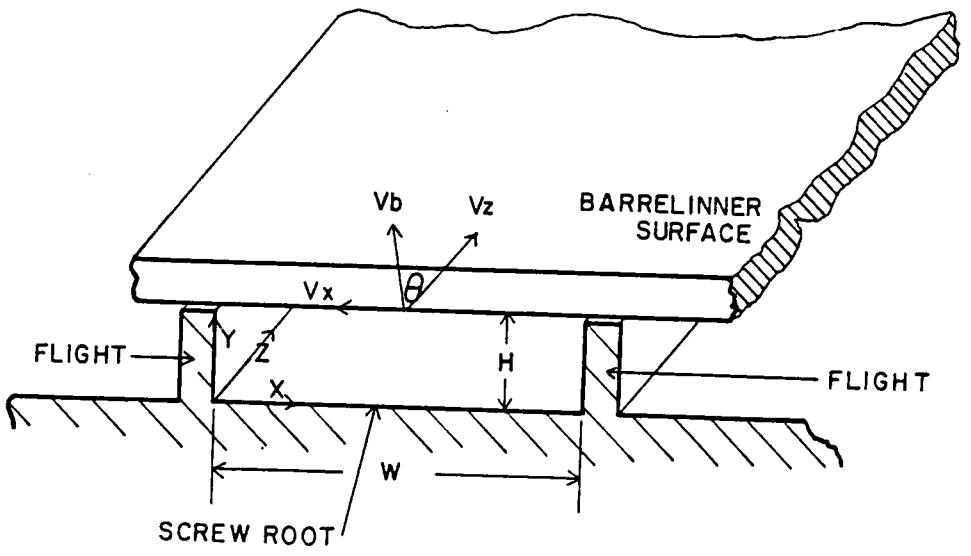

Figure 2.17. Rectangular representation of the flow channel in single screw extruders. From [76].

Strain (WATS) was conceived [64,65,66]. In Tadmor and Klein [77], WATS is defined to be:

$$\text{WATS} \equiv = \int_{t_0}^{\infty} f(t)\, dt$$

$$= \int_{2/3}^{1} f(y/H)\, d(y/H)$$

where y/H is the reduced channel depth and the second equation is true only for the parallel plate approximation in the single screw geometry. In this definition the melting process and flow in the cross-channel direction are neglected. Figure 2.18 shows the weighted average total strain as a function of pressure to drag flow ratio at various helix angles. The value of WATS is fixed for a given geometry and operating conditions; a large value represents good mixing and a smaller value poor mixing. The total strain approaches infinity at $\varphi = -1$, which occurs at closed discharge. Bigg and Middleman [78] have extended the WATS concept to power law fluids, which for this flow geometry are represented by the equation:

$$\mu = m\, [(dv_x/dy)^2 + (dv_z/dy)^2]^{(n-1)/2}$$

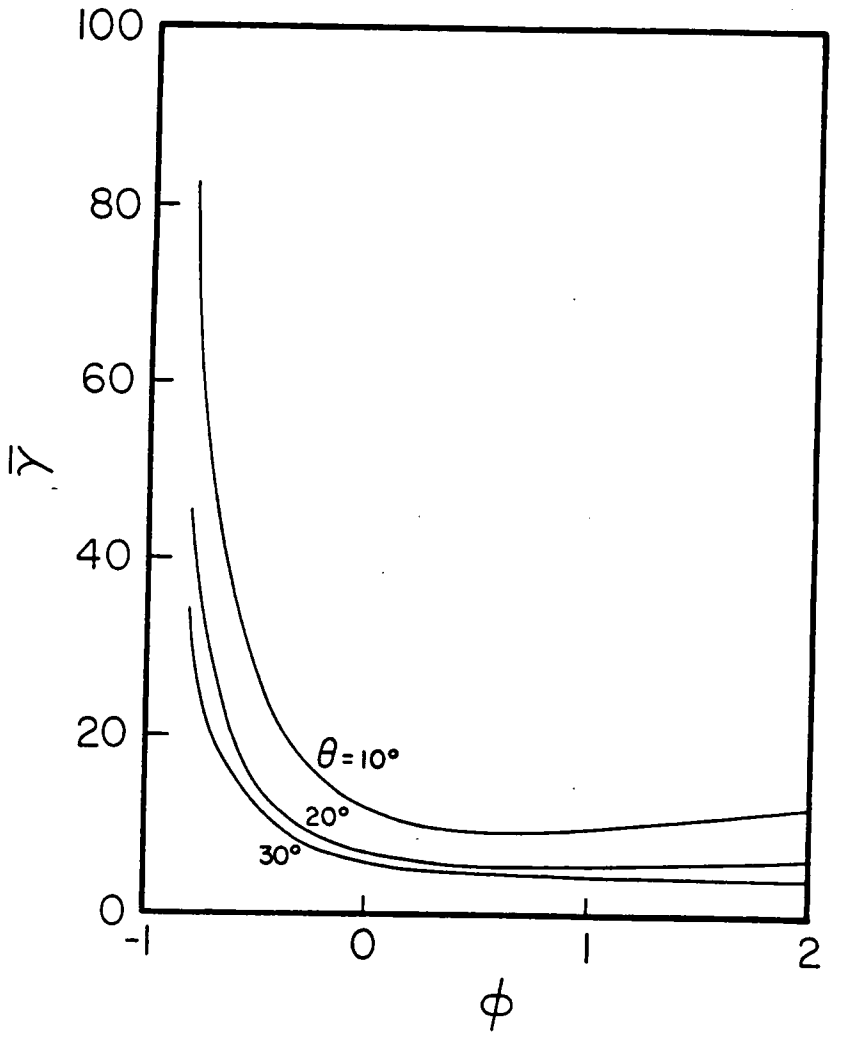

Figure 2.18. The weighted average total strain as a function of φ at various helix angles. From [76].

in which m is the consistency index and n the power law index. The residence time distribution was obtained using a dye tracer technique and the experimental results agreed well with the theoretical predictions.

The mixing in single screw extruders, although relatively uniform, is generally poor [72]. The narrow RTD of single screw extruders is diagrammed in Figure 2.19, and is indicative of mixing uniformity. In Figure 2.20 the relative residence time as a function of initial position is shown; more than 80% of the material has a relative residence time of 2 or less, again demonstrating the narrow residence time distribution. Only the material that passes over the screw flights is exposed to high shear. The bulk of the material thus is not reoriented at the flights, causing the development of an orientation parallel to the channel bottom, regardless of the initial orientation of a particle [72].

This section has reviewed the theoretical work done on the theory of mixing in the past fifty years, as well as its application to the single screw geometry. The next chapter will give the experimental procedure and analyze the equipment and instruments used in this research, focusing on the problems encountered with the particular materials and operating conditions employed.

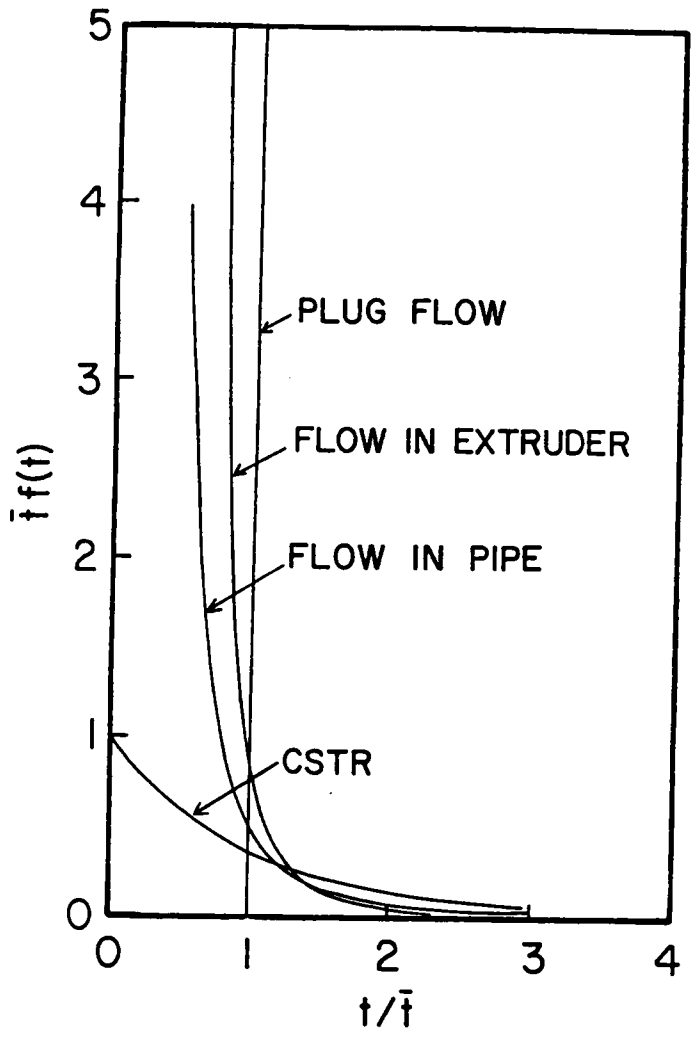

Figure 2.19. The residence time distribution function versus reduced time for various flows for isothermal flow of a Newtonian fluid. From [77].

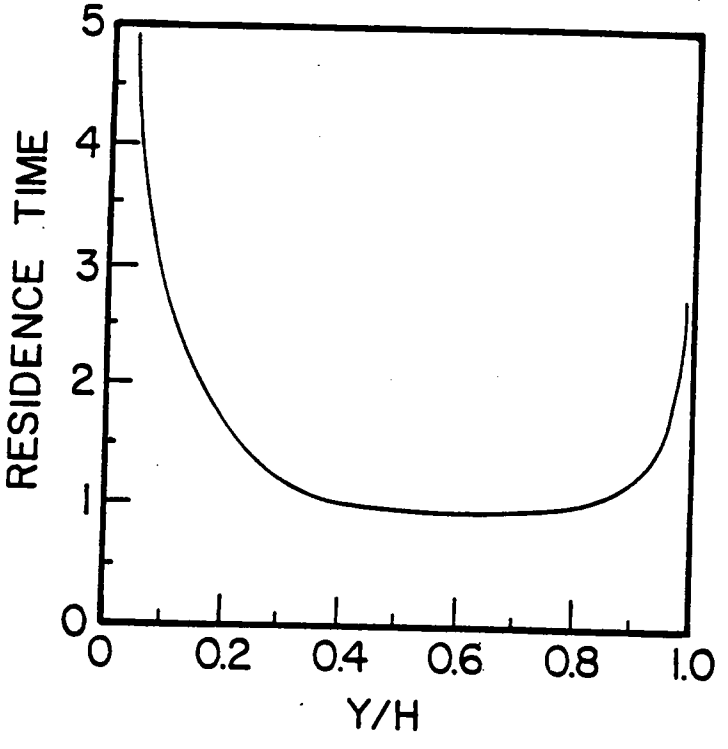

Figure 2.20. Relative residence time as a function of initial position in a single screw extruder. From [79].

3. EXPERIMENTAL INVESTIGATION

The experimental plan of investigation used to study the polyblends is discussed in this chapter. The chapter is divided into six sections. The materials used are described in section 3.1. The single screw extrusion process is described in section 3.2. The next two sections discuss the procedures used in characterizing the rheology of the blends, both for cone and plate and capillary measurements. The procedures used for mechanically testing some of the blends are given in section 3.5. Lastly, the scanning electron microscopy and characterization of the morphology of the various blends under differing processing conditions is discussed in section 3.6. The difficulties encountered and methods to overcome them are elaborated upon in the appropriate sections. The results of the experimental investigation and the pursuant calculations will then be discussed in chapter 4.

3.1 Materials

The two engineering thermoplastics used were polycarbonate (PC) and nylon 6,6 (N66). The polycarbonate was LEXAN ($M_w \approx 25000$), General Electric's commercial resin. Its glass transition temperature is 149°C (as determined from differential scanning calorimetry). The polyamide ($M_w = 30000$) was obtained from Monsanto Plastics and Resins Company, Pensacola, Florida. This batch had a melting point of 245°C.

The liquid crystal polymer (LCP) studied was an experimental copolymer of 60 mol% p-hydroxybenzoic acid with 40 mol% poly(ethylene terephthalate) (60PHB-PET), synthesized by Tennessee Eastman Company, Kingsport, Tennessee. The preparation and physical properties of this copolymer have been described in detail elsewhere [58].

3.2 Extrusion

As both nylon 6,6 and the copolyester tend to retain moisture, special precautions had to be taken to ensure that the pellets were dry before any processing or measurements were taken on them. After drying in an oven in vacuo at 110°C for not less than 72 hours pellets of the liquid crystal copolyester with either N66 or PC were tumbled in mixtures of 10, 30, 50, and 70% by weight of the LCP. The tumbled pellets were then extruded through a Killion 1" (2.54 cm) laboratory extruder at 40 RPM with capillary die diameters of 0.635 cm (1/4"), 0.3175 cm (1/8"), and 0.159 cm (1/16"). Open discharge, with no die or breaker plate, was also run for the 70% PC blend. The screw itself was of square pitch and constant taper with an initial root diameter of 1.4 cm increasing over the 50.9 cm length to 2.2 cm. Table 3.1 details the operating conditions of the extruder. The extrudate was immediately quenched in an ice water bath to preserve the structure obtained. The extrusion temperature was 260°C for the PC blends and 275°C for the N66 blends; the processing temperatures chosen were the lowest practical, maximizing the viscosity of the LCP.

The pressure gradient was measured by two pressure transducers, one located at the exit of the screw and one

TABLE 3.1

Extruder Operating Conditions

Run #	Blend	Temp.(°C)	Die (cm)	RPM
1	70% N66/LCP	275	.3175 x 15.24	40
2	70% N66/LCP	275	.3175 x 8.89	40
3	50% N66/LCP	275	.3175 x 15.24	40
4	70% N66/LCP	275	.1588 x 8.89	40
5	90% N66/LCP	275	.3175 x 15.24	40
6	50% N66/LCP	275	.1588 x 8.89	40
7	90% N66/LCP	275	.1588 x 8.89	40
8	30% N66/LCP	275	.3175 x 15.24	40
9	30% N66/LCP	275	.1588 x 8.89	40
10	90% N66/LCP	275	.635 x 15.24	40
11	50% PC/LCP	260	.3175 x 15.24	40
12	70% PC/LCP	260	.3175 x 15.24	40
13	30% PC/LCP	260	.3175 x 15.24	40
14	90% PC/LCP	260	.3175 x 15.24	40
15	10% PC/LCP	260	.3175 x 15.24	40
16	50% PC/LCP	260	.1588 x 8.89	40
17	30% PC/LCP	260	.1588 x 8.89	40
18	90% PC/LCP	260	.1588 x 8.89	40
19	70% PC/LCP	260	.1588 x 8.89	40
21	90% PC/LCP	260	.635 x 15.24	40
22	70% PC/LCP	260	none	40

15.24 cm (6") upstream. The results were recorded on a chart recorder. The mass flow rates were also measured by weighing one minute timed samples for each run.

3.3 Cone and Plate Rheology

After pelletizing and redrying the extrudate, dynamic oscillatory and steady shear data were obtained on a Rheometrics Mechanical Spectrometer (model 605) for all blend compositions as well as for the individual components. The temperatures were identical to the previous processing temperatures. All data were taken using the cone and plate fixtures with a cone radius of 1.25 cm and an angle of 0.1 radian. Multiple runs were made in most cases to obtain a measure of the relative error and to determine whether the results were repeatable. Steady shear viscosities were measured at low shear rates ($<10\ sec^{-1}$) with a gap width of .05 mm between the tip of the truncated cone and the lower plate. The upper shear rate limit varied slightly among the blends and was due to the expulsion of polymer from between the plates, causing a drastic reduction in the torque measurement. Angular frequencies between 0.1 and 100 sec^{-1} were obtained in the dynamic oscillatory mode.

The steady shear viscosity and complex viscosity are determined from well known equations given in the RMS operations manual [81]. This calculation process was fully automated.

In the dynamic mode, measurements must be taken in

the linear response region. By conducting strain sweeps at a constant shear rate, the limits of this region may be determined. Within these limits, one should operate at as high a strain as possible for low viscosity samples in order to increase the torque and thus decrease the relative error. Typical strain sweeps are shown in Figures 3.1 and 3.2. Although the thermoplastics show linear responses up to relatively high strains, when blended with the LCP in the extruder nonlinearities appear at strains as low as 8 or 9%. Hence, all dynamic data were taken at 5% strain in order to remain well within the linear region.

Difficulties also arose with polymer oxidation, particularly with the N66 blends. Although the samples remained in the vacuum oven until placed in the RMS, the hot air in the rheometer oven caused a crust to form on the edge of the sample after ten or fifteen minutes above the melting point. The result of the oxidation was an increase in the torque measurement of more than one decade, as documented in Figure 3.3. This difficulty was partially overcome by using a baffled lower plate which was flooded with polymer instead of the flat plate with the exposed edges. The effect the baffled system had on the viscosity of N66 as a function of time is demonstrated in Figure 3.4. As can be seen from the figure,

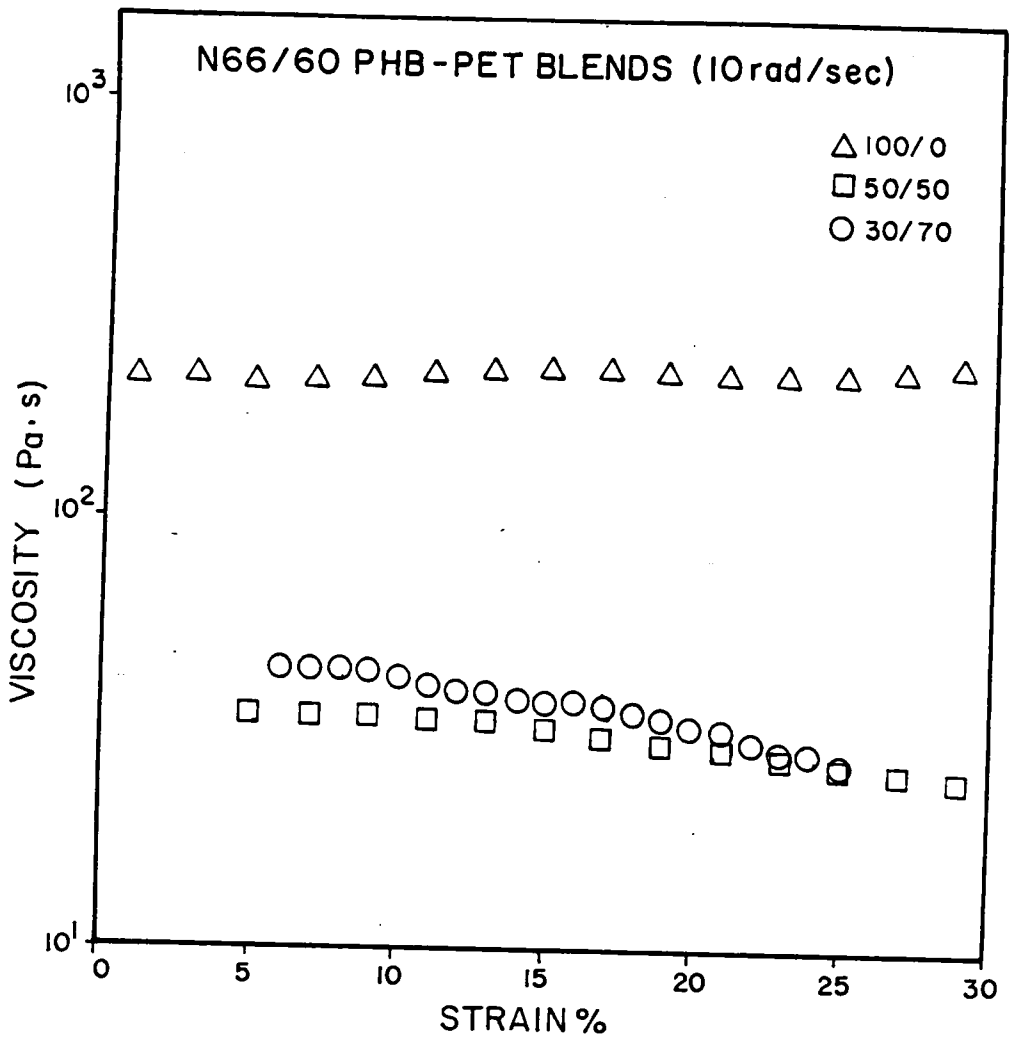

Figure 3.1. Dynamic strain sweep of N66 blends at 275°C and 10 sec^{-1}. Cone/plate mode on RMS.

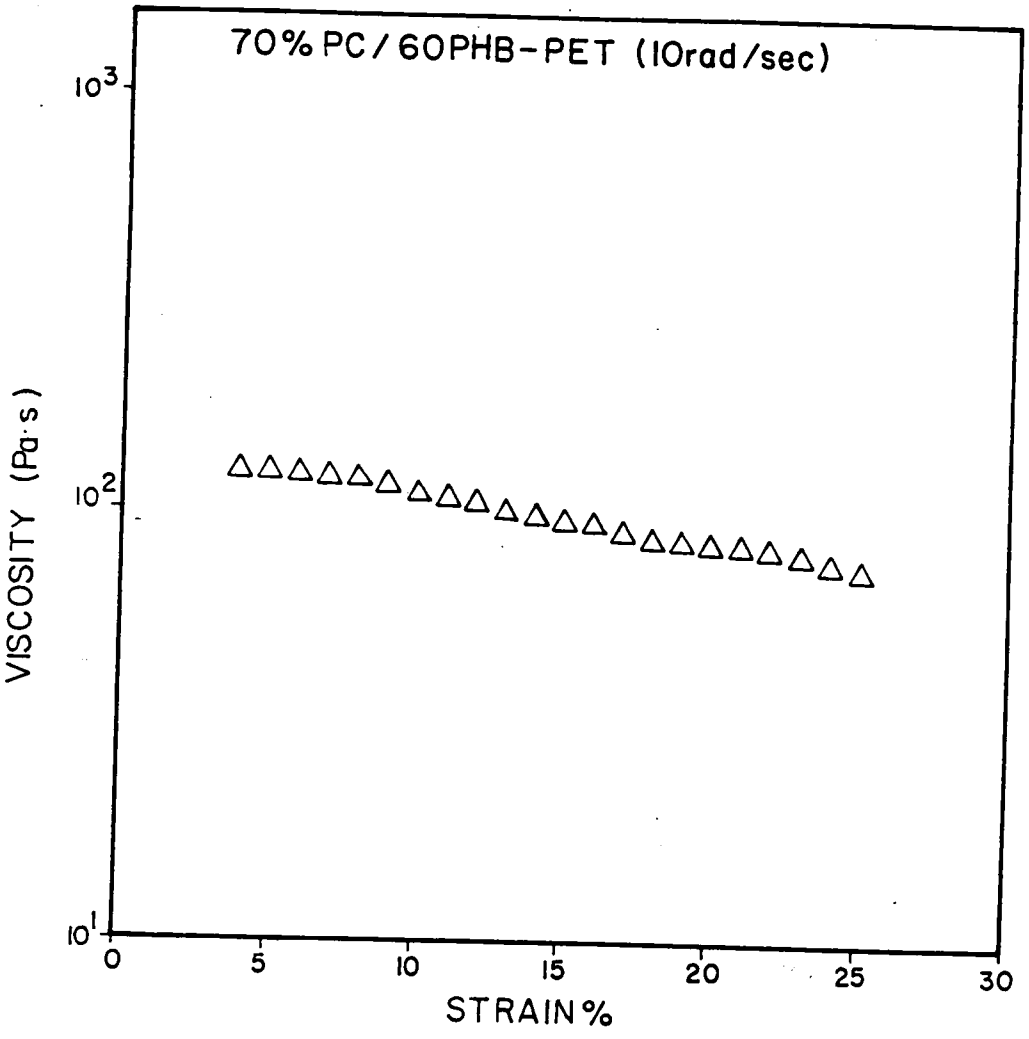

Figure 3.2. Dynamic strain sweep of 70/30 PC/LCP at 260°C and 10 sec^{-1}. Cone/plate mode on RMS.

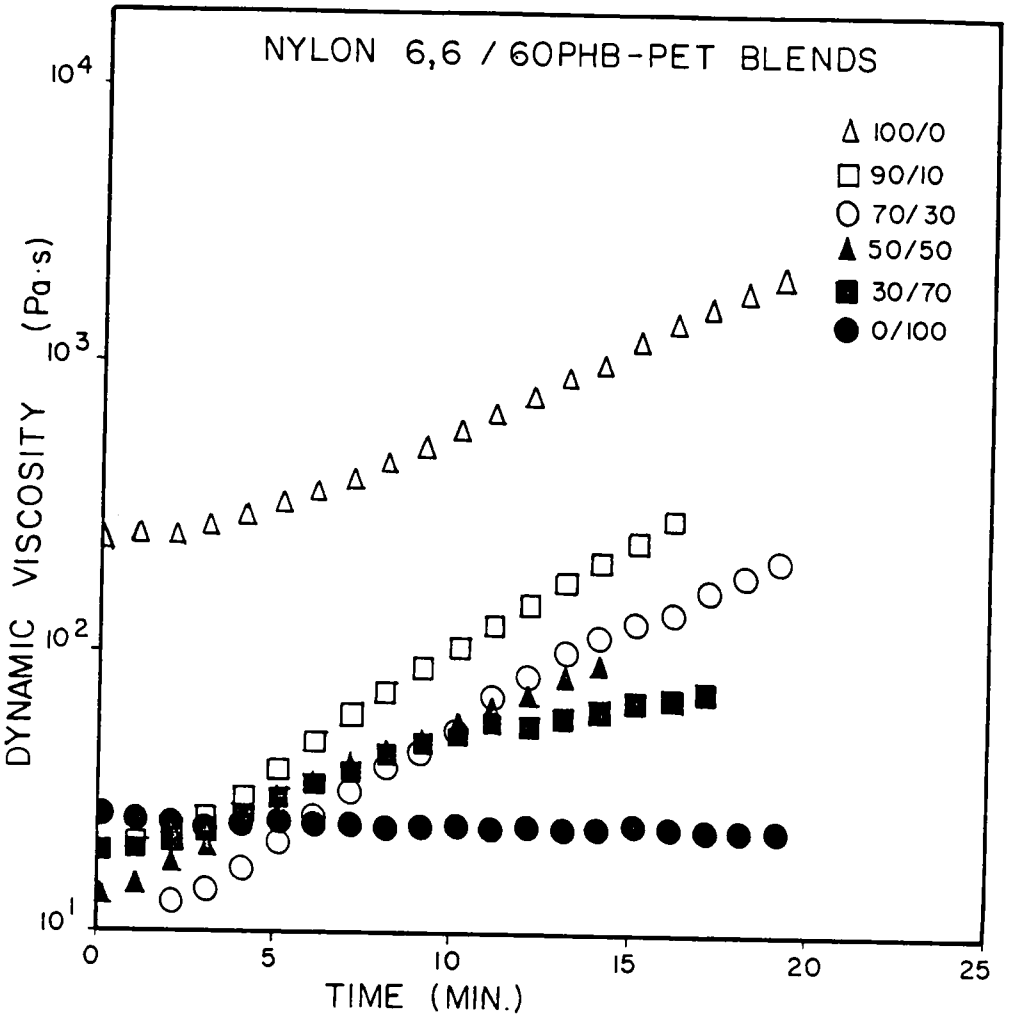

Figure 3.3. Dynamic time sweep of N66 blends at 275°C and 10 sec^{-1} for an unbaffled system.

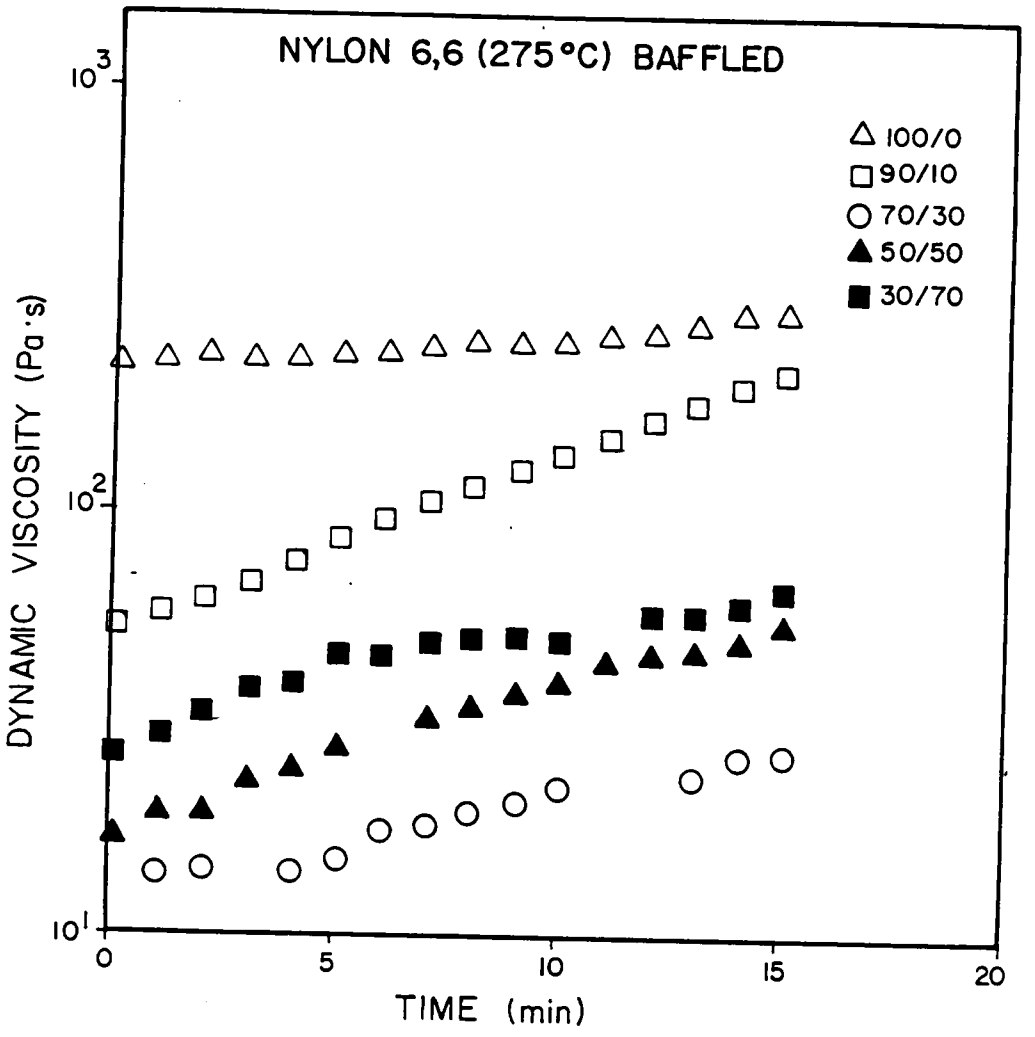

Figure 3.4. Dynamic time sweep of N66 blends at 275°C and 10 sec^{-1} for the baffled system.

at small times the relaxation of the boundary condition causes minimal error in the viscosity of N66. Subsequently, all N66 blends were run with a baffle, despite the consequent failure to satisfy the boundary condition of a spherical surface. The data were not further corrected for oxidation because the time involved for each run was generally less than ten minutes. Figure 3.5 is a time sweep of the PC blends, showing some apparent degradation for blends containing 30% or more LCP at low times. This transient behavior probably reflects a changing morphology as it dies out after ten to fifteen minutes; the LCP itself exhibits no such behavior. All samples were equilibrated at the run temperature for fifteen to twenty minutes before the measurements were started in order to remove any orientation imposed by previous processing. The micrographs in chapter 4 indicate that no residual orientation remained.

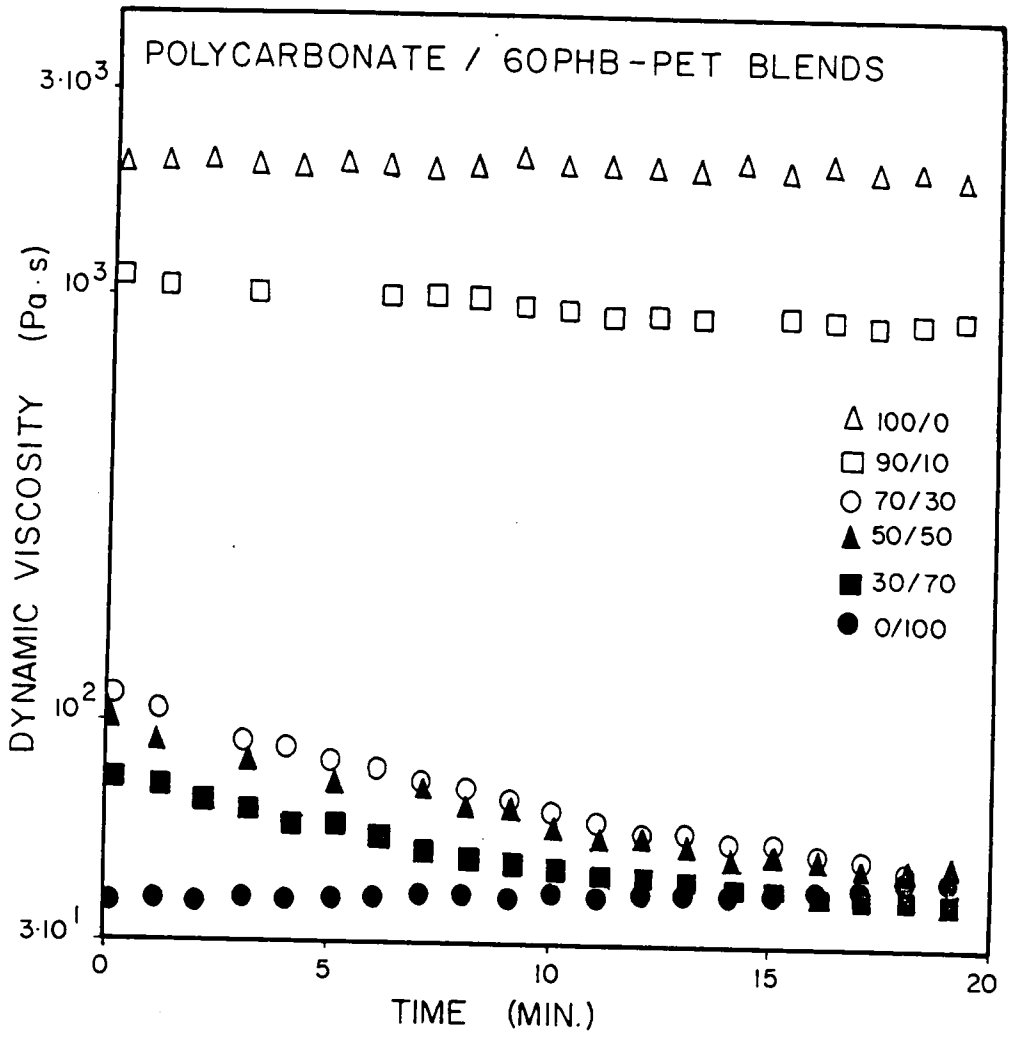

Figure 3.5. Dynamic time sweep of PC blends at 260°C and 10 sec^{-1}.

3.4 Capillary Rheology

Measurements were taken on an Instron Capillary Rheometer (model 3211) in order to obtain high shear rate viscosity data, typically above 100 sec-1, depending on the sample. The polymer was fed into a reservoir which had been heated up to the desired temperature with band heaters and tamped down to remove entrapped air. A stainless steel plunger is used to drive the polymer through the capillary die. The plunger speed was varied from .03 to 20 cm/min to obtain a wide range of shear rates. The force on the plunger is measured by a load cell which has a maximum load of 1600 Kg_f, setting the upper shear rate limit for high viscosity blends. Four length to diameter ratios were used for the capillaries: 15.22, 37.11, 75.11, and 110.22. In each case the die had a diameter of .027" (.069 cm.). For a given die geometry two parameters were measured: the speed of the plunger and the steady state force. These variables were used to evaluate the shear stress at the wall, which is given by:

$$\tau_w = \Delta PR/2L$$

where ΔP is the pressure drop across the capillary of length L and diameter R. The pressure drop is defined as the force on the plunger divided by its cross-sectional

area, A_p:

$$\tau_w = F/[4A_p(L/D)]$$

where D is the capillary diameter.

The pressure drop measured by the transducer must be corrected for entrance effects. This correction is made by taking data over a range of shear rates for several capillaries of different L/D's and extrapolating a pressure drop versus L/D plot to zero length at each shear rate. This type of plot, commonly referred to as a Bagley Plot, gives the pressure loss in the entrance region as the y-intercept so that the shear stress may be corrected accordingly:

$$\tau_w = (\Delta P - \Delta P_{ent})/[4(L/D)]$$

The shear rate is evaluated from the plunger speed and for pseudoplastic fluids the Rabinowich correction is applied in the following manner:

$$\dot{\gamma}_w = (3n+1)/4n * 8V/D$$

where

$$n = d \ln \tau_w / d \ln(8V/D)$$

and V, the mean velocity of the liquid (cm/sec), may be related to the crosshead speed, V_{xh} (cm/min), and the ratio of barrel to capillary diameters as follows:

$$V = V_{xh}/60 * (D_b/D)^2$$

The viscosity is given by he ratio of the wall shear stress to the corrected wall shear rate.

Three sources of error were encountered in the capillary viscosity measurements. Since the pressure drop across the capillary is used to evaluate the data, it is assumed that the pressure on the load cell is equal to that at the capillary entrance. This assumption neglects the drag force between the barrel and the plunger and between the polymer and barrel. The former was found by driving the plunger through an empty barrel and recording the force. Here this value was negligible in comparison to the magnitude of the force recorded when the reservoir contained polymer. The friction between the polymer melt and the barrel becomes significant at low shear rates when the barrel is full and can be reduced by running the low crosshead speeds when the reservoir is nearly empty. An additional error was introduced for the blends containing high fractions of LCP because no steady force could be obtained in many cases. In these instances an average value was employed. Most speeds were run at least twice to obtain an estimate of the error in the results. For blends containing large fractions of LCP, the width of the oscillation of the recorder pen at "steady state" was also used as a measure of the inherent error in determining the viscosity of that particular blend.

3.5 Mechanical Testing

Samples to be mechanically tested were obtained from plaques injection molded in an Arburg Allrounder (model 221-55-250) from pellets dried in the same manner as for extrusion. Tests were limited to the three components and blends of 70% thermoplastic with 30% liquid crystal copolyester. Plaques were nominally 1/16" (.159 cm) thick and strips for flexural analysis as well as tensile specimens were cut so that their major axes were parallel to the flow direction in the mold. Specimens were cut at room temperature where possible; the pure PC plaques had to be heated above their T_g in order to cut tensile specimens because of polycarbonate's toughness. Likewise the 70% N66 plaques were heated to eliminate tearing of the tensile specimen during cutting. Tests were conducted in all instances on an Instron Mechanical Tester (model 1122) with the samples at equilibrium with the surroundings, which was approximately 35% relative humidity and 26°C. Three to five specimens were taken for each of the pure components and the 30% LCP blends. Crosshead speeds ranged from 0.5 to 5 mm/min for the tensile tests, depending on the type of test and the elongation to break of the particular blend. All flexural tests were done at a deformation of 5 mm/min.

3.6 Scanning Electron Microscopy

The primary goal of this research is the determination of the morphology of the blends as a function of processing history. Toward this end samples from the single screw extrudater, RMS, and Instron Capillary Rheometer (ICR) were analyzed by scanning electron microscopy (SEM). Two-inch specimens from each extruder run were cut from the extrudate coil and assumed to be typical of the output. Specimens were obtained from the RMS by quickly cooling the sample in the oven after deformation and then removing the solid disc. This process was facilitated by applying a mold release agent to the plates prior to the run. Blends of 70/30 PC/LCP and 70/30 N66/LCP were studied in the RMS. Shear rates ranged from .1 to 100 sec^{-1} and strains from 30 to 10,000. Instron samples were obtained from a 0.178 cm (.07") die with L/D's of 7.82, 21.4, and 40. Only the 70% PC blend was studied in the ICR. This composition was chosen after analyzing the single screw extrudate morphology and finding that particular composition to show the greatest promise of an oriented fibrous morphology. Tables 3.2 and 3.3 show the processing conditions for which microstructural analysis was conducted for the RMS and ICR studies.

TABLE 3.2

Morphology Analysis: RMS

#	Shear Rate (sec^{-1})	Viscosity (Pa*s)	Strain	Stress (Pa)
		70% PC/LCP (260°C)		
0	0	-	0	0
1	0.1	442.6	30	44.3
2	1	82.5	30	82.5
3	10	26.3	100	263
5	1	82.2	100	82.2
6	10	34.5	300	345
7	1	170.4	300	170
8	10	21.7	1000	217
9	100	10.8	5000	1080
10	10	32.6	5000	326
11	100	16.5	10000	1650
		70% N66/LCP (275°C)		
1	0	-	0	0
2	10	20.8	1000	208
3	100	5.5	10000	550

TABLE 3.3

Morphology Analysis: ICR

70% PC/LCP (260°C)

#	Capillary D (cm)	L/D	V_{xh} (cm/min)
1	0.179	7.82	0.6
2	0.179	7.82	2
3	0.179	7.82	6
4	0.179	7.82	20
5	0.179	21.4	0.6
6	0.179	21.4	2
7	0.179	21.4	6
8	0.179	21.4	20
9	0.179	40	0.6
10	0.179	40	2
11	0.179	40	6
12	0.179	40	20

Samples were prepared for SEM analysis by extracting the engineering thermoplastic from the blend with formic acid in the case of the nylon 6,6 or methylene chloride in the case of polycarbonate. This process left the LCP phase intact since it was insoluble in the solvents chosen. Extraction of PC was carried out in a Soxhlet apparatus for 4 hours or until the extraction was complete, as determined by weight loss measurements. The nylon samples could not be effectively recovered from the formic acid in the Soxhlet apparatus due to the predominant droplet in matrix morphology. Thus, the N66 blends were etched in formic acid. An Ultramet II sonic cleaner was used to greatly reduce the time required to remove the N66 from the surface of the sample. The samples were then mounted with silver conducting paint and coated with 100-150 Angstroms of gold prior to analysis. A Jeol JSM-35C scanning electron microscope was used with an accelerating voltage of 15kV. Photomicrographs were taken with Polaroid type 55 film primarily at 480x magnification. In some instances 940x, 4000x, or 4800x magnifications were used to obtain higher resolution.

4 RESULTS AND DISCUSSION

This study was conducted in order to determine what influence processing history has on the structure of these polyblend systems, as well as find out whether the blends are stable and what desirable melt and solid state properties they posess. The results and discussion of this work have been divided into seven sections. Some thermodynamic considerations particularly in relation to the compatibility of the blends studied are discussed briefly in section 4.1. The morphology obtained from single screw extrusion is detailed in section 4.2. In order to better correlate the results, more well-defined flow fields were used in addition to the industrially important extrusion process. Thus, the morphology developed in steady simple shear flow is analyzed in the third section. This simple flow field is roughly analogous to the complex one present in the channel of the screw. In section 4.4 the structure of the blend morphology generated in a capillary rheometer is examined and compared to that obtained in the previous two sections. Capillary flow is similar to that experienced by the material in the die of the single screw extruder,

and therefore any morphology that would develop in that portion of the melt processing is also approximated. Next, the rheology of the blends is focused on and its relation to the microstructure examined. Section 4.5 covers the steady shear and dynamic viscosity obtained in the Rheometrics Mechanical Spectrometer. The capillary data are then analyzed in section 4.6 and discussed in terms of the morphology that may be present. Together, these sections on rheology reinforce each other, but the results leave some unanswered questions concerning what precisely causes the flow behavior that the polyblends exhibit. The last section reviews the mechanical property tests conducted because the properties of a polyblend are of primary importance. Tensile and flexural moduli have been determined to give an indication whether the properties of the thermoplastics can be enhanced with the addition of the LCP. Whether or not the mechanical properties reflect the morphology of the injection-molded specimens is also discussed.

4.1 Thermodynamic Considerations

As discussed in chapter 2, most polymer blends are immiscible due to the low entropy of mixing in macromolecular systems relative to the large positive value of the enthalpy of mixing. Table 4.1 summarizes some parameters calculated for N66, PC, 60 mol% PHB/PET and their blends. Calculations were based on procedures outlined in the thermodynamics section of the literature review except that experimental values in the literature were used where available. The interfacial tension is significantly greater for the N66 blends than for the PC blends, a difference reflected in the high positive spreading coefficient for LCP on N66 compared to the negative one for LCP on polycarbonate. Since these values are only rough estimates, they should only be considered in a qualitative manner. One would suspect based on these data that the adhesion between the nylon and the LCP would be superior to that between the PC and the LCP. Also, at low fractions of polycarbonate, the blends may show some miscibility since the chi parameter is less than 0.5.

TABLE 4.1

Thermodynamic Parameters

Polymer	δ (cal/cm3)$^{\frac{1}{2}}$	γ (dyn/cm)
Nylon 6,6	13.7	46.3
Polycarbonate	11.2	29.9
60PHB/40PET (LCP)	12.3	35.0

Polymer Pair	χ_{12}	γ_{12} (dyn/cm)	λ_{12}
N66/LCP	0.674	1.57	+9.73
PC/LCP	0.416	0.40	-5.50

4.2 Blend Morphology: Single Screw Extruder

Blends with varying content of LCP and with different die geometries were processed through a single screw extruder. The flow conditions (pressure buildup and flow rate) in the extruder for each run are given in Appendix B. The absolute value of the pressure to drag flow ratio was calculated to be less than 0.2 in all cases except run #7, indicating that most of the flow was generated by the drag of the polymer on the screw. Shear rates and stresses at the wall in the extruder were calculated for a power law fluid using equations derived in Tadmor and Klein [77], and are shown in Table 4.2. The shear rate was between 50 and 60 sec-1 except for run #7, and the shear stress at the barrel wall ranged from 150 to 24900 Pa due to the difference in the viscosity among the different blends. Most runs, though, had a wall shear stress less than 1000 Pa. The shear stress in the die, calculated from simple Poiseuille flow relations, varied more among the runs than did the stress in the extruder, from essentially zero to 23000 Pa.

The extrudate was examined with a scanning electron microscope (SEM) as detailed in the previous chapter. The LCP remaining after the PC has been extracted is shown in Figure 4.1 for different blend ratios. Ten

TABLE 4.2

Extruder Shear Rates and Stresses

Run #	$\dot{\gamma}_w$ (sec-1)	τ_w (kPa)	$\tau_{w,die}$ (kPa)
1	53	0.16	1.64
2	60	0.19	13.6
3	49	0.15	0
4	58	0.18	4.0
5	59	0.49	1.6
6	59	0.18	1.9
7	102	0.85	15.0
8	54	0.23	0.71
9	54	0.23	0.61
10	58	0.48	3.3
11	51	0.69	0.55
12	50	3.32	0.55
13	51	0.58	0.71
14	50	24.4	13.1
16	54	0.72	1.9
17	51	0.58	1.2
18	51	24.9	23.0
19	50	3.32	6.1
21	49	24.2	2.2

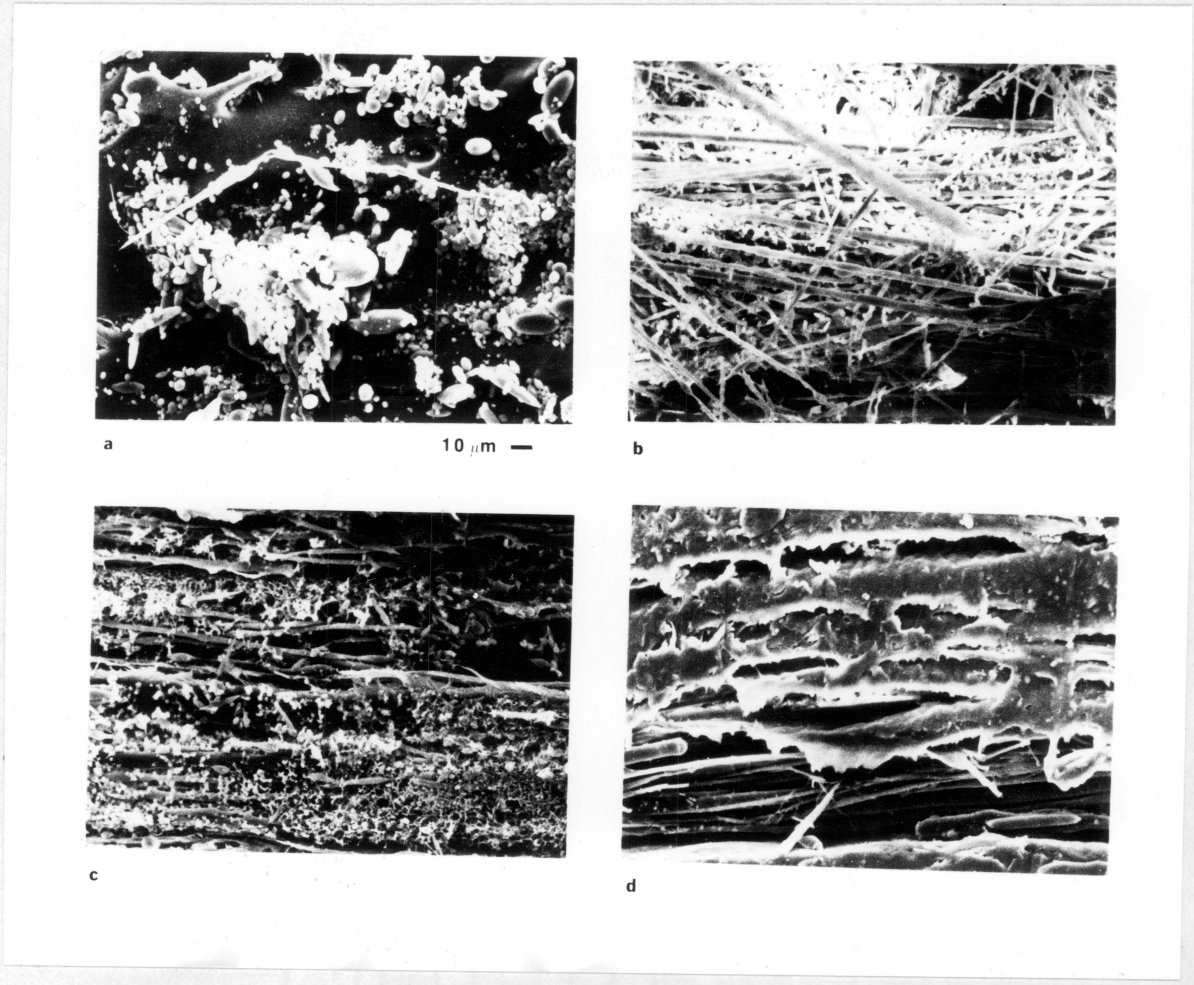

Figure 4.1. Scanning electron micrographs of extruded polycarbonate blends after extraction of PC. a, 10% LCP; b, 30% LCP; c, 50% LCP; d, 70% LCP. 480 x.

percent liquid crystal is shown in Figure 4.1a, thirty percent in Figure 4.1b, fifty percent in Figure 4.1c, and seventy percent in Figure 4.1d. In each case the die used was 0.1588 cm in diameter and 8.89 cm in length. At the lowest content, the LCP forms a discrete droplet phase in a PC matrix. The smaller drops exhibit little deformation from a spherical shape, but the drops around 10 μm in diameter tend to elongate noticeably, as may be seen clearly in Figure 4.2a at 4000x magnification. In contrast to the ten percent LCP, the structure of thirty percent LCP consists of numerous ultrafine fibers, shown in Figure 4.1b and 4.2b at 4000x magnification. These highly oriented fibers represent only part of the structure because at the higher magnification a significant quantity of droplets on the order of one μm may also be discerned. For the purposes of this study, orientation refers only to the alignment of the bulk LCP phase, and not to its crystalline structure. Some of the fibers and orientation are retained at fifty percent (Figure 4.1c), but the LCP also formed a fine web-like network structure throughout the sample. When the liquid crystal phase is dominant, a bulky LCP structure is formed along with some fibrous texture.

For all but the lowest LCP composition a distinct

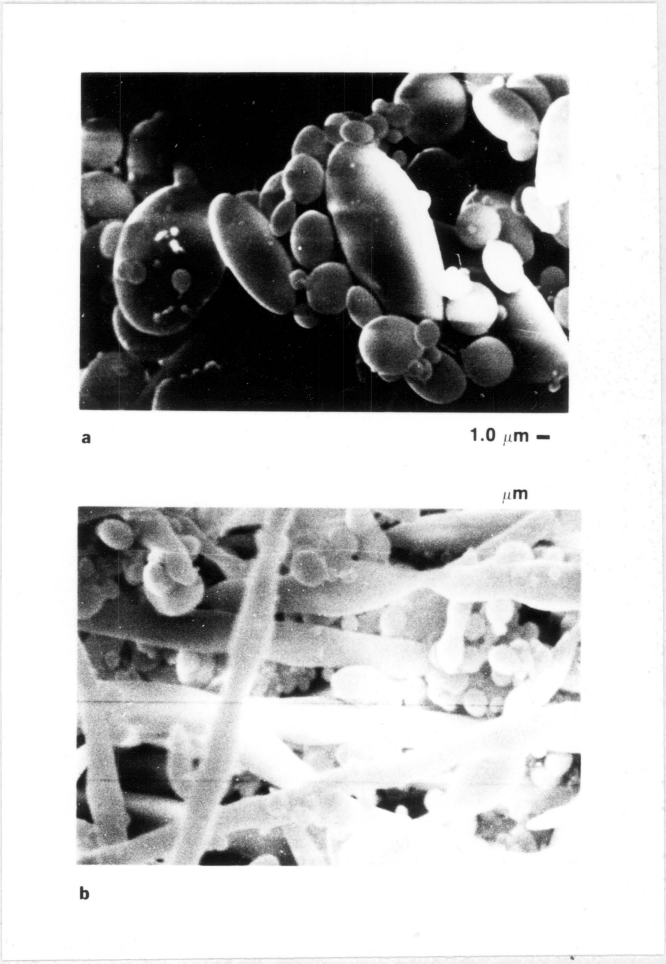

Figure 4.2. Micrographs of extruded PC blends after extraction of PC. a, 10% LCP; b, 30% LCP. 4000 x.

orientation in the flow direction is noticed. One explanation for the lack of fibrillation at ten percent LCP is that the small volume fraction of the minor component renders the coalescence of droplets in the thrmoplastic matrix unlikely. Without such coalescence, the surface energy of the smaller particles, according to the theory of hydrodynamic stability, is too large for deformation to occur (see chapter 2). Thus fibrillation depends on some critical volume fraction that makes coalescence of the disperse phase in a given flow field statistically significant. The change in the morphology with the cross-section in some cases may be attributable to either phase migration of one component, establishing a concentration gradient, or to a less than thorough mixing process in the screw channel. Among these four blend ratios, fibrillation is promoted to a greater extent at thirty percent LCP; thus, the consequent studies focused primarily on this particular blend ratio.

The effect of shear rate on the microstructure of 30% LCP in PC is examined in Figure 4.3. Three different geometries were employed: the small die already mentioned was used in obtaining the structure in Figure 4.3a, a larger die, 0.3175 cm x 15.24 cm, was used in the second photograph, and finally, no die or breaker plate assembly was used in obtaining the morphology in Figure 4.3c.

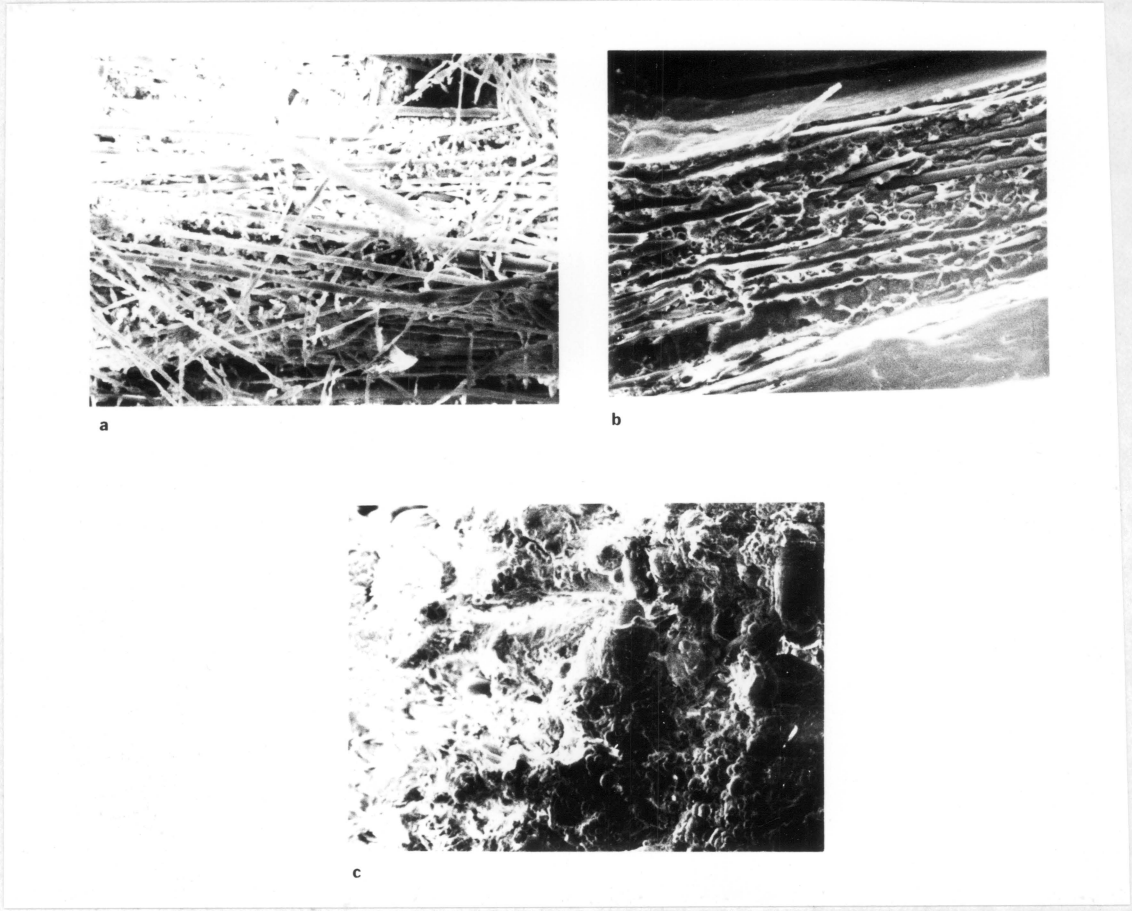

Figure 4.3. Micrographs of extruded 30% LCP blends after extraction of PC. a, 0.1588 cm x 8.89 cm die used; b, 0.3175 cm x 15.24 cm die used; c, no die or breaker plate used. 480 x.

From the ultrafine fibers seen in samples extruded with the smallest die, the orientation diminishes in the succeeding photos. With a larger die, some fibers may be seen, but the structure is not constant across the diameter of the extrudate. With no die all orientation is lost, leaving the LCP in a droplet phase. The fibrillation of the 70% PC blend did increase with the shear stress in the die, as can be seen in comparing runs 12 and 19 (Figure 4.3), in which the 0.3175 cm and 0.1588 cm diameter dies were used, respectively. Between these two runs, the shear stress in the extruder itself was identical. Thus, the fibrillation of the extrudate seems to be imparted by the flow in the die itself, and the shear flow in the screw has only the less direct importance of homogenizing the tumbled pellets in the melt state.

Three blend ratios of N66 with LCP are shown in Figure 4.4. Thirty percent LCP (Figure 4.4a) exhibits some fiber formation, although the liquid crystal is the matrix component in the lower half of the picture. Due either to a phase migration phenomenon or to incomplete mixing in the barrel, the morphology is complex. This photograph is magnified 940 x in order to show detail. At higher concentrations of LCP, namely 50 and 70%, the copolyester becomes the dominant phase, as seen in

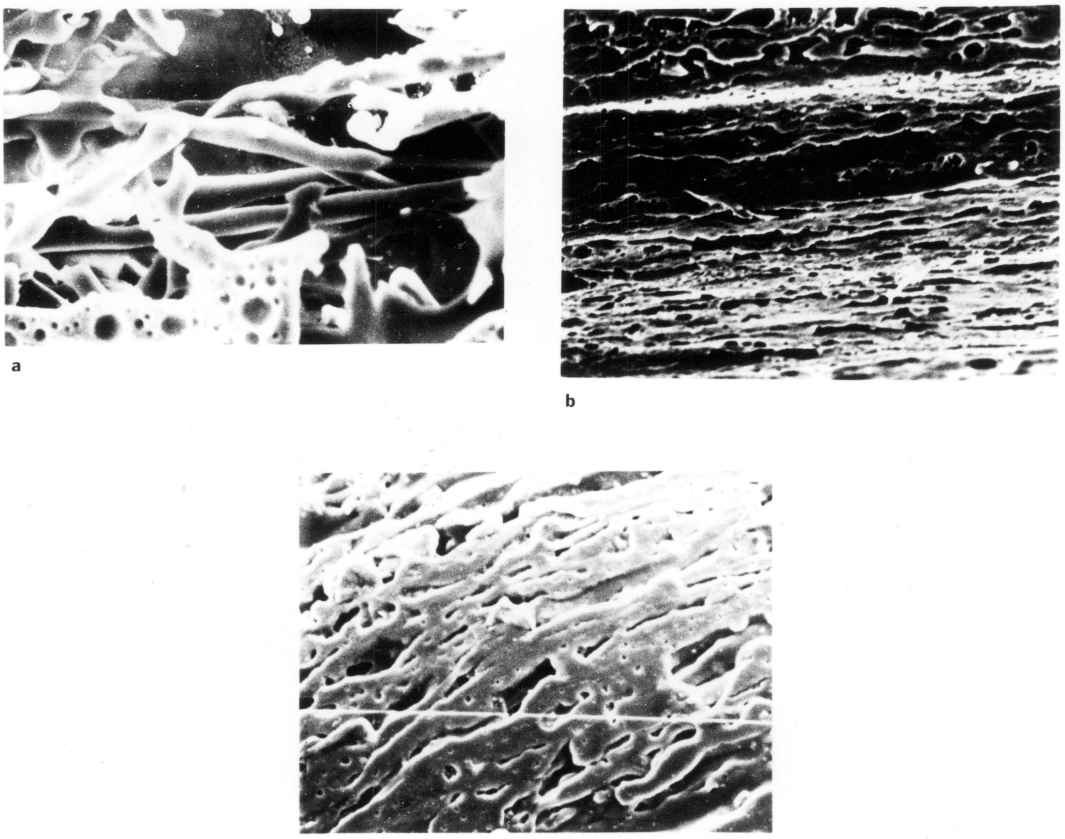

Figure 4.4. Micrographs of extruded N66 blends after extraction of N66. a, 30% LCP; b, 50% LCP; c, 70% LCP. 480 x.

Figures 4.4b and 4.4c. The flow direction in the latter case is inclined about 30 degrees from the horizontal. The structure of the 50% blend is not invariant with the cross-section, as may be seen in Figure 4.5. The first micrograph, reproduced from the previous figure, was taken near the edge of the specimen. At the center, shown in Figure 4.5b, the liquid crystal appears in droplet form after etching with formic acid. The orientation achieved near the edge is not present here. As with some PC blends, this gradient in concentration, and hence orientation and morphology, may be due either to nonuniform mixing or to phase migration. Further interpretations of the extruder results will be made after the cone-&-plate and capillary studies have been analyzed in order to more effectively separate the contributions of the screw and the die to the morphology of the extrudate.

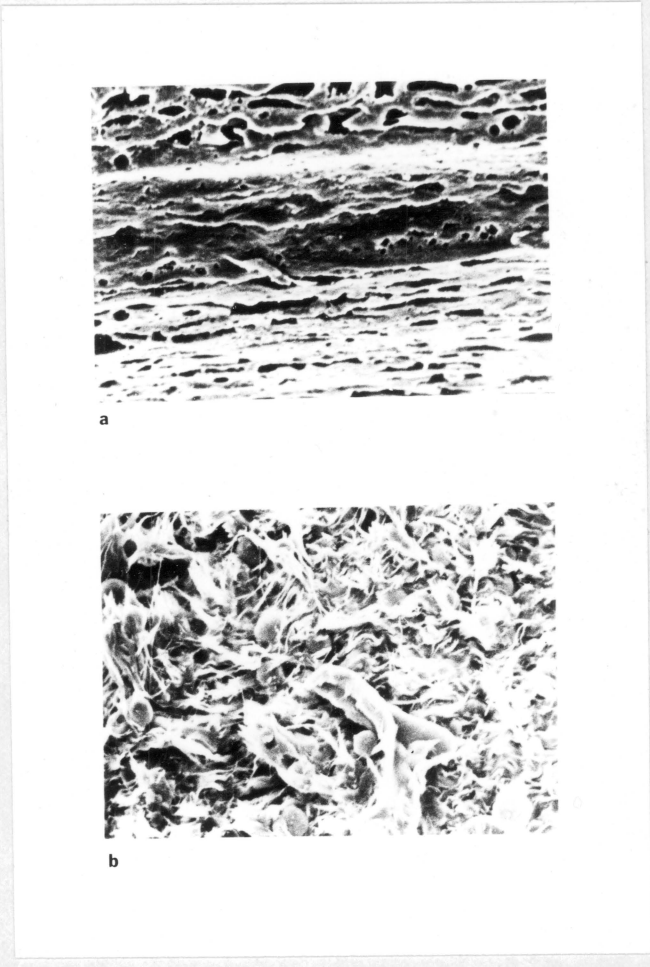

Figure 4.5. Micrographs of extruded 50% LCP after extraction of N66. 480 x.

4.3 Blend Morphology: Steady Shear

Studies of 70% thermoplastic blended with LCP in the extruder were analyzed in the Rheometrics Mechanical Spectrometer to determine the structure of the blend systems after being deformed in a uniform shear field. All samples were annealed for fifteen to twenty minutes at the processing temperature in order to remove any previous orientation due to processing. The micrograph in Figure 4.6 shows the structure of 70% PC blends after this thermal treatment and washing away the thermoplastic. The ultrafine fibers present after extrusion have been replaced by a droplet-in-matrix morphology in which the LCP is dispersed in droplet form in a continuous matrix of PC. Nor does shear flow in the RMS impart a fibril morphology to the samples within the range of shear stresses studied. Values of τ ranged from 45 to 1650 Pa, depending on the shear rate used. Increasing the shear rate from 0.1 to 100 sec^{-1}, shown in Figure 4.7, only serves to make the drops more uniform and smaller in size. The larger drops that were ellipsoidal at 0.1 and 1 sec^{-1} in Figures 4.7a and 4.7b appear to have been broken up into smaller, more spherical drops. The sample sheared at the highest rate was taken at 940x magnification, compared to only 480x

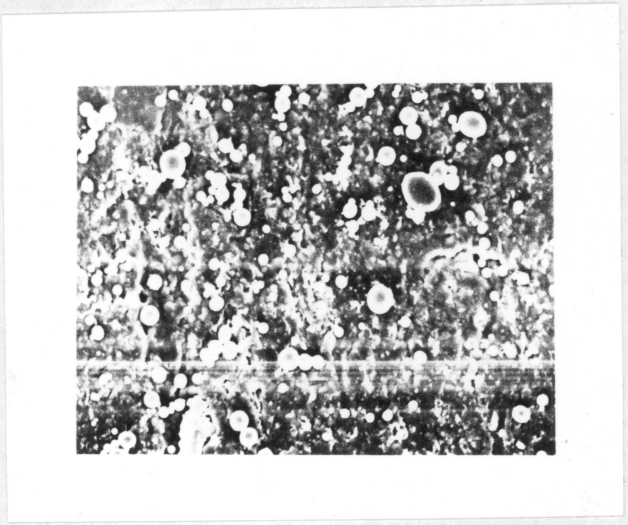

Figure 4.6. Micrograph of 30% LCP after extraction of PC. RMS sample with no applied shear, annealed for 15 minutes. 480 x.

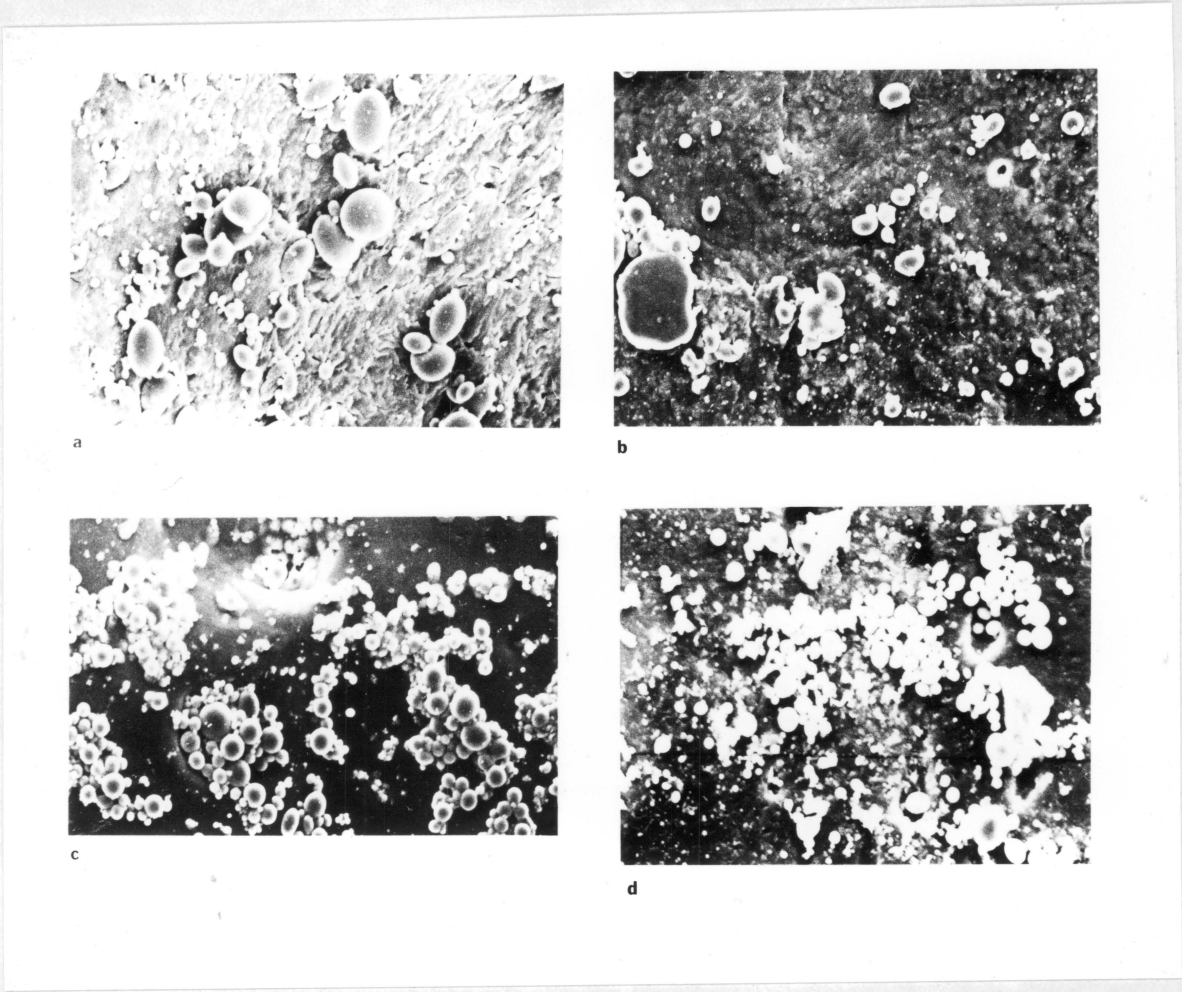

Figure 4.7. Micrographs of 30% LCP after extraction of PC for increasing shear rates. a, 0.1/sec; b, 1.0/sec; c, 10/sec; d, 100/sec. 480 x (except c which is 940 x).

for the others. Because of the several orders of magnitude difference in the shear rates, not all samples could be deformed for the same total strain without introducing time as a factor. Thus, in order to eliminate the total strain as a variable, two different shear rates are compared at different total strains in Figure 4.8. The samples shown in the first two micrographs were deformed at 1 sec^{-1} at strains of 30 and 100, respectively. The last two were sheared at 10 sec^{-1} for strains of 100 and 5000. No difference in droplet size or distribution occurred when two samples were sheared at the same rate for different lengths of time. Thus, the homogenization process is a function only of the shear rate for a given blend composition and temperature.

Nylon 6,6 blends with 30% LCP showed similar behavior. Micrographs of an undeformed sample, one sheared at 10 sec^{-1}, and one sheared at 100 sec^{-1}, are reproduced in Figure 4.9. Little orientation remained in the unsheared sample after annealing for fifteen minutes. The texture of the disc becomes more uniform at the highest rate of deformation, as was the case with the polycarbonate blends. In no instance was any orientation or fibrillation found as the result of deformation in the steady shear field within the experimental limits of this

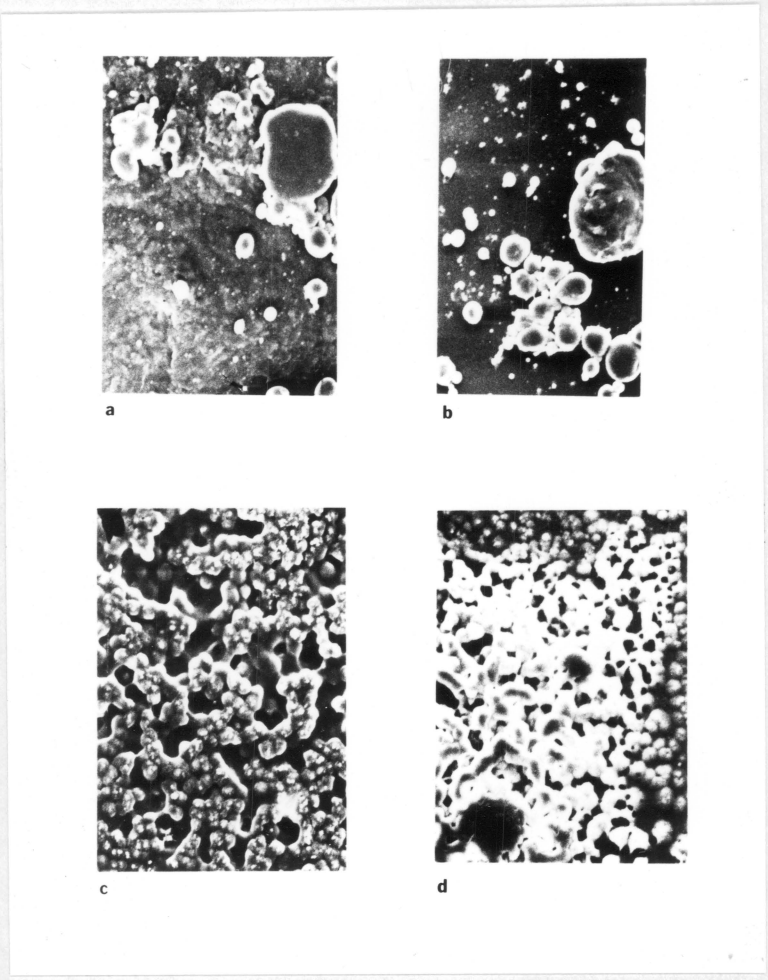

Figure 4.8. Micrographs of 30% LCP after deformation in RMS and extraction of PC. a, strain of 30 at 1/sec; b, strain of 100 at 1/sec; c, strain of 100 at 10/sec; d, strain of 5000 at 10/sec. 480 x.

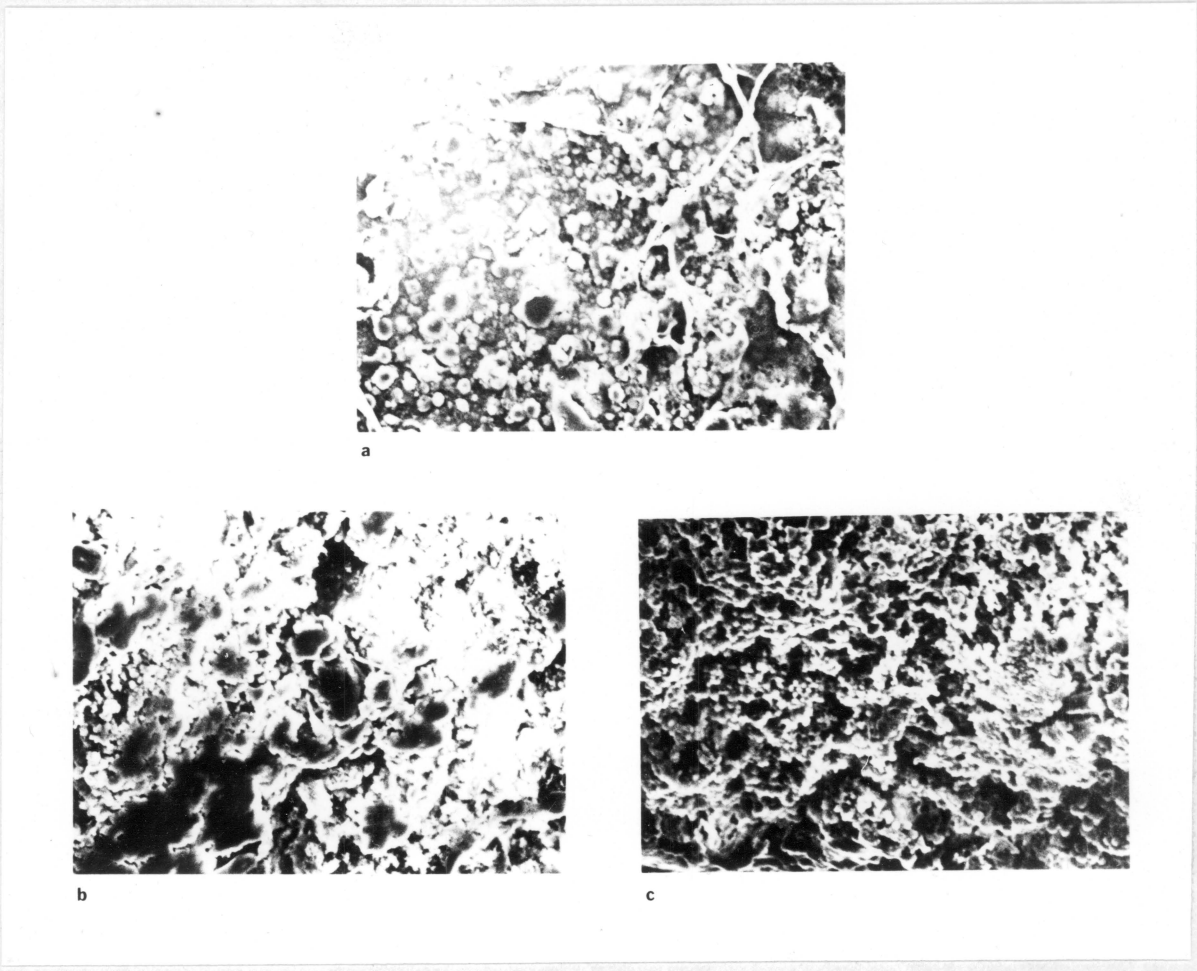

Figure 4.9. Micrographs of 30% LCP after deformation in RMS and extraction of N66. a, no shear; b, 10/sec; c, 100/sec. 480 x.

investigation.

Other researchers [27] have found fibrillation to occur in a uniform shear field, as explained in the literature review, but only for stresses greater than about 4000 Pa. Because of the very low viscosity of the 30% LCP blends and the upper shear rate limit imposed by the machine, the maximum shear stress obtainable in this study was only 1650 Pa. Hence, although a simple steady shear field may possibly cause fibrillation of this polymer blend at higher shear stresses, none was detected in this study.

4.4 Blend Morphology: Capillary Rheometer

In order to generate known flows other than simple shear, 70% PC blends were processed in the Instron Capillary Rheometer with varying L/D capillary ratios. The force and plunger speed were recorded and from these numbers viscosity, shear rate, and wall shear stress were obtained. Three shear rates and three different die geometries at each rate were run to analyze the structure of the extrudate.

Micrographs of samples extruded from the lowest L/D (7.82) capillary are shown in Figure 4.10. Fibrillation was observed to occur readily in all samples extruded from this capillary for shear rates from 45.7 to 457 sec^{-1}. Wall shear stresses were in the range of 4000 Pa to approximately 45,000 Pa. The first three micrographs were taken at increasing shear rates. All photographs show numerous ultrafine fibers oriented in the direction of flow. Two perceptible differences are the qualitative one that at the highest rate the fibers tend to be of smaller diameter and that the presence of phase inversion can be detected at 457 sec-1. This concentration gradient is shown in Figure 4.10d. This photograph was taken near the outer edge of the sample, and may be distinguished from the one in Figure 4.10c

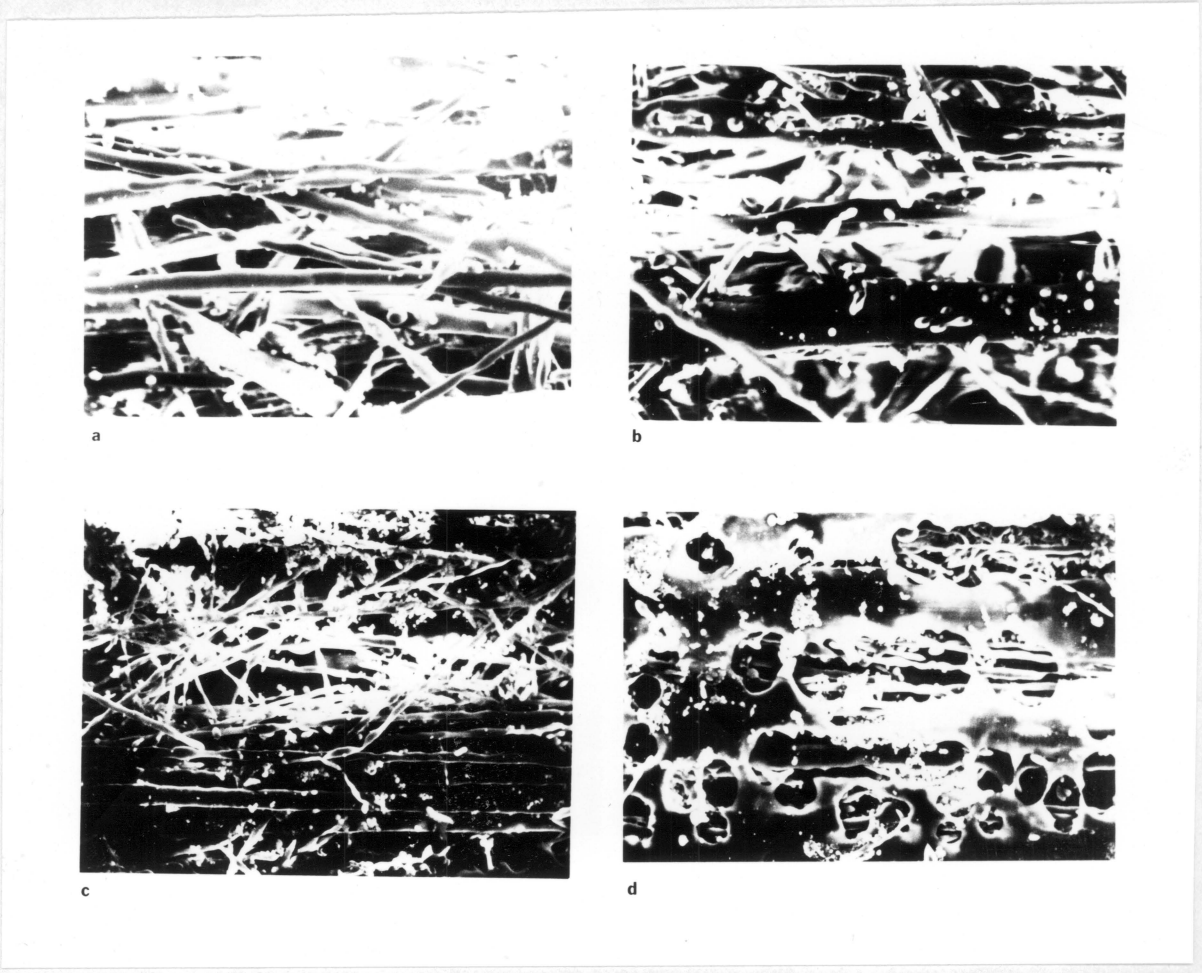

Figure 4.10. Micrographs of 30% LCP after extraction of PC. Samples extruded through ICR with capillary diameter of 0.178 cm and L/D of 7.82. a, 45.7/sec; b, 137/sec; c, 457/sec, center of sample; d, 457/sec, edge of sample. 480 x.

from the center of the specimen. The higher concentration of the LCP near the edge appears as a matrix from which near-spherical droplets of PC have been extracted.

This phase migration is similar in effect to the nonuniformity that is observed in some samples processed in the single screw extruder. In those cases though, the shear stress in the die was 6.1 kPa or less, except for the 90% PC blend which showed no signs of fibrillation anyway. As can be seen from Table 4.3, the phase inversion, not present for any but the highest shear rate, occurs at a wall shear stress of 22 kPa for the smallest L/D. Thus, nonconstant morphology as exhibited by the 70% PC in the large die is possibly the result of less than ideal mixing in the extruder. Likewise, the variation seen in the 30% PC blend probably arises from poor melt blending of the tumbled pellets during extrusion.

The fibrous structure was no longer present in the extrudate for the L/D ratio of 21.4, as shown in Figure 4.11. Micrographs a, b, and d represent increasing shear rates. Figure 4.11c is a 4800x magnification of the specimen sheared at the intermediate shear rate showing greater detail of the phase separation. The coral-like texture is the PC after being etched with methylene

TABLE 4.3

Instron Morphology Study

Material: 70/30 PC/LCP
Temperature: 260°C

Capillary L/D	Shear Rate (sec-1)	Wall Shear Stress (kPa)
7.82	45.73	3.77
7.82	137.2	8.76
7.82	457.3	22.0
21.4	45.73	5.22
21.4	137.2	12.6
21.4	457.3	32.9
40.0	45.73	8.19
40.0	137.2	19.0
40.0	457.3	47.8

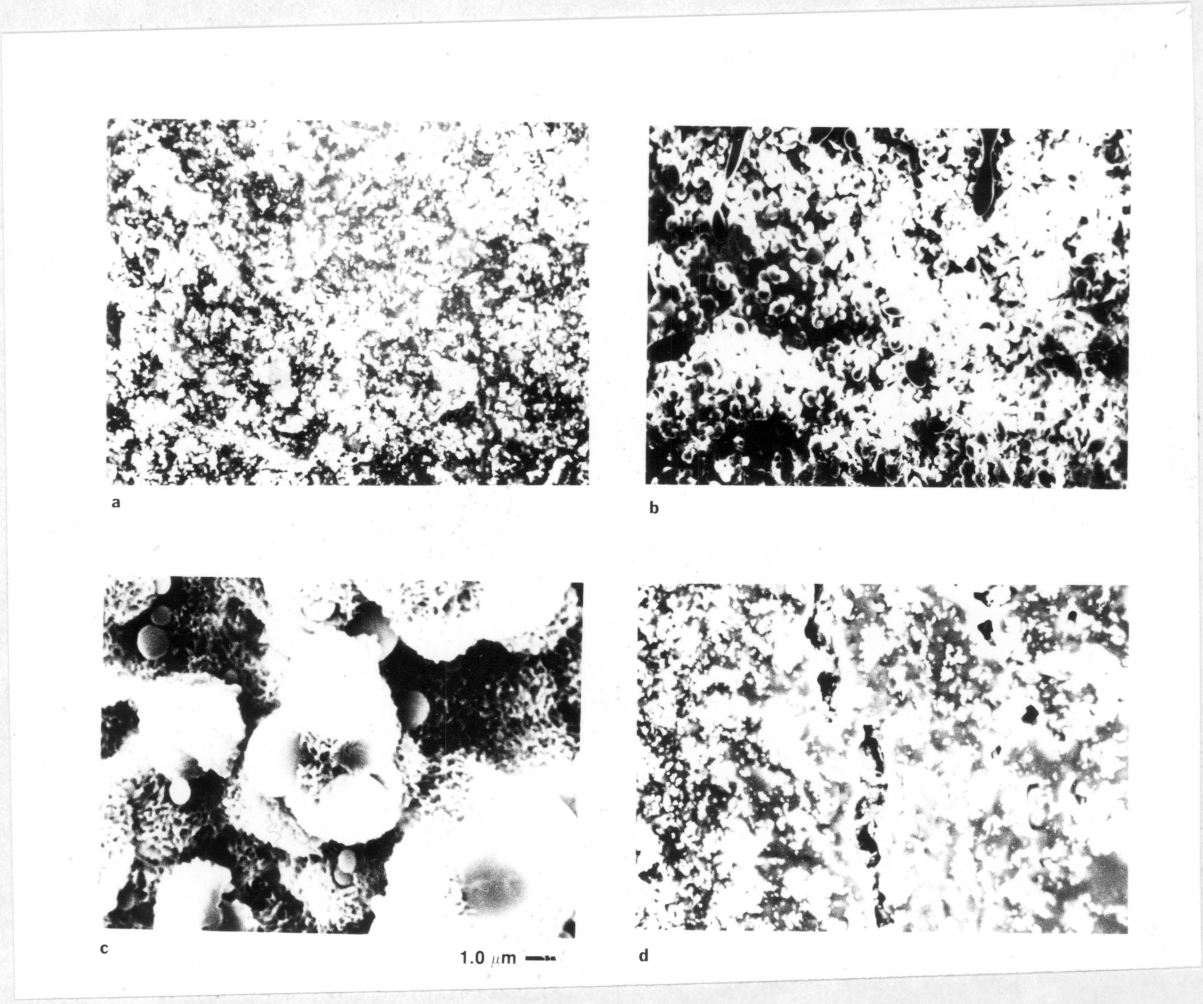

Figure 4.11. Micrographs of 30% LCP after extraction of PC. Samples extruded through ICR with L/D of 21.4. a, 45.7/sec; b, 137/sec; c, 137/sec at 4800 x; d, 457/sec. a, b, and d at 480 x.

chloride. The smooth droplets are the copolyester. All orientation and fibrillation appears to be lost, although some signs of macroscopic phase separation may be seen at the highest shear rate, with the outer sheath consisting primarily of the lower viscosity LCP.

One explanation for the difference between the morphology of the specimens extruded through the shortest and intermediate range L/D capillaries is that the effects of any extensional forces at the converging entrance to the die may have been lost due to the relaxation of the structure in the shear flow field of the capillary itself. This explanation alone does not suffice because the longest L/D (40) shows some orientation at the highest shear (Figure 4.12). The micrograph of the lowest plunger speed is enlarged 4800x to show phase details otherwise not apparent; Figures 4.12b and 4.12c are magnified only 480x. The droplet-in-matrix structure is prevalent at all but the highest shear rate. In the latter case, some fibers aligned along the flow direction are noticeable. This morphology does not preclude significant droplet structure, which can be seen in the lower portion of Figure 4.12c.

Several authors have studied polyblend morphology after processing in a capillary rheometer [24,26,28,

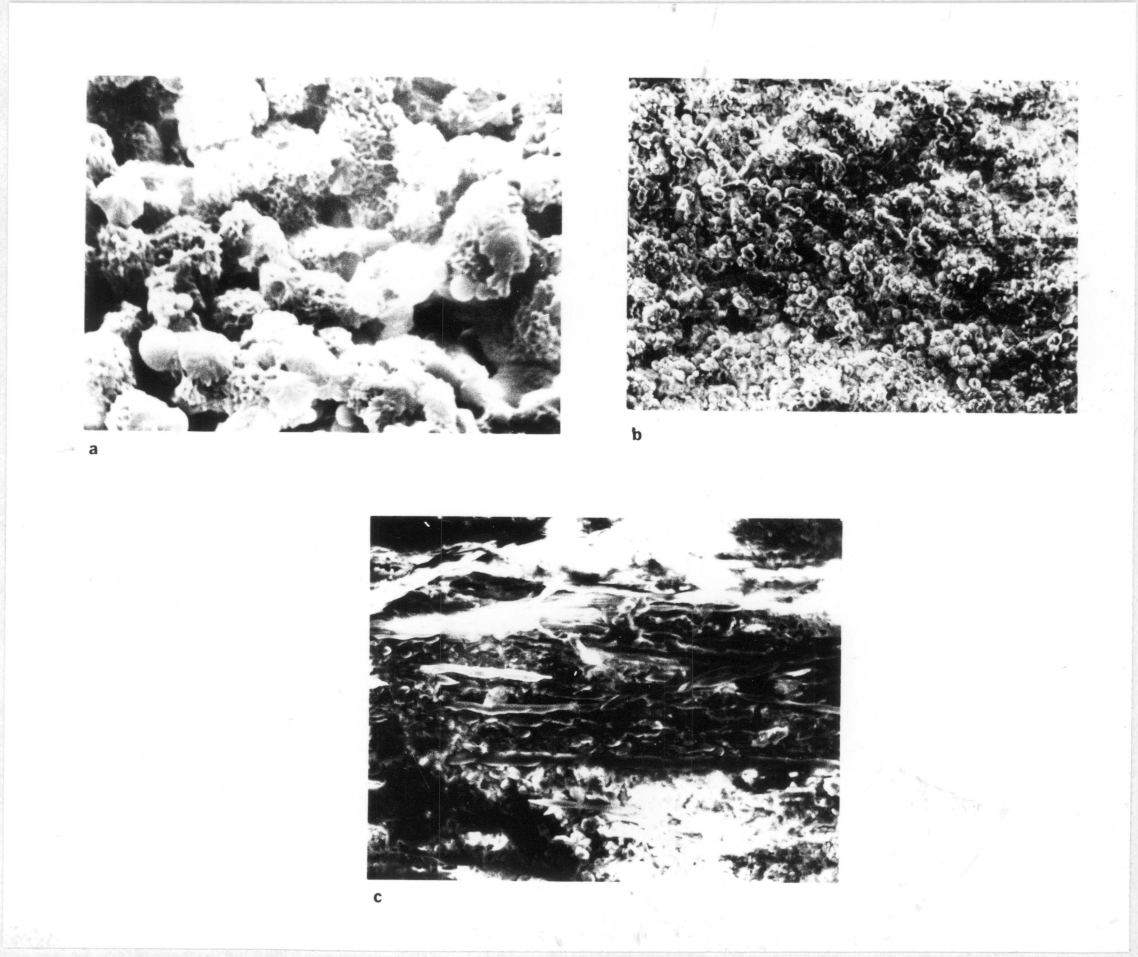

Figure 4.12. Micrographs of 30% LCP extruded through ICR with L/D of 40 after extraction of PC. a, 45.7/sec at 4800 x; b, 137/sec; c, 457/sec. b and c at 480 x.

32,80]. Most researchers have attributed the observed fibrillar structure to the converging flow at the entrance of the capillary which causes coalescence and extension of the domains. Van Oene [32] reported some difference in the homogeneity of the extrudate depending on the L/D of the die. Longer capillaries tended to result in a finer dispersion in the blend, although the morphology was not altered.

The morphology of these polyblends under different processing histories has been examined. Once one knows what structure is present under given processing conditions, it is of both theoretical and practical interest to determine how, or if, this morphology affects the solid state and melt properties of the polyblend. Thus, these properties will be examined in the remainder of the chapter.

4.5 Blend Rheology: Cone & Plate

The flow properties have been characterized with the Rheometrics Mechanical Spectrometer both in steady shear and dynamic oscillatory shear fields. Shear rate - viscosity data for the PC blends are shown in Figure 4.13 for steady deformation. The unblended copolyester data have been taken from reference [61]. The error bars give an uncertainty in the measurements as determined from the differences observed for multiple runs at the same conditions. Polycarbonate itself does not shear thin, maintaining a viscosity of about 2000 Pa*s. With the addition of 10% LCP, the viscosity is cut in half and some shear thinning is noticeable at shear rates of 1 sec^{-1} and higher. With a higher ratio of LCP, the liquid crystal tends to dominate the flow properties. The three blends studied in this range all show shear thinning behavior comparable to the copolyester. When the viscosity data are plotted at a fixed shear rate versus composition as shown in Figure 4.14 for two different shear rates, the effect of blending is more readily apparent. Pronounced negative deviation behavior may be seen at high LCP contents. The results cannot be used to predict a viscosity minimum as a function of composition due to the error in the measurements as indicated by the

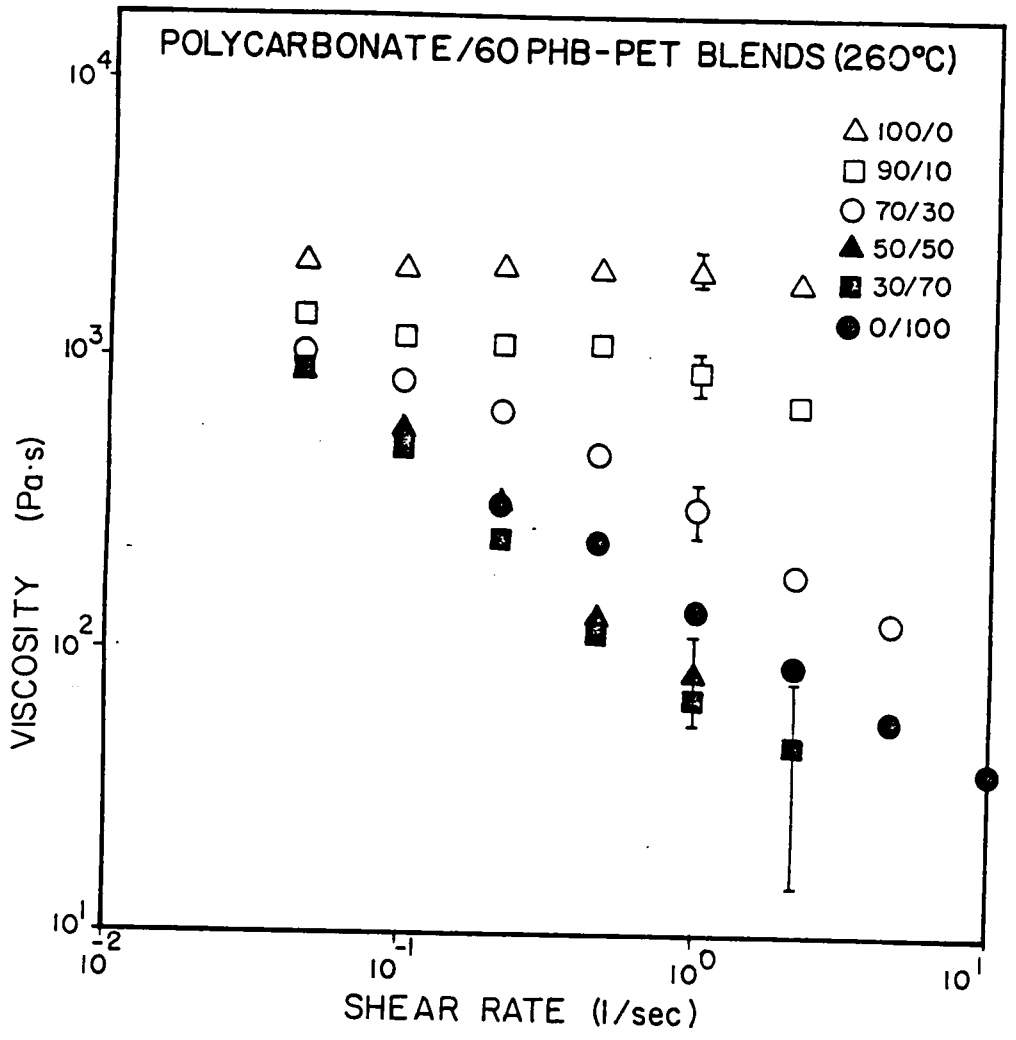

Figure 4.13. Steady shear viscosity of polycarbonate blends from RMS in cone & plate mode. The first number appearing in the key denotes the weight fraction of PC, the second that of the LCP.

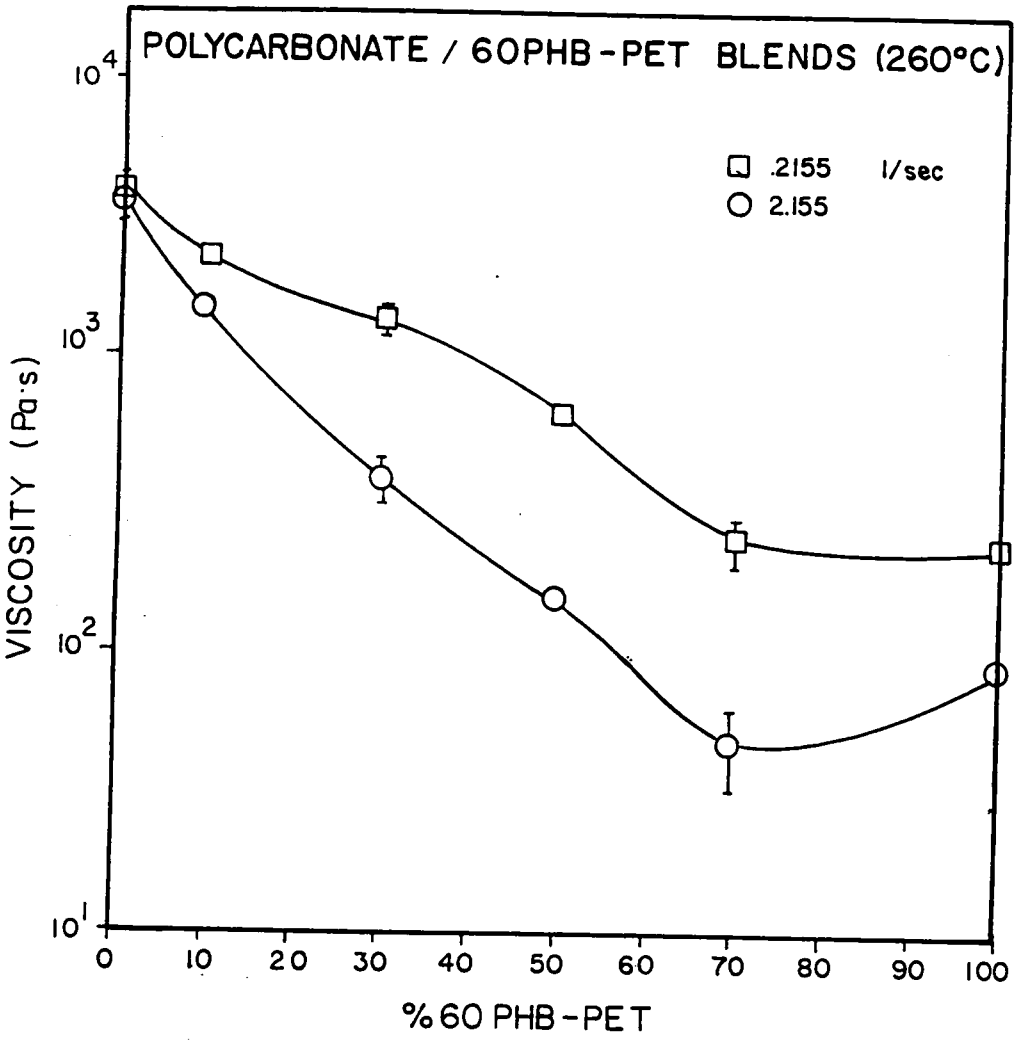

Figure 4.14. Steady shear viscosity of PC blends as a function of composition for two shear rates in the RMS.

error bars in the figure.

The dynamic results in Figure 4.15 follow the same pattern, except that the 30% LCP blend retains some of the PC flow behavior. A more abrupt change is noticeable in Figure 4.16 at 50% LCP. The dramatic decrease in viscosity, although the rate of shear thinning remains essentially constant, is evidence of a phase inversion in which the LCP becomes the predominant phase. Since no fibrillation occurs for small strain oscillatory deformations, this viscosity reduction is probably due to PC being present in a droplet dispersion, and hence contributing less to the flow properties than it would in a continuous matrix. The micrographs from the extrudate samples (Figures 4.1-4.4) reinforce this notion of an overall phase inversion occurring at some concentration of the LCP. The outer sheath tends to show inversion of the phases at a lower bulk minor component concentration than would be anticipated. Within the limits of this study, the trends of both the dynamic and steady shear behavior on the composition diagram are the same for different shear rates, although the effect of increasing the shear rate on the viscosity is more pronounced in the steady shear mode.

The N66 blends show an even more accentuated negative deviation from linearity on a viscosity - composition

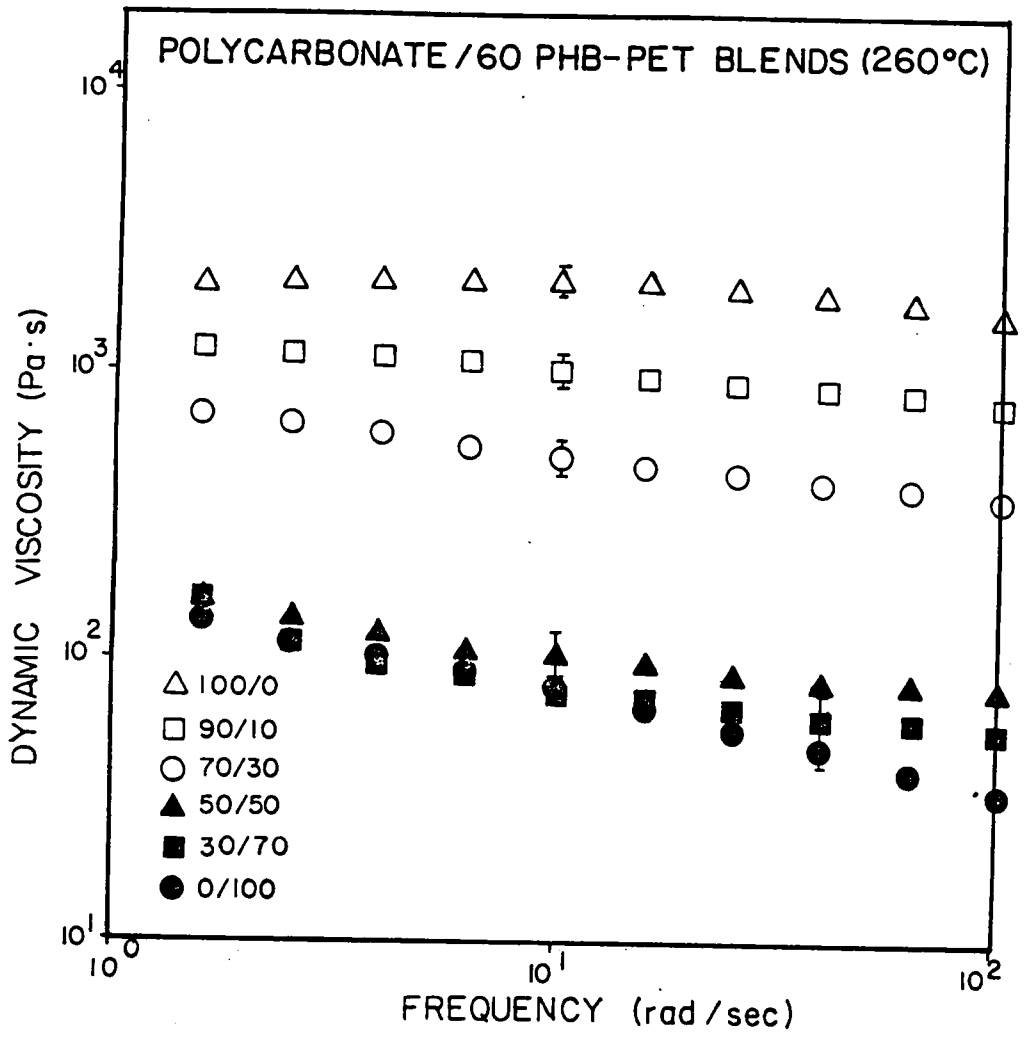

Figure 4.15. Dynamic viscosity of PC blends from the RMS.

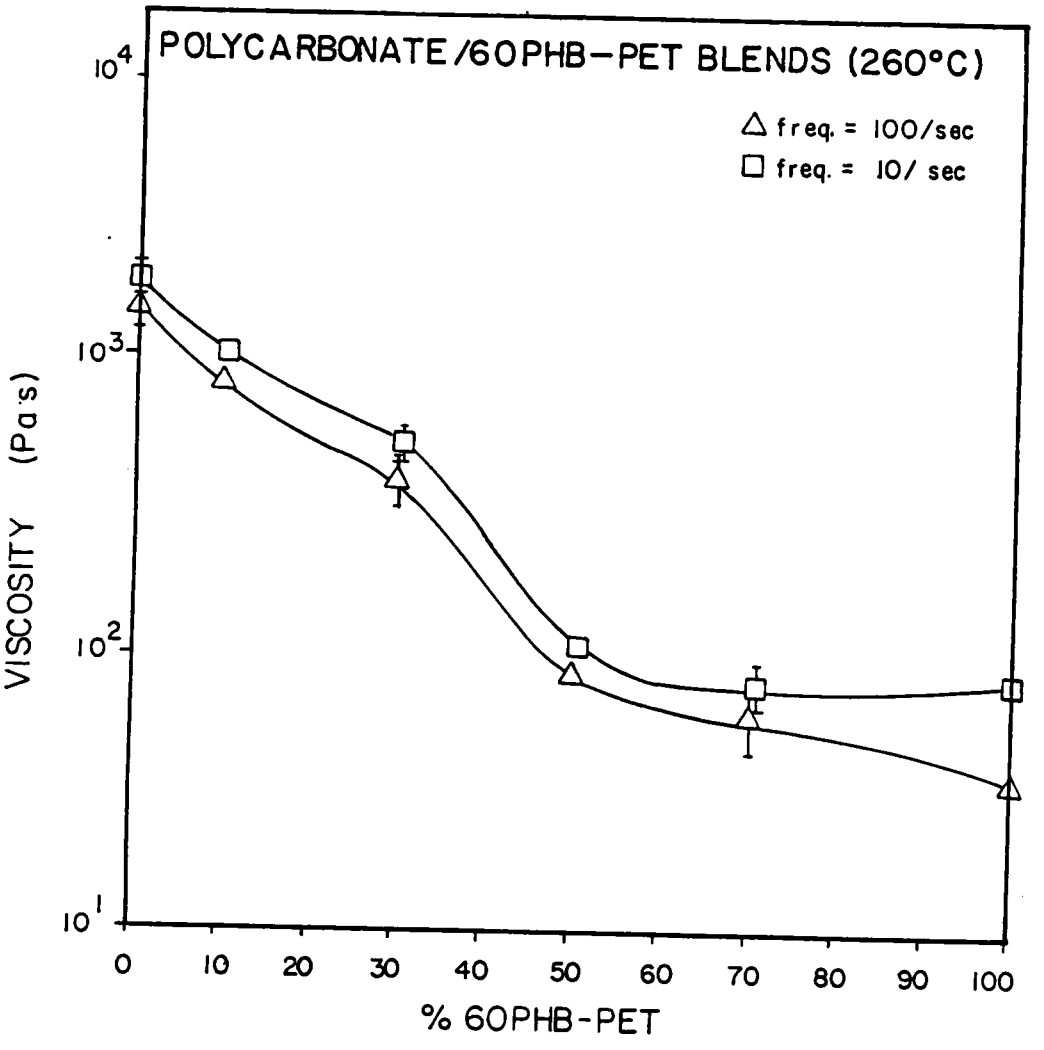

Figure 4.16. Dynamic viscosity of PC blends as a function of composition at two shear rates from the RMS.

plot than do the PC blends. Steady shear behavior is summarized in Figure 4.17, where, within experimental error, all blends behave precisely as does the copolyester itself. Nylon's viscosity remains fairly constant at 400-700 Pa*s or so, whereas the blends shear thin to a high degree at the rates examined. At ten reciprocal seconds all blends show viscosities from 10 to 30 Pa*s.

The dynamic viscosities of the N66 blends are reproduced in Figure 4.18. As with the PC blends, the amount of shear thinning decreases in the dynamic mode. As may be seen from Figure 4.19, an intermediate minimum in viscosity as a function of composition appears to occur between 10 and 50% LCP. Due to the experimental error no particular blend ratio may be postulated to show an absolute minimum in viscosity. Increasing the angular frequency serves only to shift the data vertically downward; the viscosity-composition trends remain the same.

As mentioned in the literature review, intermediate minima have been noted by other researchers. However, none has been able to satisfactorily explain this phenomenon either in terms of the microstructure present or by an acceptable rheological theory. The negative deviation of the samples deformed in the steady shear

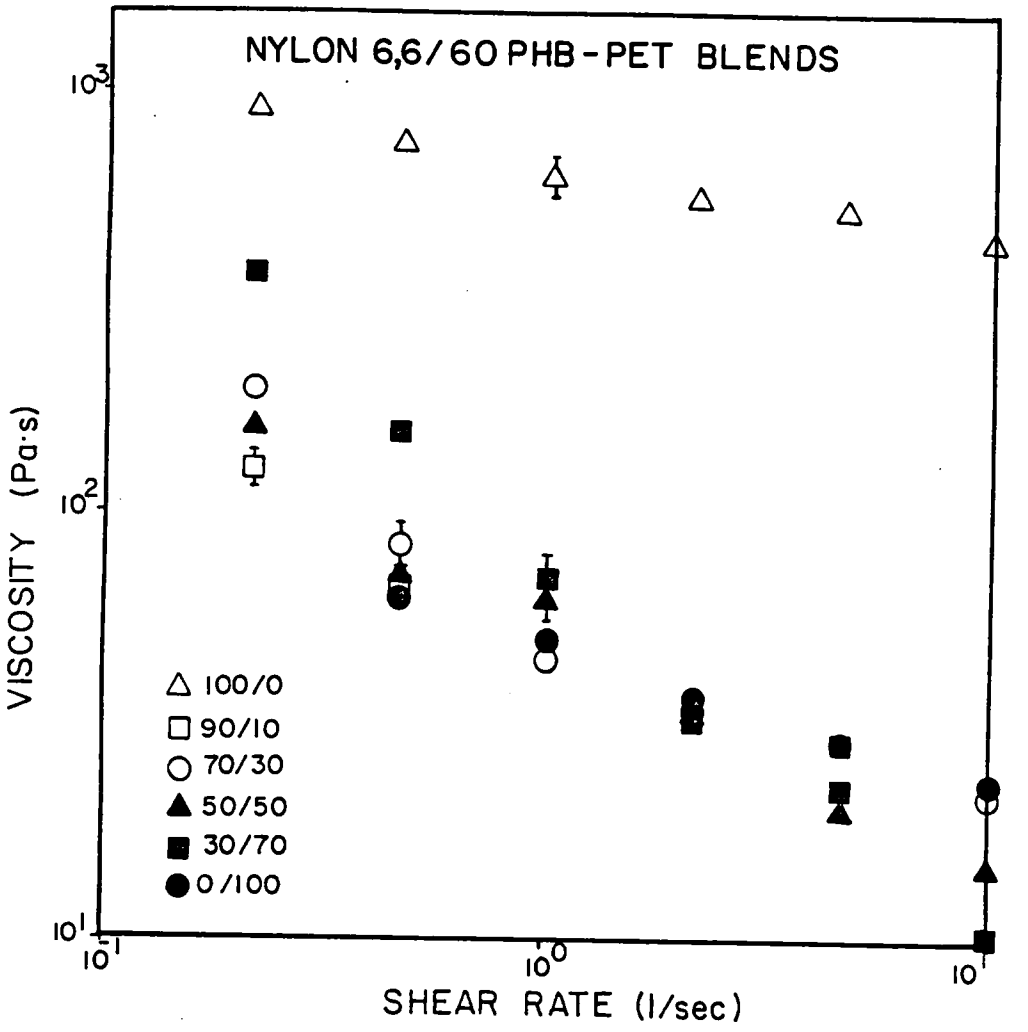

Figure 4.17. Steady shear viscosity of N66 blends from RMS. The first number appearing in the key denotes the weight percent of N66, the second that of the LCP.

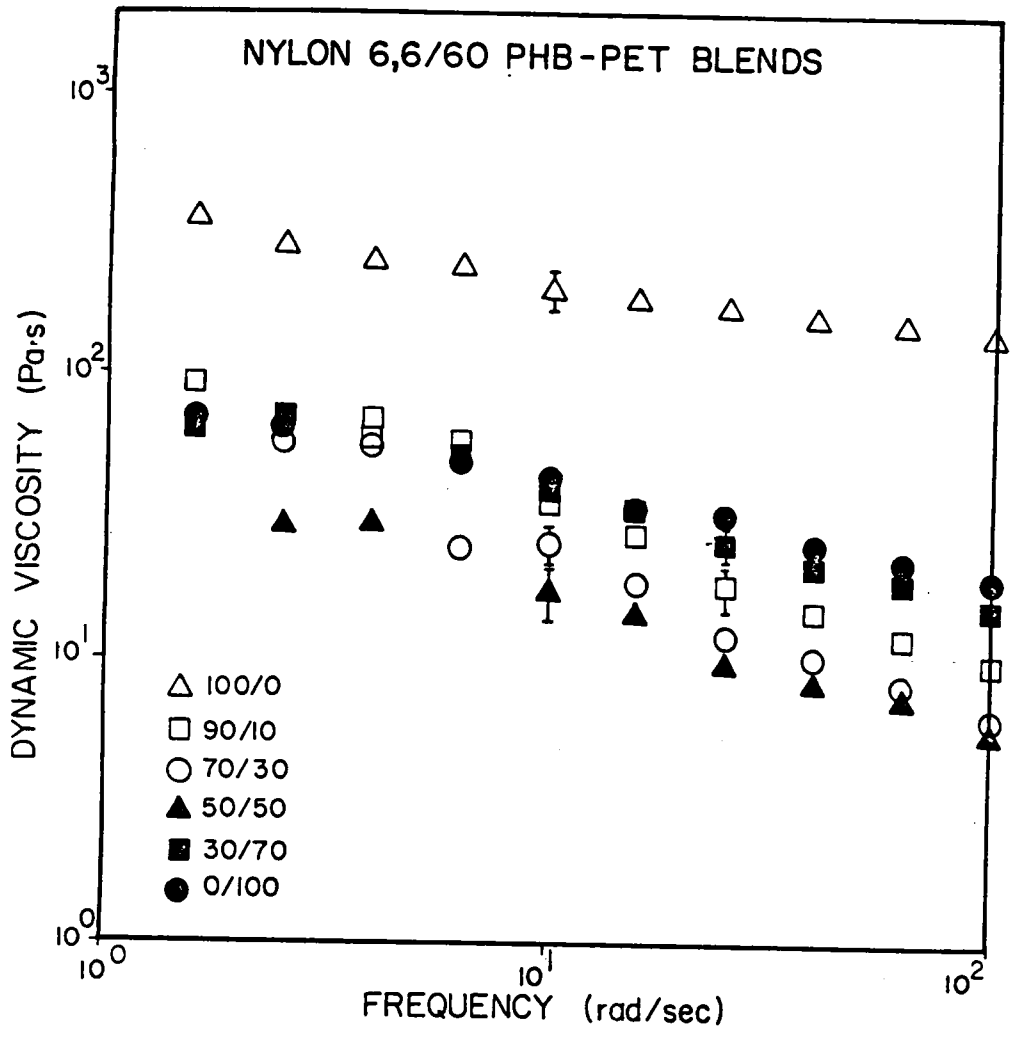

Figure 4.18. Dynamic viscosity of N66 blends from the RMS.

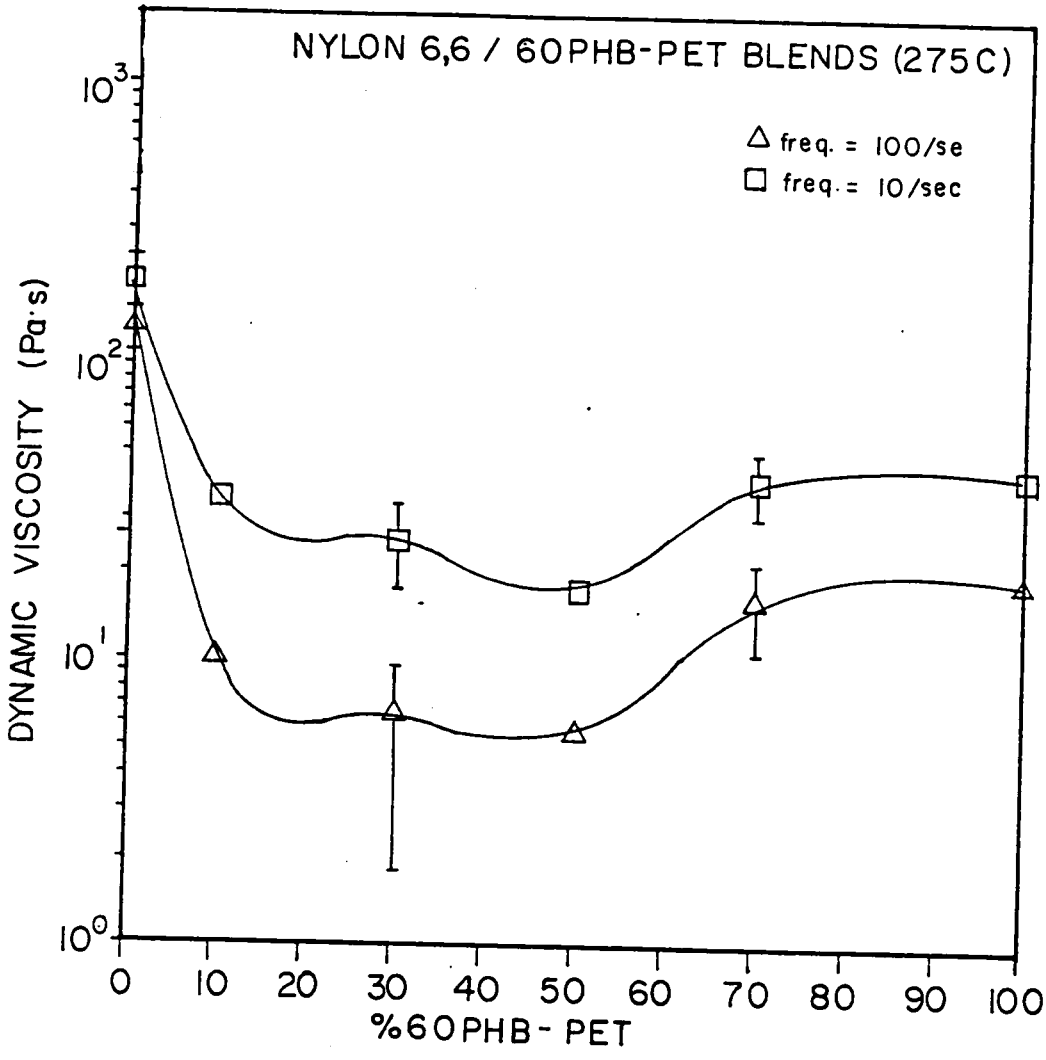

Figure 4.19. Viscosity of N66 blends as a function of composition for two shear rates from the RMS.

mode is difficult to account for in terms of the droplet morphology present in the blends processed in the RMS. Nor does the capillary morphology explain the rheological behavior, as will be seen in the next section.

4.6 Blend Rheology: Capillary Rheometer

The viscosity of PC and N66 and their blends with the LCP was measured between ten and 10000 sec-1 in the Instron Capillary Rheometer (ICR). These results are reported in Tables 4.4 and Table 4.5. The PC results are summarized in Figure 4.20. Pressure drop versus L/D plots (Bagley plots) for all blends are reproduced in Appendix B. The error bars indicate the differences obtained in the force when more than one reading was taken at a given speed for a barrel load. The trends are similar to the shear data in the RMS, with 30% LCP and higher reflecting the flow properties of the LCP to a great extent; the 10% LCP blend showed behavior similar to the PC, but with an absolute value of viscosity of about half of the homopolymer. The compositional dependence of the viscosity may be seen more readily in Figure 4.21. The marked decrease in the viscosity at 30% LCP and 1000 sec-1 may represent either the fibrillation of the LCP or a phase migration behavior in which the minor component concentrates at the outer wall where the stress and shear rate values have been calculated. As with the cone-&-plate data, the copolyester capillary viscosity data were obtained from reference [61]. The combined cone-&-plate and capillary data in Figure 4.22

TABLE 4.4

Instron Capillary Data of PC Blends

Shear Rate (sec^{-1})	τ_w (Pa)	Viscosity (Pa*s)
Polycarbonate (260 C)		
12.44	11.56	929.2
41.47	41.69	1005.4
124.4	130.2	1046.7
414.7	444.0	1070.6
1244	1342.	1078.8
PC/LCP 90/10 (260 C)		
11.92	6.09	510.7
39.74	19.58	492.8
119.2	56.58	474.6
397.4	180.1	453.3
1192.	516.6	433.3
PC/LCP 70/30 (260 C)		
12.69	1.66	130.8
42.31	3.54	83.73
126.9	7.07	55.67
423.1	15.05	35.57
1269.	29.96	23.61
PC/LCP 50/50 (260 C)		
235.3	3.46	14.71
784.3	8.78	11.19
2353.	20.46	8.70
PC/LCP 30/70 (260 C)		
253.2	2.88	11.36
844.1	6.97	8.26
2532.	15.62	6.17
8441.	37.73	4.47

TABLE 4.5

Instron Capillary Data of N66 Blends

Shear Rate (sec-1)	τ_w (Pa)	Viscosity (Pa*s)
Nylon 6,6 (275 C)		
11.86	3.71	313.1
39.52	10.71	270.9
118.6	28.13	237.3
395.2	81.03	205.0
1186.	212.6	179.3
90/10 N66/LCP (275 C)		
390.1	2.39	6.12
780.2	4.24	5.44
1170.	5.94	5.07
3901.	16.1	4.13
70/30 N66/LCP (275 C)		
410.8	1.26	3.07
1232.	2.39	1.94
2465.	3.57	1.45
4108.	4.80	1.17
50/50 N66/LCP (275 C)		
812.9	2.38	2.93
1219.	3.30	2.70
2439.	5.76	2.36
4064.	8.68	2.14
30/70 N66/LCP (275 C)		
415.4	1.03	2.49
1246.	2.17	1.74
4154.	4.90	1.18

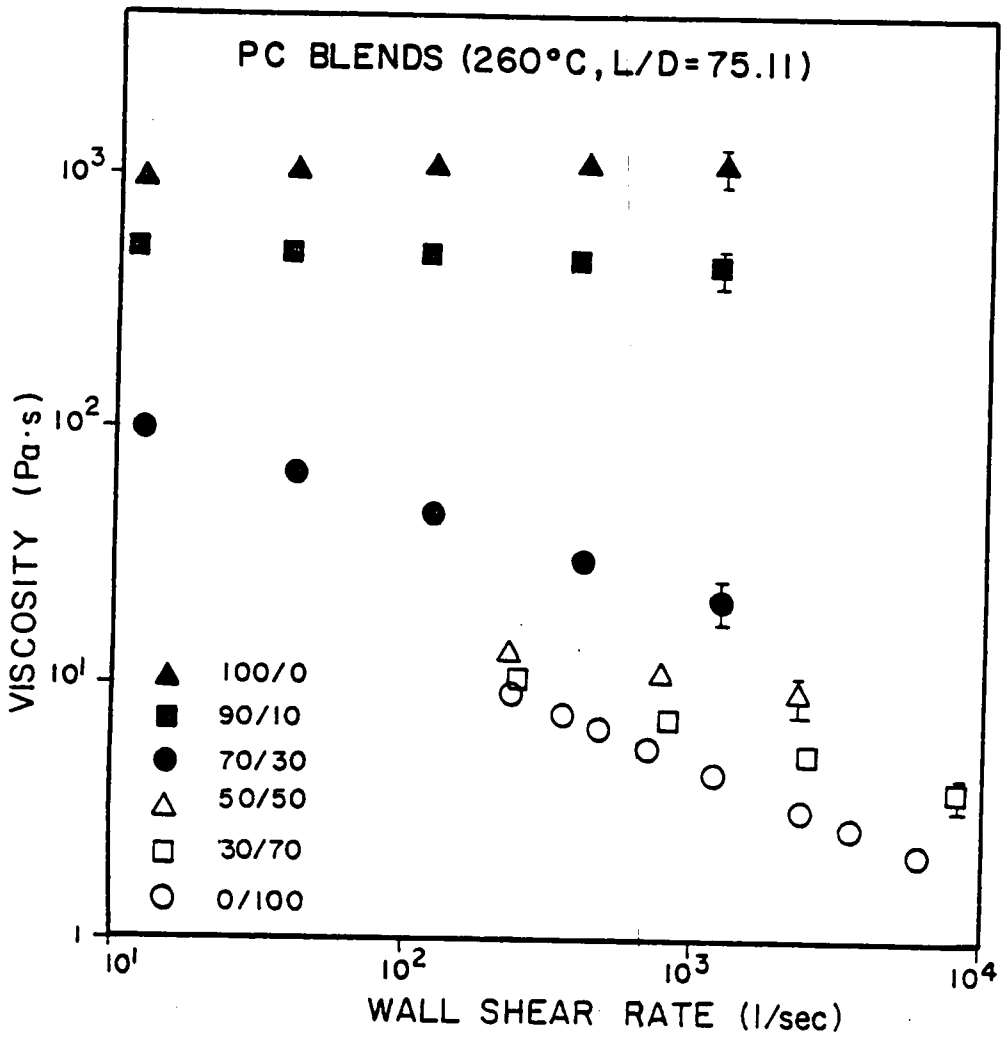

Figure 4.20. Viscosity of PC blends from the ICR for an L/D of 75.11 and a capillary diameter of 0.0686 cm.

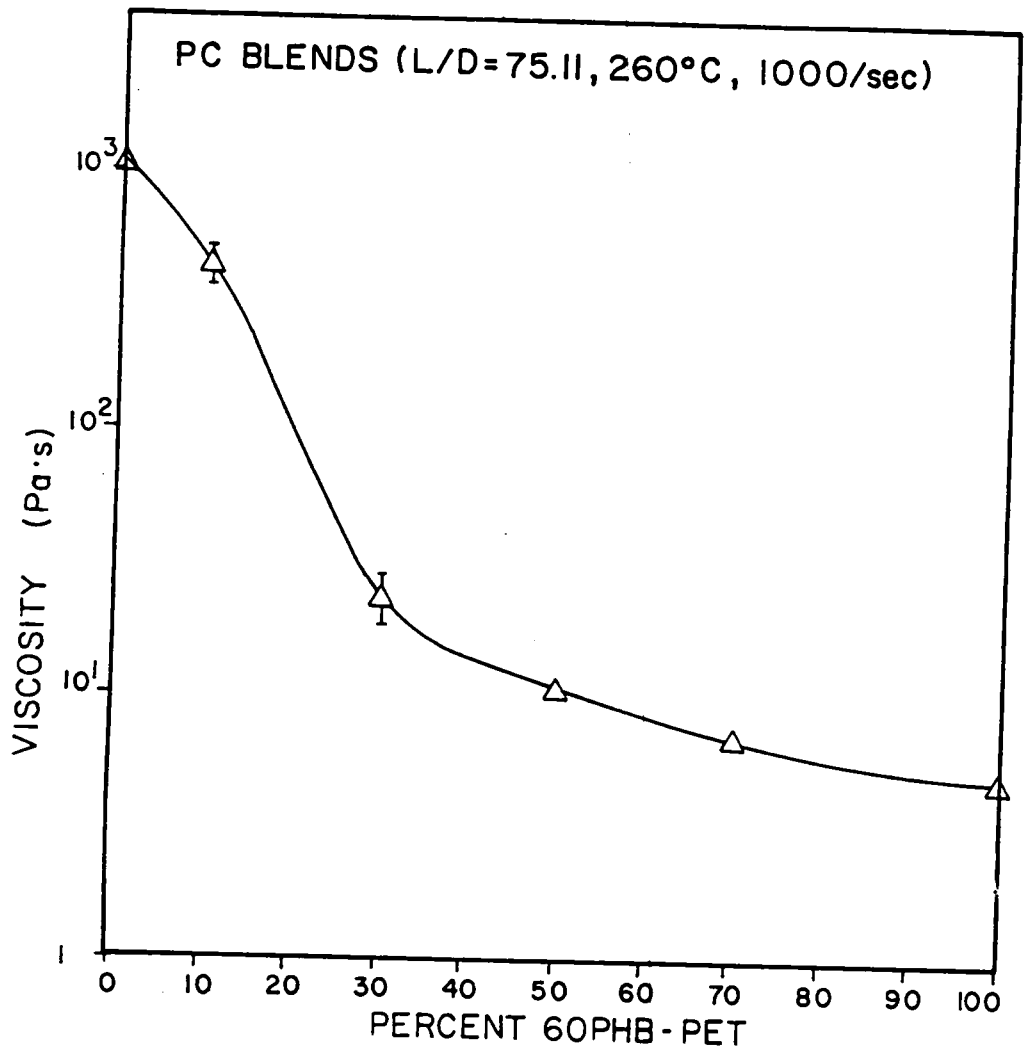

Figure 4.21. Viscosity of PC blends at 1000/sec as a function of composition from the ICR.

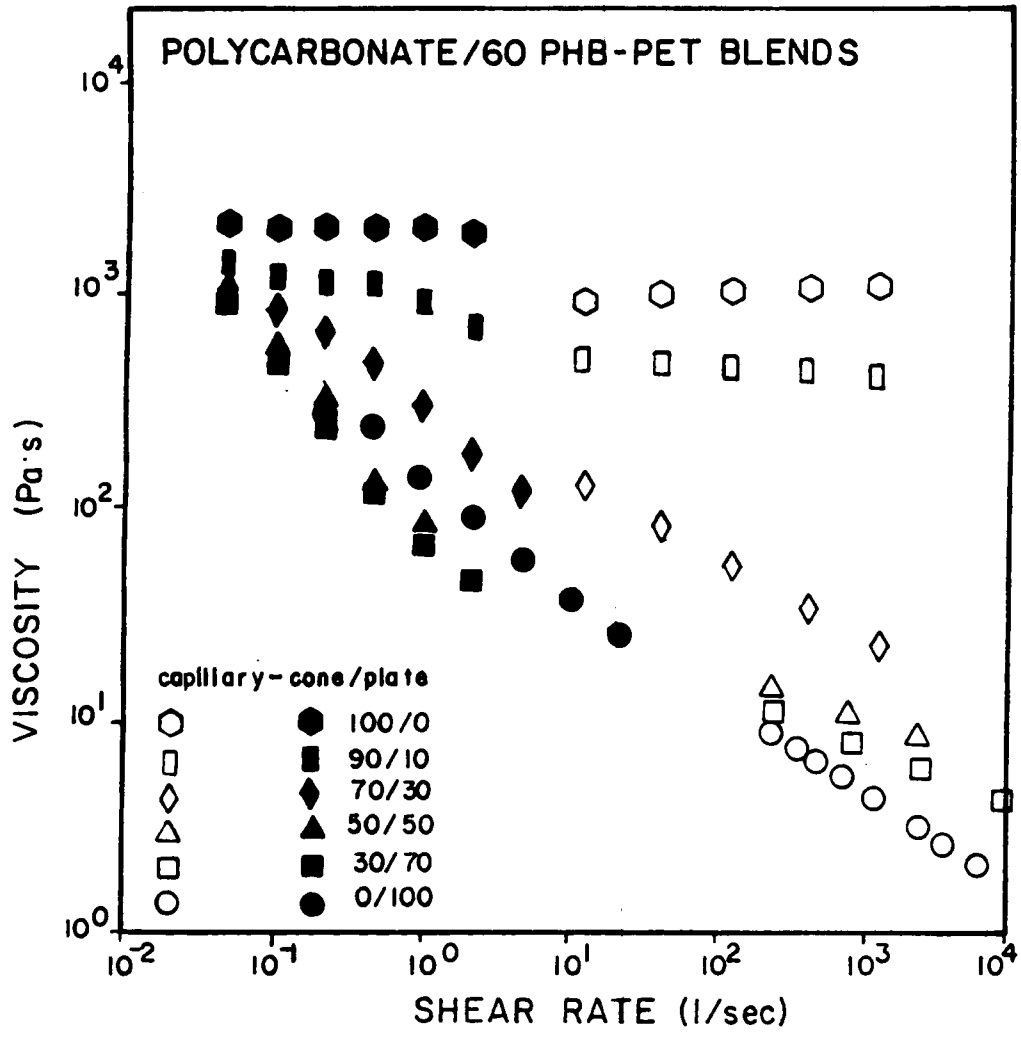

Figure 4.22. Combined viscosity data from RMS and ICR for PC blends.

show good agreement as far as general trends are concerned, but the capillary data are slightly higher or lower than the cone-&-plate data, depending on the blend ratio. The capillary data are higher than expected for moderate LCP content, but for the 90% and 100% PC the viscosity is somewhat lower than in the RMS. violation of the no-slip boundary condition at the wall of the capillary for high content PC blends may account for this latter discrepency. Most data points do lie within the estimated experimental error given by the error bars in Figures 4.13 and 4.20.

The N66 capillary blend viscosity results are correlated in Figures 4.23-4.25. The values obtained in the ICR show nearly the same trends as did the cone-&-plate measurements. The remarkable decrease in viscosity at only 10% LCP is reproduced in Figure 4.23. Data obtained ranged from 10 to 4000 sec-1, and are reported on a viscosity versus composition graph in Figure 4.24. From a viscosity of nearly 200 Pa*s for the N66 homopolymer at 1000 sec-1, the value quickly dropped to a minimum by 30% LCP, which has a magnitude similar to that of the pure LCP. This minimum remained constant within experimental error at a value of around 3 Pa*s with the addition of more LCP. The combined cone-&-plate and capillary results in Figure 4.25 for the N66 poly-

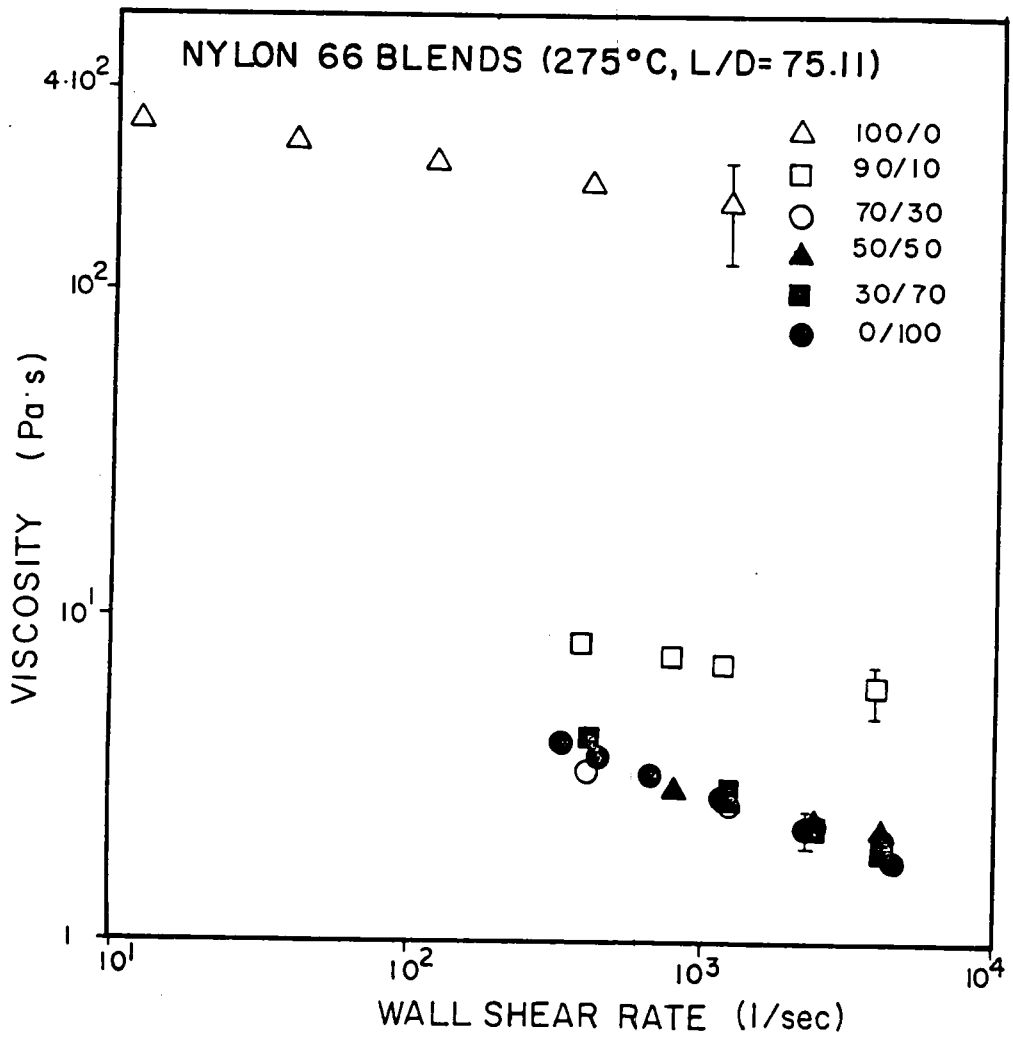

Figure 4.23. Viscosity of N66 blends from the ICR.

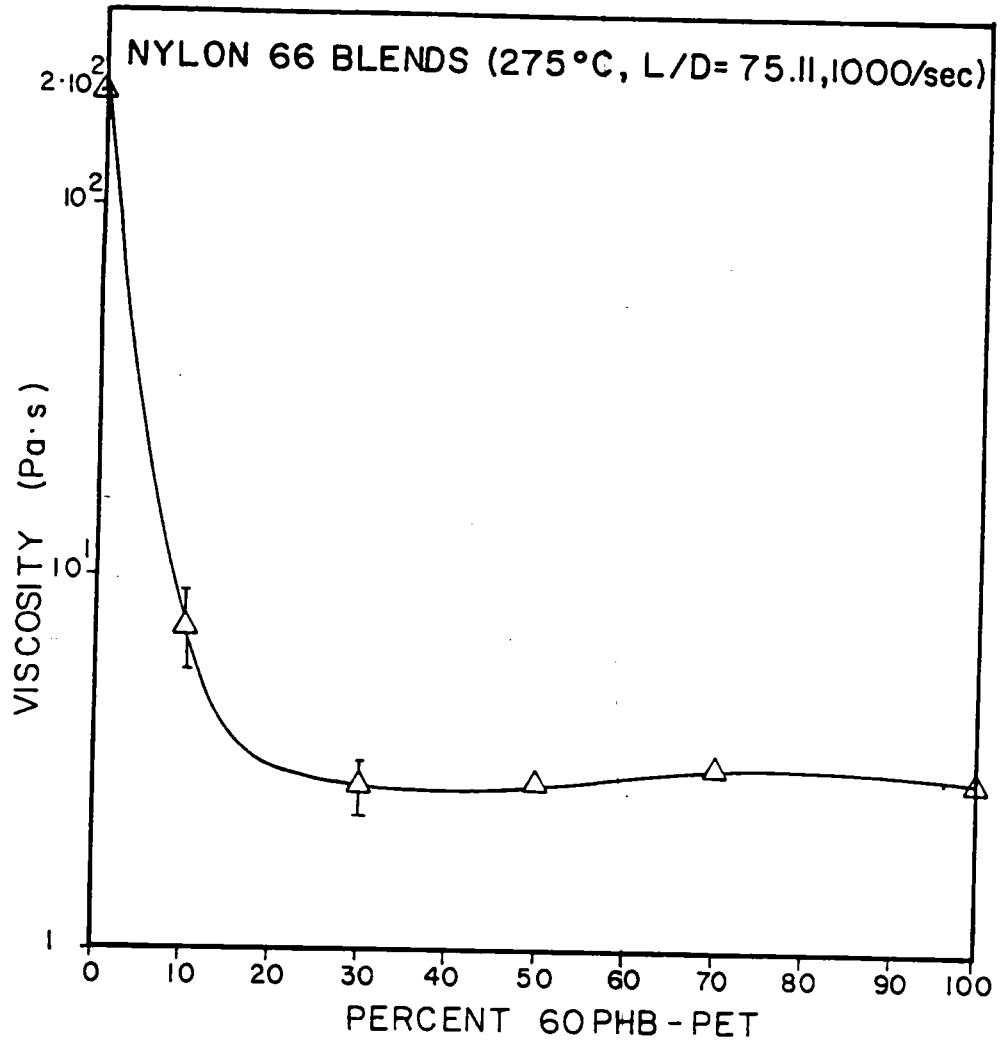

Figure 4.24. Viscosity of N66 blends at 1000/sec as a function of composition from the ICR.

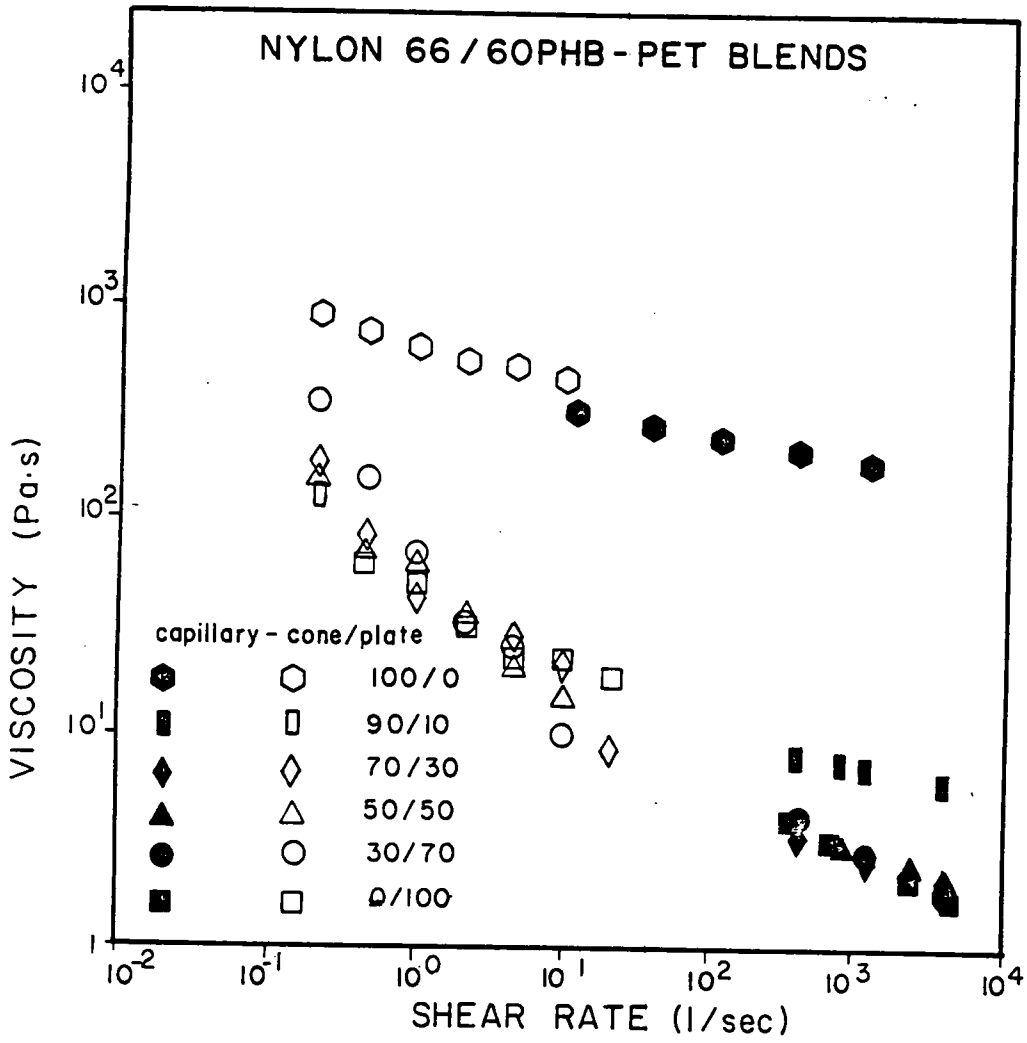

Figure 4.25. Combined viscosity data of N66 blends from the RMS and ICR.

blends show remarkably good agreement. The viscosities at all compositions fall within the error bars established in Figures 4.17 and 4.23.

The rheology of the thermoplastic/LCP blends is very difficult to correlate with any fibrous texture in the system. The viscosity measurements in the ICR were taken at an L/D of 75, so the morphology, although not directly examined because the small diameter made such analysis extremely difficult, was assumed to be similar to that seen in the higher L/D's in section 4.4. Thus, as with the RMS, the properties measured do not represent the fibrillar structure, but rather a droplet-in-matrix morphology. The major difference between the two cases is that in the capillary the morphology was dynamic as the fibers formed in the entrance region of the die were broken apart in the capillary itself. The samples in the RMS, on the other hand, had lost their previously imposed orientation before any measurements were taken.

The rheological parameter most frequently correlated with the morphology of a binary polymer blend is the viscosity ratio of the minor to major component, S. When this value is unity or less, a fine dispersion in the extrudate is the typical result. When the minor component has a higher visosity than the major one, however, a

coarse dispersion usually occurs [24,26,28,32,33,80]. Vinogradov has established a relationship between the fibrillar structure of PS/PE blends with S and the shear stress level during processing, as explained in the literature review. The values of S for the LCP/ thermoplastic systems under consideration are given in Figure 4.26. This value varied from less than 0.005 for PC blends in the capillary rheometer to 0.13 for N66 blends at low shear rates in the RMS. Thus, when one considers the blends in which the LCP was the predominant phase (70%), more than four orders of magnitude of S were spanned. In no case was there evidence of fibrillation of the thermoplastic, which always had a greater viscosity than the liquid crystal copolyester. Fibrillation of the LCP occurred for all values of S studied when it was present at 30% by weight.

Two important moduli of the solid polymer are examined in the next section. Here again, though, the measurement of properties of a fibrillar blend structure was not possible since the injection-molded specimens' morphology did not consist of the desired ultrafine fibrils.

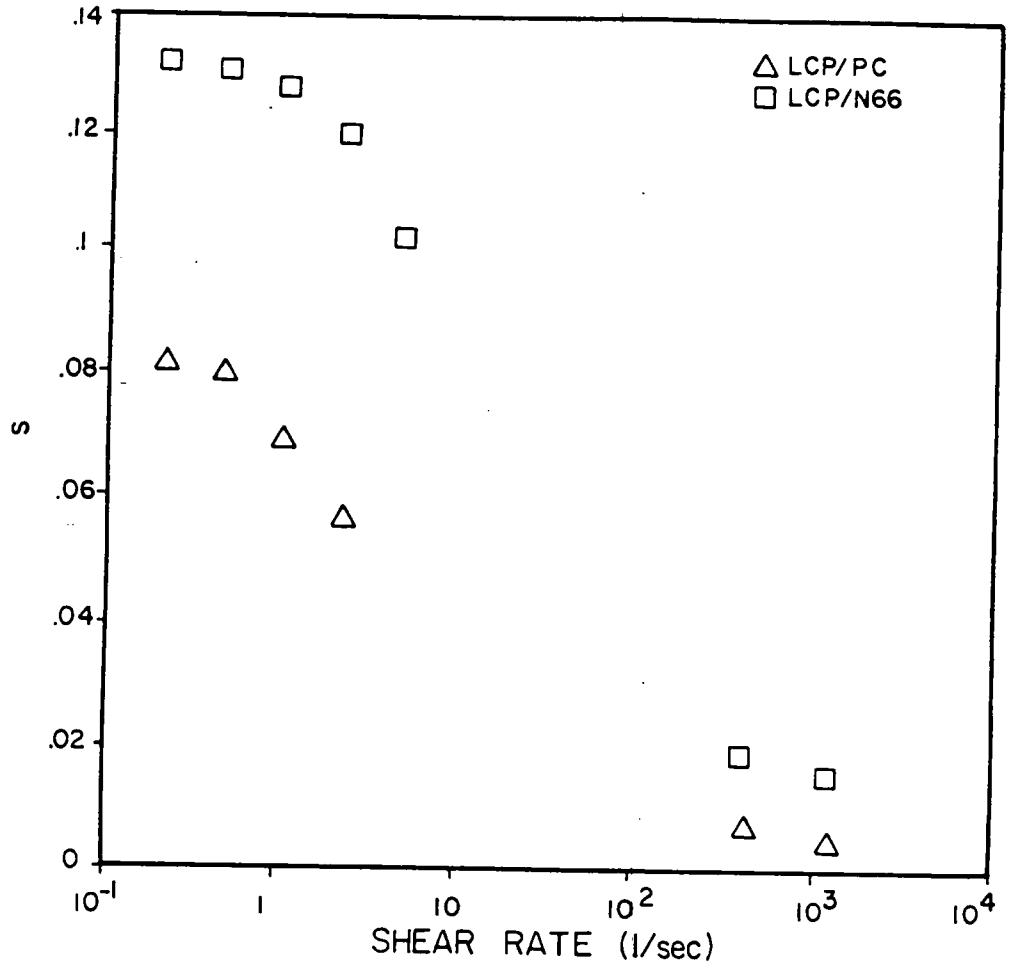

Figure 4.26. Viscsoity ratio of LCP to thermoplastic for the shear rates studied in the RMS and ICR.

4.7 Mechanical Properties of the Blends

In order to obtain an estimate of two mechanical properties, the tangent moduli of elasticity in tension and in bending, E_T and E_B, were determined for each thermoplastic, the copolyester, and 30% LCP blends. This blend ratio was chosen in preference to any other since extrudate samples exhibited the highest degree of fibrillation at 30% LCP and a continuous structure of the liquid crystalline polymer was expected to result in the greatest enhancement in mechanical properties of the blend because the moduli of the LCP are a decade higher than the thermoplastics studied. Specimens were cut from injection-molded plaques as outlined in chapter 3. The results are reported along with the standard deviations in Table 4.6. All measurements were taken along the flow direction in the mold. The moduli for PC and its blends are summarized in Figure 4.27. The results for N66, PC, and the LCP agreed well with those reported in the literature [58,63,64,65].

Both flexural and tensile moduli increased linearly with composition (within experimental uncertainty). The tensile modulus of the 30% LCP blend was 1651 MPA, an improvement of over 50% compared to pure PC, but considerably less than the value of 2704 MPa for the

TABLE 4.6

Modulus Calculations

Blend	$\langle E_T \rangle$ (MPa)	σ (MPa)	$\langle E_B \rangle$ (MPa)	σ (MPa)
N66	1282	87.9	1796	91.5
70 N66	1668	82.0	3764	199.8
PC	1088	18.1	2092	26.8
70 PC	1651	269.8	4254	163.6
LCP	2704	209.0	12623	353.1

All values along the flow direction in the mold.

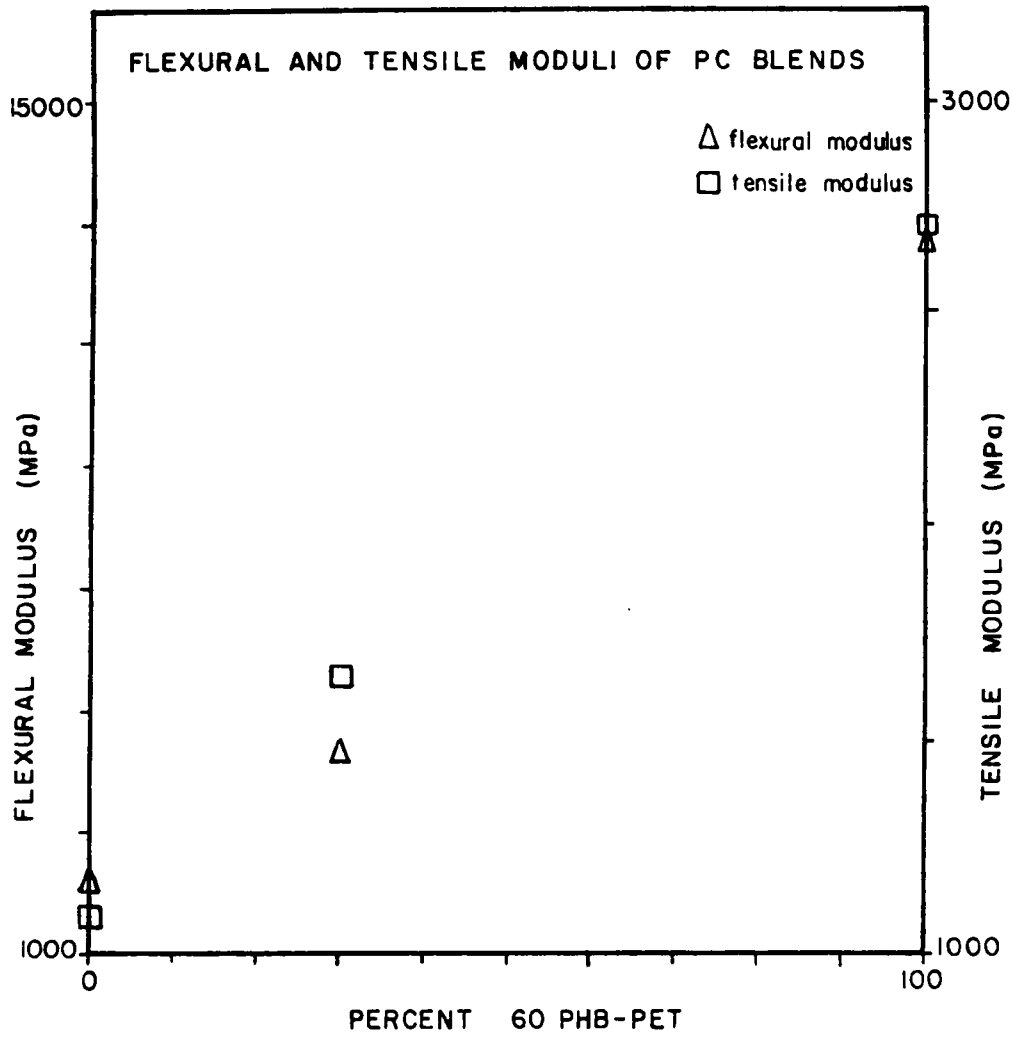

Figure 4.27. Flexural and Tensile Moduli of PC blends. Values taken at 35% humidity and 26°C along the flow direction.

copolyester. The flexural modulus doubled from 2092 to 4254 MPa with the addition of the LCP, but again was far short of the LCP value of 12,623 MPa. On the next page similar results are seen for the N66 blends (Figure 4.28). The 30% LCP blend here had a tensile modulus of 1668 MPa and a flexural modulus of 3764 MPa, up 30 and 210%, respectively, from the values for N66.

The micrograph in Figure 4.29 shows the structure of a molded plaque of 30% LCP after the thermoplastic PC was extracted with methylene chloride. The greatest orientation is expected at the surface where extensional fountain flow occurs during molding. The morphology present is not that of droplet-in-matrix and shows some alignment along the flow direction in the mold, but certainly no ultrafine fibers are formed.

This section concludes the results and discussion. The morphology of the polyblends processed in the extruder as well as in a uniform shear field and in a capillary were analyzed and related to the processing conditions. The viscosity was measured in the cone-&-plate and the capillary instruments and showed a distinct negative deviation which could at least partly be accounted for in terms of the morphology present. Lastly, modulus values were obtained for 30% LCP blends and compared to the component properties. Next, some

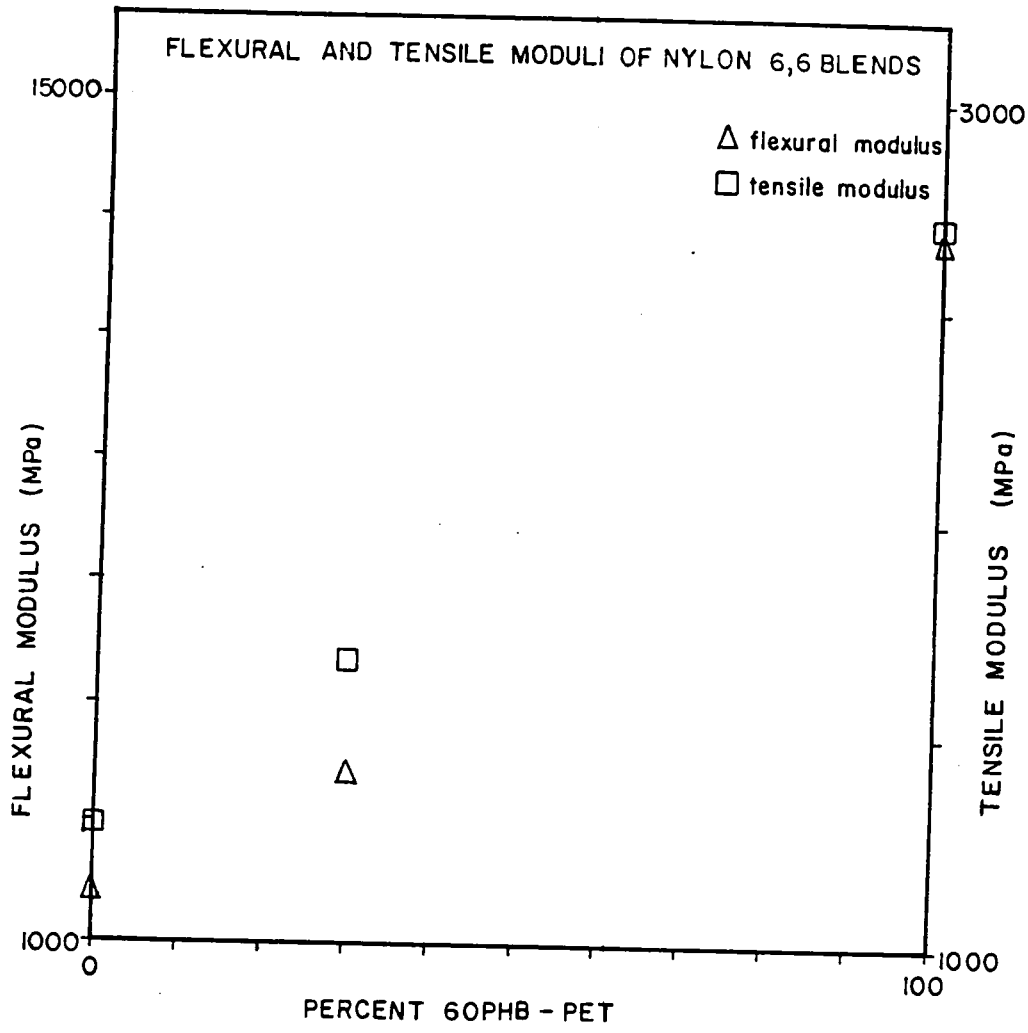

Figure 4.28. Flexural and Tensile Moduli of N66 blends. Values taken at 35% relative humidity and 26°C along the flow direction.

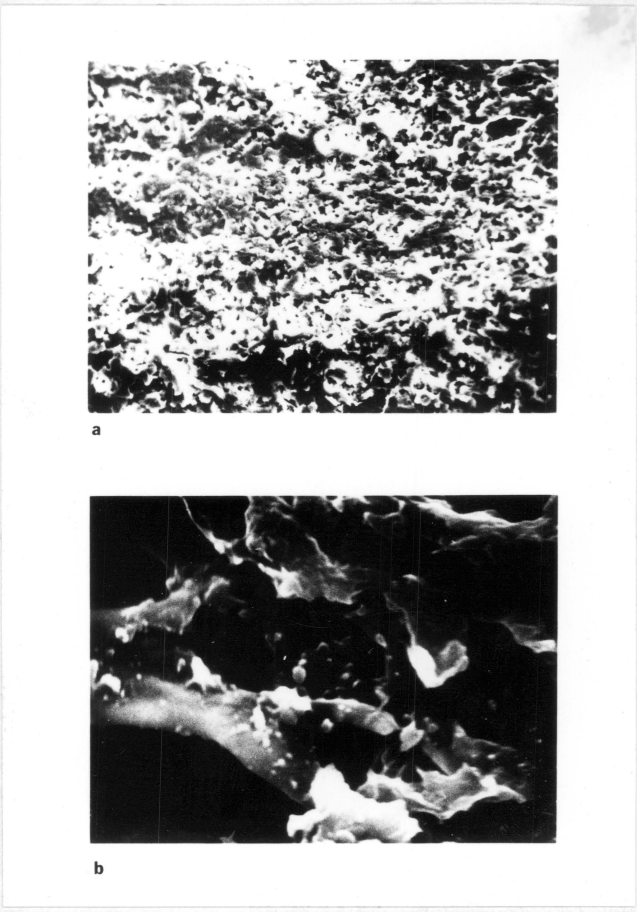

Figure 4.29. Micrographs of injection molded samples of 30% LCP after extraction of PC. Top surface of plaque at a, 480 x; b, 4800 x.

conclusions will be drawn from the results and a few recommendations made for further work with these thermoplastic/LCP blends and polymer blends in general.

5 CONCLUSIONS AND RECOMMENDATIONS

An investigation of the morphology of a 60 mole% PHB/PET copolymer blended with nylon 6,6 and polycarbonate under different processing conditions has been undertaken. The rheological and mechanical behavior of these blends has also been investigated. The following conclusions and recommendations are made with respect to the results and discussion presented in chapter 4.

5.1 Morphology

1. The formation of ultrafine fibers in the extrudate from the single screw extruder is a function of the fraction of LCP in the polyblends studied. This conclusion qualitatively agrees with other investigations reported in the literature [28,33,80]. With both N66 and PC blends, 30 weight% LCP showed a fine fibrous texture; other blend ratios showed no such morphology. The lower concentration limit of the fibrillar structure is a function of the interfacial surface tension of the particulate phase; at low volume fractions not enough material is present to permit the coalescence of the droplets that is necessary to reduce the surface energy enough to promote elongation of the domains. The upper limit to fibrillation exists because of the phase inversion that occurs when the LCP becomes the matrix component.

2. Extruded 30% LCP blends exhibited different morphologies depending on the level of shear stress developed in the die. With no die or breaker plate assembly, the LCP remained dispersed in a matrix of polycarbonate. Increasing the shear rate in the die by decreasing its diameter promoted fibrillation of the extrudate. Thus it

appears that the fibrous morphology is imparted to the melt blend in the die or the entrance of the die, and not in the channel of the screw.

3. Samples deformed in the Rheometrics Mechanical Spectrometer showed no fibrillation under the conditions studied, which ranged up to 1650 Pa shear stress and 100 sec^{-1} shear rate for total strains up to 10,000. Increasing the shear rate did serve to homogenize the sample, but the 30% LCP blends still retained a droplet-in-matrix morphology.

4. Samples extruded through the Instron Capillary Rheometer, however, showed a high degree of fibrillation for the shortest capillary for all shear rates analyzed with SEM. Specimens extruded through longer L/D's showed little or no fibrous texture. Rather, a coral-like texture was seen after etching. Thus, the fibrillation of these systems appears to be dependent on the extensional flows present at the converging entrance to the capillary, and the capillary flow itself seems to cause any orientation developed at the entrance to relax.

5. The viscosity ratio also is critical in determining the morphology of the blend. The minor component must

have a viscosity no greater than the major one for fibrillation to result. Within the limits of the composition ratios discussed above, fibrillation occurred when extensional forces dominated for all cases in which the minor component had a lower viscosity.

6. Annealing melt-blended samples above their melting point tended to rapidly remove any previously imposed orientation.

7. Although the nylon blends are qualitatively less compatible than the PC blends with LCP, this result is not reflected in the mechanical properties or the morphology of the various polyblends.

5.2 Rheology

1. The viscosity of the PC blends reflects that of the liquid crystal polymer at only 30% LCP for the steady shear and capillary tests. The dynamic viscosity of the blends showed a sharp decline at 50% LCP. In all cases, the PC blends show significant negative deviation behavior when the viscosity is plotted against composition. Because the morphology present in the instruments is not generally fibrous, one cannot correlate the rheology with this texture.

2. Nylon blends exhibited an extreme degree of negative deviation on a viscosity - composition plot. Only 10% LCP in the N66 blends reduced the viscosity to essentially that of the liquid crystal copolyester. In this regard, steady shear and dynamic oscillatory results in the cone-&-plate apparatus as well as the values obtained in the capillary rheometer agreed well. As with the PC blends, it is difficult to correlate the flow behavior with a fibrous LCP texture. Nor can the high degree of negative deviation seen be explained in terms of an acceptable rheological theory at present.

5.3 Mechanical Properties

The tensile and flexural moduli of 30% LCP blends with both N66 and PC showed a linear increase (within experimental error) between the values for the thermoplastics and those of the copolyester. The structure of the injection-molded plaques, although showing an alignment along the flow direction in the mold, did not consist of ultrafine fibers at the outer edge of the plaque.

5.4 Recommendations

In view of the conclusions made above, as well as work done by other researchers, several recommendations may be proposed for future work in this area.

1. Since a wide range of viscosity ratios was not obtainable for the particular systems studied, a correlation of morphology with that parameter was not possible, except in noting that at high contents of LCP when the thermoplastic was the disperse phase, there was no evidence of fibrillation of either N66 or PC. In order to obtain several different viscosity ratios, it is recommended that other LCP's with higher viscosities at the processing temperatures of the thermoplastics be blended and then analyzed with SEM. Although it is suspected that the minor component should have a viscosity no greater than the major one for fibrillation to occur, this hypothesis should be further tested for liquid crystalline polymer systems.

2. Additional morphological studies on these blends should be conducted in the Instron and RMS. In the latter case it should be determined whether any orientation or morphology that may develop relaxes before the

sample can be quenched. By conducting shear measurements at a constantly decreasing temperature, any imposed orientation should be retained; also, higher stresses should be obtained. The influence on the morphology of the shear flow in the capillary needs to be further examined, perhaps using a smaller diameter capillary which would permit running a wider range of shear rates. In addition to longer L/D's, a greater variance in shear stress will thus be obtained, perhaps permitting one to postulate a minimum critical stress required to produce fibrils as other researchers have done.

3. As a further measure of morphological relaxation, unquenched as well as quenched specimens from the ICR should be compared by means of SEM to determine whether any relaxation of the sample occurs after the first few seconds after extrusion.

4. More steady shear and dynamic data, particularly the first normal stress difference, N_1, and the storage and loss moduli, G' and G", should be analyzed to further quantify the visco-elastic properties of the polyblends.

5. The mechanical properties of these blends need to be more completely characterized. In addition to deter-

mining the tensile and flexural properties for each blend ratio, other aspects of mechanical behavior, such as impact strength, should be examined to get a better indication of the possible usefulness of these materials. In this regard, more morphological studies on the injection-molded plaques, both at the edge and near the center of the specimens, need to be conducted so that any perceived property enhancement may be better correlated with the structure present.

6. To achieve an optimum blending ratio for these systems, 20% and 40% LCP should be melt-blended and examined with SEM for the development of a fibrillar morphology. These blends should also be analyzed in terms of solid state and melt behavior.

7. Using another processing history to compare with those already studied, such as processing in a twin screw extruder where higher stresses and different flow patterns are encountered, would be useful as far as industrial applications are concerned. Some work in this area has been conducted by others, but no generaliztion has yet been made concerning the morphology of polyblends processed in a twin screw mechanism.

8. This work should be generalized by examining other systems to find out whether other LCP polyblends exhibit similar characteristic morphologies, the high degree of negative deviation of viscosity, and mechanical property enhancement. In all cases the thermodynamic properties such as interfacial tension and adhesion should be experimentally obtained in order to determine what influence miscibility or the degree of immiscibility of the blends has on the properties.

REFERENCES

1. R.L. Scott, J. Chem. Phys. 17, 279(1949).

2. P.J. Flory, J. Chem. Phys. 9, 660(1941).

3. P.J. Flory, J. Chem. Phys. 10, 51(1942).

4. M.L. Huggins, J. Chem. Phys. 9, 440(1941).

5. M.L. Huggins, Ann. N.Y. Acad. Sci. 43, 1(1942).

6. J.H. Hildebrand and R.L. Scott, "The Solubility of Nonelectrolytes," 3rd ed., Van Nostrand-Reinhold, Princeton, N.J., 1950.

7. J.H. Hildebrand and R.L. Scott, "Regular Solutions," Prentice-Hall, Englewood Cliffs, N.J., 1962.

8. K.L. Hoy, J. Paint Technol. 42, 76(1970).

9. S. Krause, Ch. 2 in "Polymer Blends" (D.R. Paul and S. Newman, eds.), Academic Press, N.Y., 1978.

10. S. Wu, Ch. 6 in "Polymer Blends" (D.R. Paul and S. Newman, eds.), Academic Press, N.Y., 1978.

11. S. Wu, J. Adhes. 5, 39(1973).

12. S. Wu, J. Phys. Chem. 72, 3332(1968).

13. L.A. Girifalco and R.J. Good, J. Phys. Chem. 61, 904(1957).

14. S. Wu, J. Macromol. Sci. C10, 1(1974).

15. S. Wu, J. Polym. Sci. C34, 19(1971).

16. E. Helfand and Y. Tagami, J. Polym. Sci. B9, 741(1971); J. Chem. Phys. 56, 3592(1972).

17. E. Helfand, J. Chem. Phys. 63, 2192(1975).

18. R.J. Roe, J. Chem. Phys. 62, 490(1975).

19. L.H. Sharpe and H. Schonhorn, Adv. Chem. Ser. 43, 189(1964).

20. W.A. Zisman, Adv. Chem. Ser. 43, 1(1964); Ind. Eng. Chem. 55, 18(1963).

21. J.E. McNutt, Adhesives Age 7, 24(1964).

22. W.H. Smarook and S. Bonotto, Polym. Eng. Sci. 8, 41(1968).

23. M. Levine, G. Ilkka, and P.Weiss, Polym. Lett. 2, 915(1964).

24. J.M. Starita, Trans. Soc. Rheol. 16, 339(1972).

25. C.D. Han, Y.W. Kim, and S.J. Chen, J. Appl. Polym. Sci. 19, 2831(1975).

26. G.V. Vinogradov, et al., Intern. J. Polymeric Mater. 9, 187(1982).

27. G.V. Vinogradov, et al., Rheol. Acta 22, 102(1983).

28. S. Danesi and R.S. Porter, Polymer 19, 448(1978).

29. W. Ho and R.S. Salovey, Polym. Eng. Sci. 21, 839(1981).

30. C. Markin and H.L. Williams, J. Appl. Polym. Sci. 25, 2451(1980).

31. F.C. Stehling, et al., J. Appl. Polym. Sci. 26, 2693(1981).

32. H. Van Oene, J. Coll. Interf. Sci. 40, 448(1972).

33. G.N. Avgeropoulos, et al., Rubber Chem. Technol. 49, 93(1976).

34. M.V. Tsebrenko, et al., Polym. Eng. Sci. 20, 1023(1980).

35. R.G. Cox, J. Fluid Mech. 37, 601(1969).

36. J. Majnusz, in "Polymer Blends" (Martuscelli, Palumbo, and Krzszewski, eds.), Plenum Press, N.Y., 1980.

37. D.C. Warmund, D.R. Paul, and J.W. Barlow, J. Appl. Polym. Sci. 22, 2155(1978).

38. T.R. Nasser, D.R. Paul, and J.W. Barlow, J. Appl. Polym. Sci. 23, 85(1979).

39. R.N. Mohn, et al., J. Appl. Polym. Sci. 23, 575(1979).

40. C.A. Cruz, D.R. Paul, and J.W. Barlow, J. Appl. Polym. Sci. 23, 589(1979).

41. L.A. Utracki and M.R. Kamal, Polym. Eng. Sci. 22, 96(1982).

42. H. Van Oene, Ch. 7 in "Polymer Blends" (D.R. Paul and S. Newman, eds.), Academic Press, N.Y., 1978.

43. M.V. Tsebrenko, et al., Vysokomol. Soed. A21, 830(1979).

44. L.A. Utracki, Z. Bakerdjian, and M.R. Kamal, J. Appl. Polym. Sci. 19, 484(1975).

45. C.K. Shih, Polym. Eng. Sci. 16, 742(1976).

46. V.N. Kuleznev, et al., Kolloid Zhion. 37, 273(1975).

47. L.A. Utracki, et al., J. Appl. Polym. Sci. 27, 1913(1982).

48. C.B. Martinez and M.C. Williams, J. Rheol. 24, 421(1980).

49. T. Nishimura, Rheol. Acta 23, 617(1984).

50. A.P. Plochocki, Ch. 21 in "Polymer Blends" (D.R. Paul and S. Newman, eds.), Academic Press, N.Y., 1978.

51. R.F. Heitmiller, R.Z. Naar, and H.H. Zabusky, J. Appl. Polym. Sci. 8, 873(1964).

52. K. Hayashida, et al., in "Proc. Fifth Intern. Congr. Rheol., Vol. 4, University of Tokyo Press, Tokyo, 1970.

53. J.F. Carley, Polym. Eng. Sci. 21, 249(1981).

54. R.A. McAllister, AIChE J. 6, 427(1960).

55. K.F. Wissbrun, J. Rheol. 25, 619(1982).

56. Asada and Onogi, Polym. Eng. Rev. 3, 324(1983).

57. D.G. Baird, Ch. 7 in "Liquid Crystalline Order in Polymers" (A. Blumstein, ed.), Academic Press, N.Y., 1978.

58. W.J. Jackson and H.F. Kuhfuss, J. Appl. Polym. Sci., Polym. Chem. Ed. 14, 2043(1976).

59. D.G. Baird, J. Appl. Polym. Sci. 22, 2701(1978).

60. R.E. Jerman and D.G. Baird, J. Rheol. 25, 275(1981).

61. A.D. Gotsis, Master's thesis, Virginia Tech, 1984.

62. G.G. Viola, PhD. dissertation, Virginia Tech, 1985.

63. M. Kohan, ed., "Nylon Plastics," John Wiley and Sons, N.Y., 1973.

64. W.E. Nelson, "Nylon Plastics Technology," Butterworth, London, 1976.

65. K. Johnson, "Polycarbonates: Recent Developments," Noyes Data Corporation, Park Ridge, N.J., 1970.

66. A.P. Plochocki, Adv. Polym. Technol. 2, 267(1982).

67. Z. Tadmor and C.G. Gogos, "Priciples of Polymer Processing," John Wiley and Sons, N.Y., 1979.

68. G.I. Taylor, Proc. Royal Soc. A-146, 501(1934).

69. R.S. Spencer and R.M. Wiley, J. Coll. Sci. 6, 133(1951).

70. Mohr, Saxton, and Jepson, Ind. Eng. Chem. 49, 1855(1957).

71. P. Hold, Adv. Polym. Technol. 2, 197(1982).

72. J.M. Ottina and R. Chella, Polym. Eng. Sci. 23, 357(1983).

73. R.A. Strasser and L. Erwin, Adv. Polym. Technol. 4, 18(1984).

74. Mohr, Saxton, and Jepson, Ind. Eng. Chem. 49, 1857(1957).

75. H.F. Irvin and R.L. Saxton, Ch. 8 in "Mixing" (Uhl and Gray, eds.), Academic Press, N.Y., 1967.

76. G. Pinto and Z. Tadmor, Polym. Eng. Sci. 10, 279(1970).

77. Z. Tadmor and I. Klein, "Engineering Principles of Plasticating Extrusion," Van Nostrand-Reinhold, N.Y., 1970.

78. D. Bigg and S. Middleman, Ind. Eng. Chem. Fundam. 13, 66(1974).

79. J.M. McKelvey, "Polymer Processing," John Wiley and Sons, N.Y., 1962.

80. A. Siegmann, A. Dagan, and S. Kenig, Polymer 26, 1325(1985).

81. Rheometrics Operations Manual (RMS 605).

APPENDIX: DATA TABLES AND FIGURES

TABLE B.1

Pressure Increase in Extruder

Run	PT 1 (kPa)	PT 2 (kPa)	dP/dL (kPa/m)
1	896	1034	21.02
2	4619	4999	57.79
3	-	-	0
4	2620	2930	47.28
5	103	1034	141.9
6	1034	1379	52.54
7	6895	11032	630.5
8	207	448	36.78
9	207	448	36.78
10	172	1034	131.3
11	-	345	52.54
12	-	345	52.54
13	276	448	26.27
14	5723	8274	388.8
15	207	345	21.02
16	621	1379	115.6
17	621	862	36.78
18	7102	16892	1492.0
19	3999	4482	73.55
21	483	689	31.52
22	-	-	0

PT 1 is located 0.1524 m before the end of screw.
PT 2 is located at the exit of the screw.

TABLE B.2

Etrudate Flowrates

Run #	Q_{exp} (cm^3/min)	Q_{calc} (cm^3/min)	$-Q_p/Q_d$
1	43.5	38.7	0.064
2	35.0	34.0	0.177
3	34.7	41.3	0
4	38.9	35.3	0.145
5	45.4	34.6	0.163
6	33.1	34.4	0.166
7	26.9	11.3	0.73
8	31.4	37.9	0.083
9	27.9	37.9	0.083
10	51.5	35.1	0.151
11	37.7	39.8	0.037
12	44.9	41.0	0.008
13	35.7	40.4	0.022
14	43.7	41.0	0.008
16	36.7	37.9	0.082
17	37.1	40.1	0.031
18	36.8	40.1	0.028
19	37.7	41.1	0.005
21	40.5	41.3	0.001

TABLE B.3

Steady Shear Viscosity of N66/LCP Blends at 275°C
Cone-&-Plate

Shear Rate	Viscosity (Pa*s)				
(sec^{-1})	100/0	90/10	70/30	50/50	30/70
0.2155	878.0	126.7	193.8	156.4	361.6
0.4642	730.3	68.2	84.6	71.6	153.0
1.0	615.9	-	46.1	62.4	71.6
2.155	543.6	33.5	34.3	36.3	33.8
4.642	505.9	29.5	29.4	20.3	23.1
10.0	436.6	-	22.2	15.0	10.4

TABLE B.4

Dynamic Viscosity of N66/LCP Blends at 275°C
Cone-&-Plate. Strain = 5%.

Frequency (sec^{-1})	Complex Viscosity (Pa*s)				
	100/0	90/10	70/30	50/50	30/70
1.585	347.1	91.2	-	-	64.6
2.512	271.0	-	56.8	29.1	60.0
3.981	242.5	68.1	54.8	28.9	58.5
6.31	229.4	56.6	24.6	-	51.1
10.0	192.4	35.0	25.9	17.1	40.3
15.85	178.7	27.0	18.9	14.4	33.5
25.12	166.7	18.4	12.2	9.45	26.1
39.81	155.2	15.0	10.3	8.27	21.6
63.1	145.4	12.3	8.04	7.21	19.1
100.0	133.5	9.93	6.29	5.54	15.6

TABLE B.5

Steady Shear Viscosity of PC/LCP Blends at 260°C
Cone-&-Plate

Shear Rate (sec^{-1})	Viscosity (Pa*s)				
	100/0	90/10	70/30	50/50	30/70
0.04642	2170	1510	-	1095	699.9
0.1	1947	1588	633.9	422.2	217.7
0.2155	-	1372	544.1	249.7	-
0.4642	2184	1128	418.4	118.2	-
1.0	1890	917.4	-	-	-
2.155	1817	931.9	-	-	-

TABLE B.6

Dynamic Viscosity of PC/LCP Blends at 260°C
Cone-&-Plate. Strain = 5%.

Frequency (sec-1)	Complex Viscosity (Pa*s)				
	100/0	90/10	70/30	50/50	30/70
1.585	1973	1217	698.6	-	165.4
2.512	2046	1153	655.5	134.2	114.2
3.981	2070	1134	607.4	122.1	95.0
6.31	2043	1081	548.3	104.9	88.8
10.0	2030	1022	507.9	100.4	75.6
15.85	1990	960.8	468.0	93.1	74.0
25.12	1930	921.3	438.3	86.7	67.3
39.81	1846	889.0	410.7	81.1	62.8
63.1	1727	847.6	390.6	81.1	60.9
100.0	1579	794.1	368.2	77.4	56.7

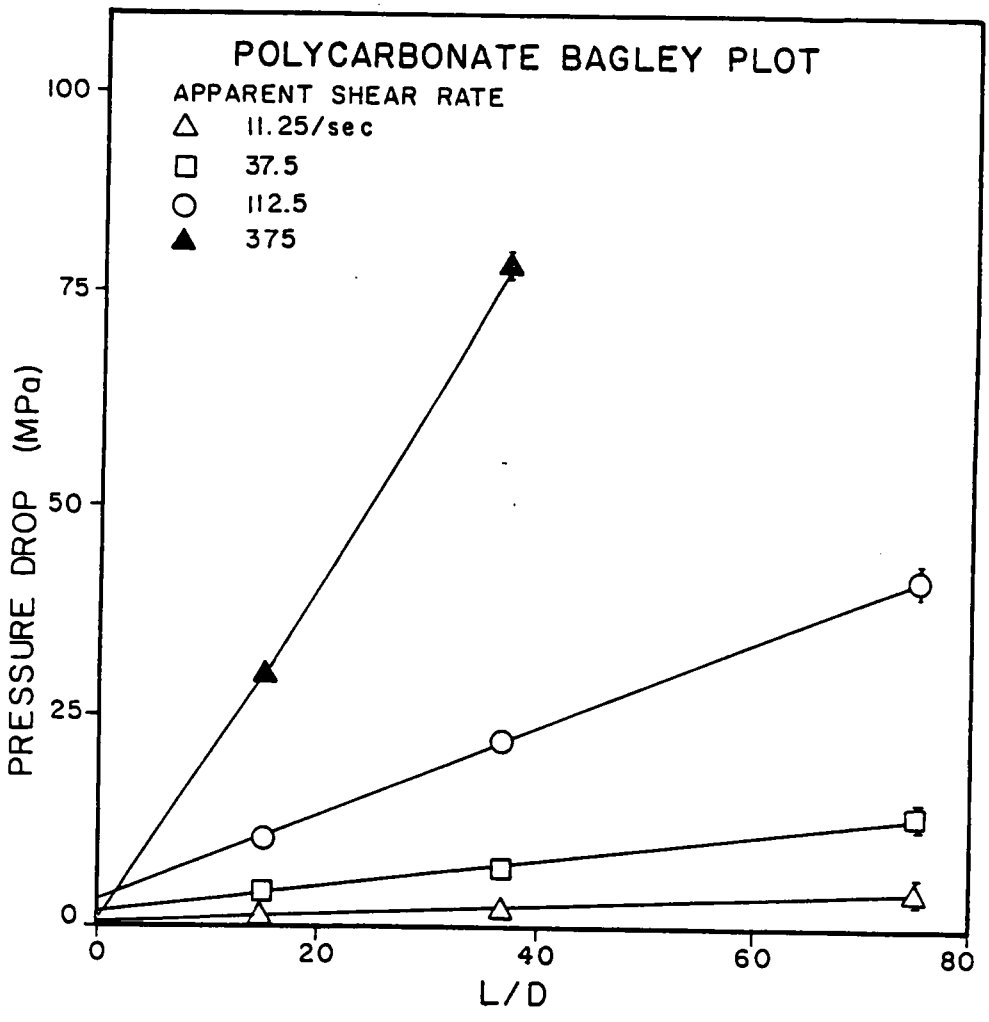

Figure B.1. Bagley Plot for Polycarbonate at 260°C. Capillary diameter = 0.0686 cm.

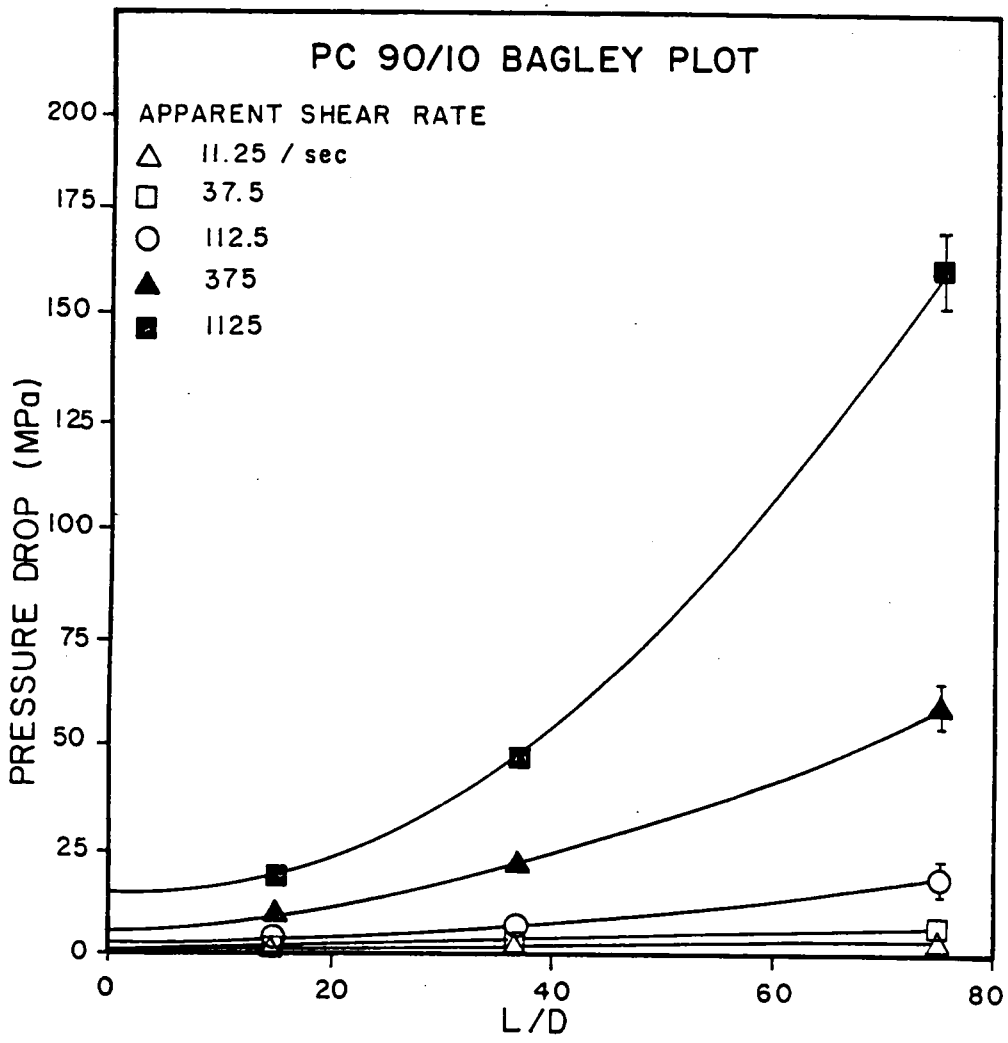

Figure B.2. Bagley Plot for 90/10 PC/LCP at 260°C. Capillary Diameter = 0.0686 cm.

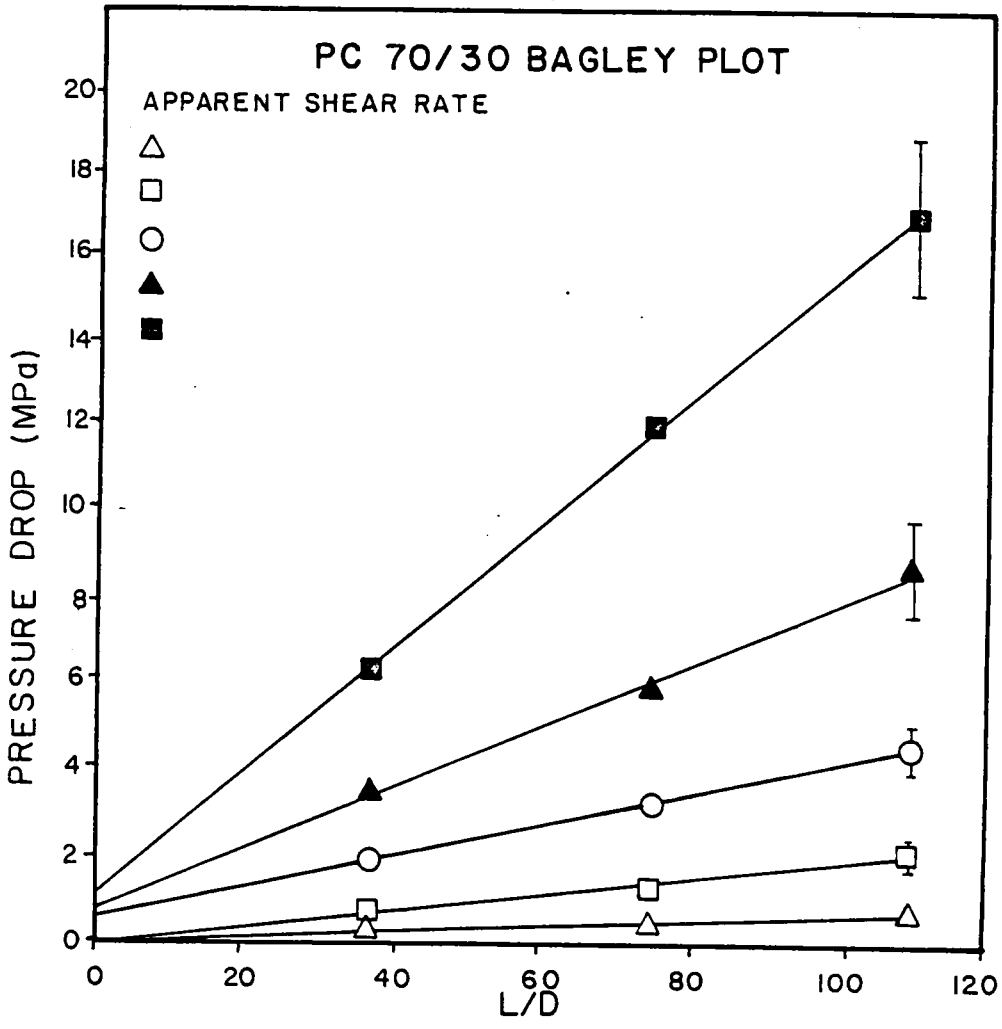

Figure B.3. Bagley Plot for 70/30 PC/LCP at 260°C. Capillary Diameter = 0.0686 cm.

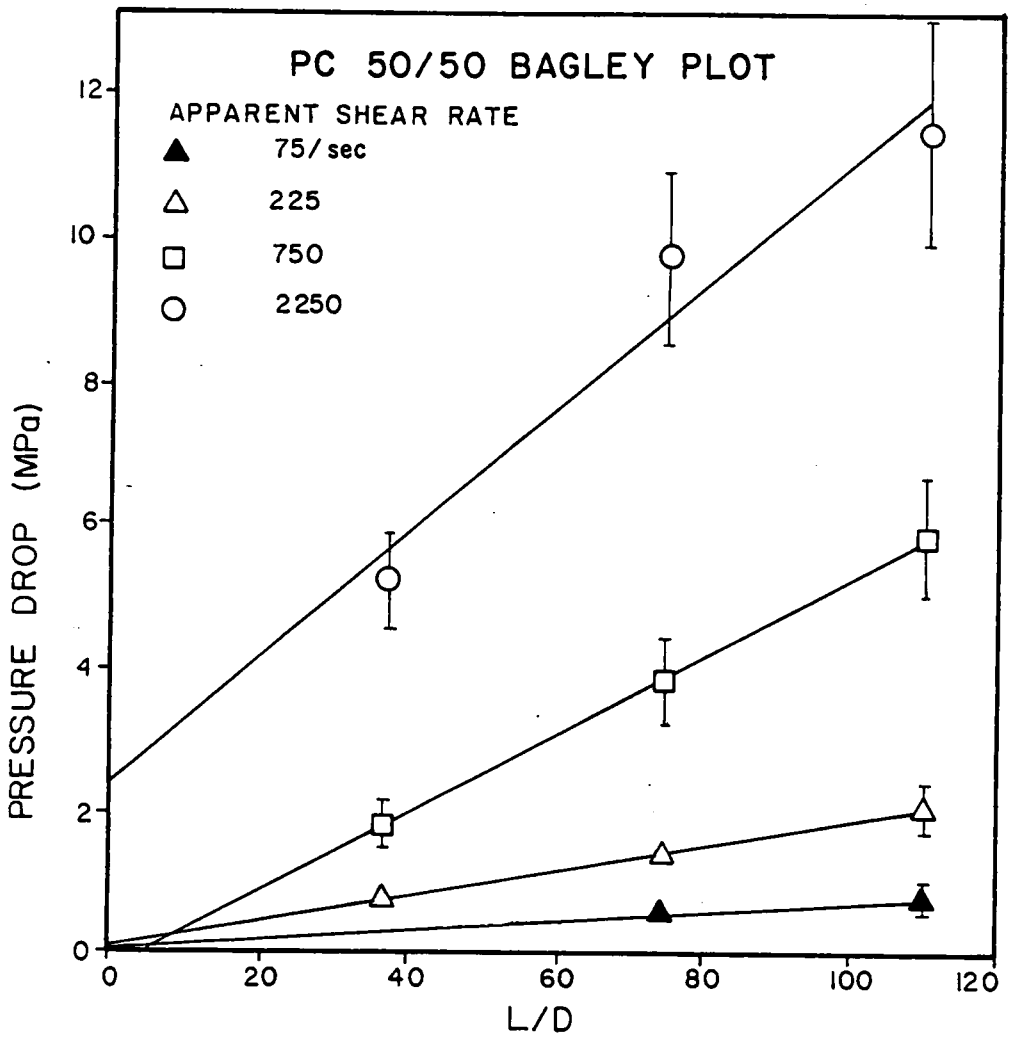

Figure B.4. Bagley Plot for 50/50 PC/LCP at 260°C. Capillary Diameter = 0.0686 cm.

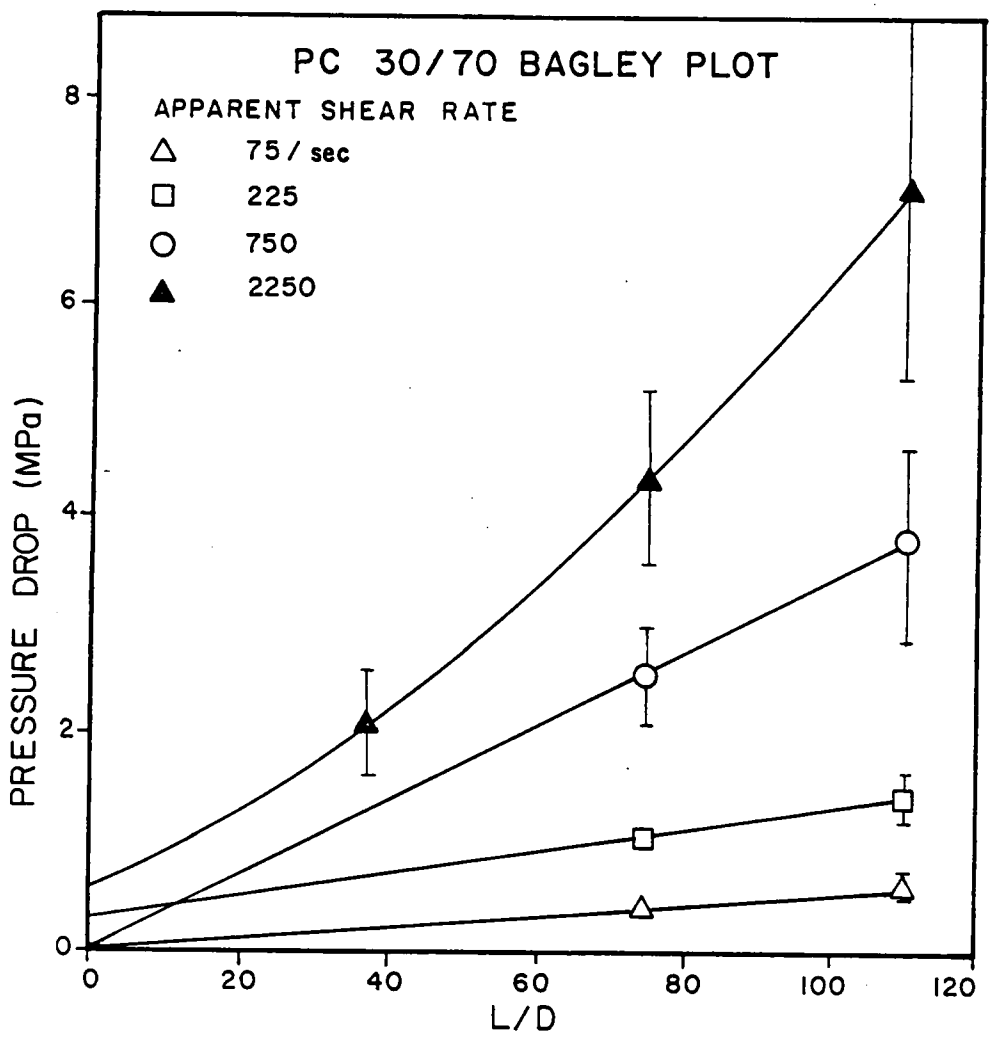

Figure B.5. Bagley Plot for 30/70 PC/LCP at 260°C. Capillary Diameter = 0.0686 cm.

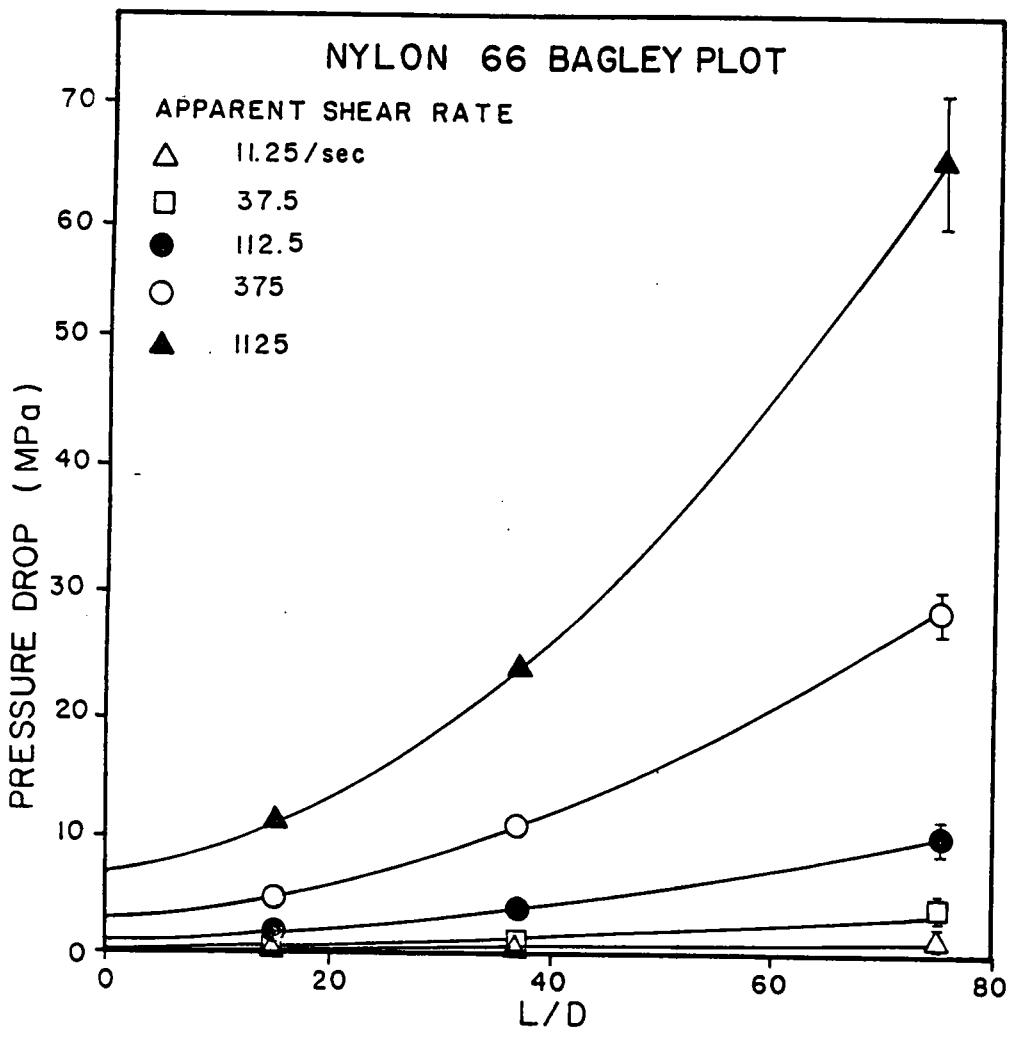

Figure B.6. Bagley Plot for Nylon 6,6 at 275°C.
Capillary Diameter = 0.0686 cm.

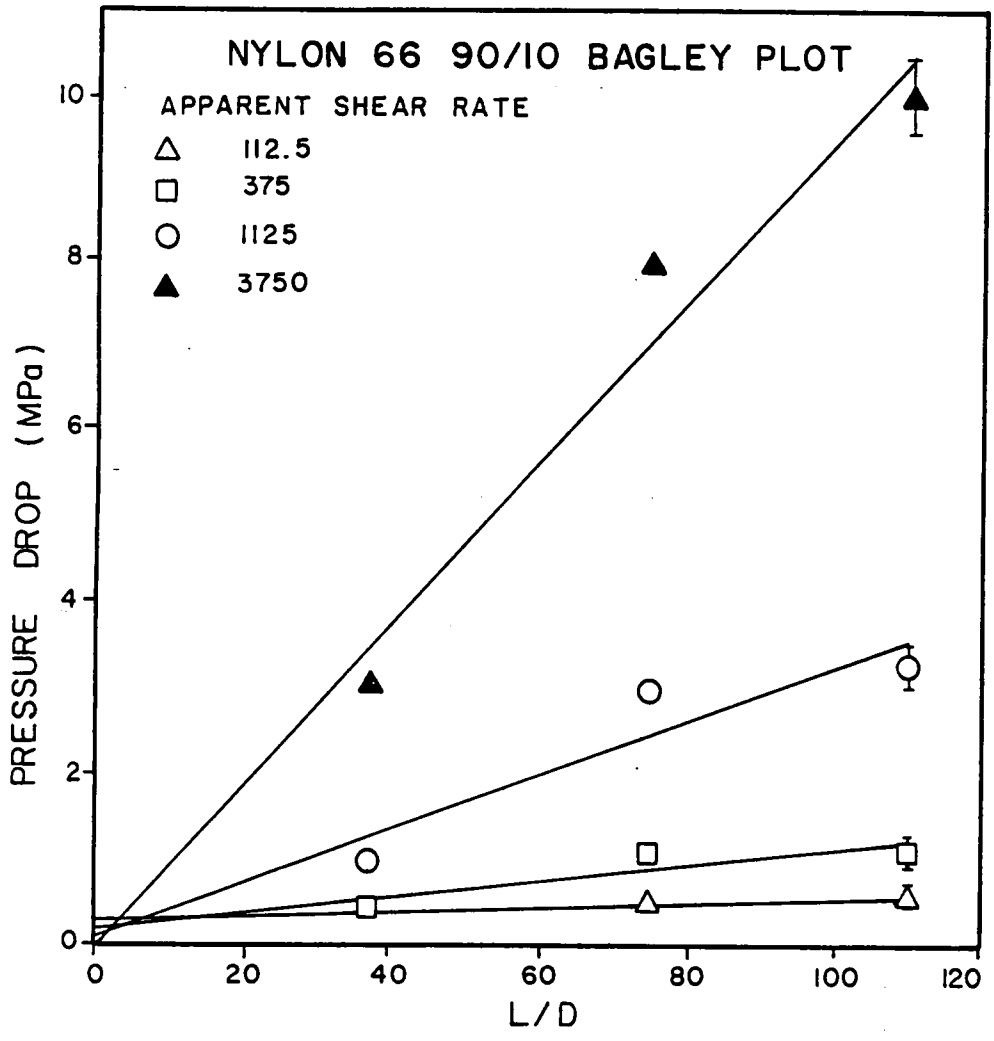

Figure B.7. Bagley Plot for 90/10 N66/LCP at 275°C. Capillary Daimeter = 0.0686 cm.

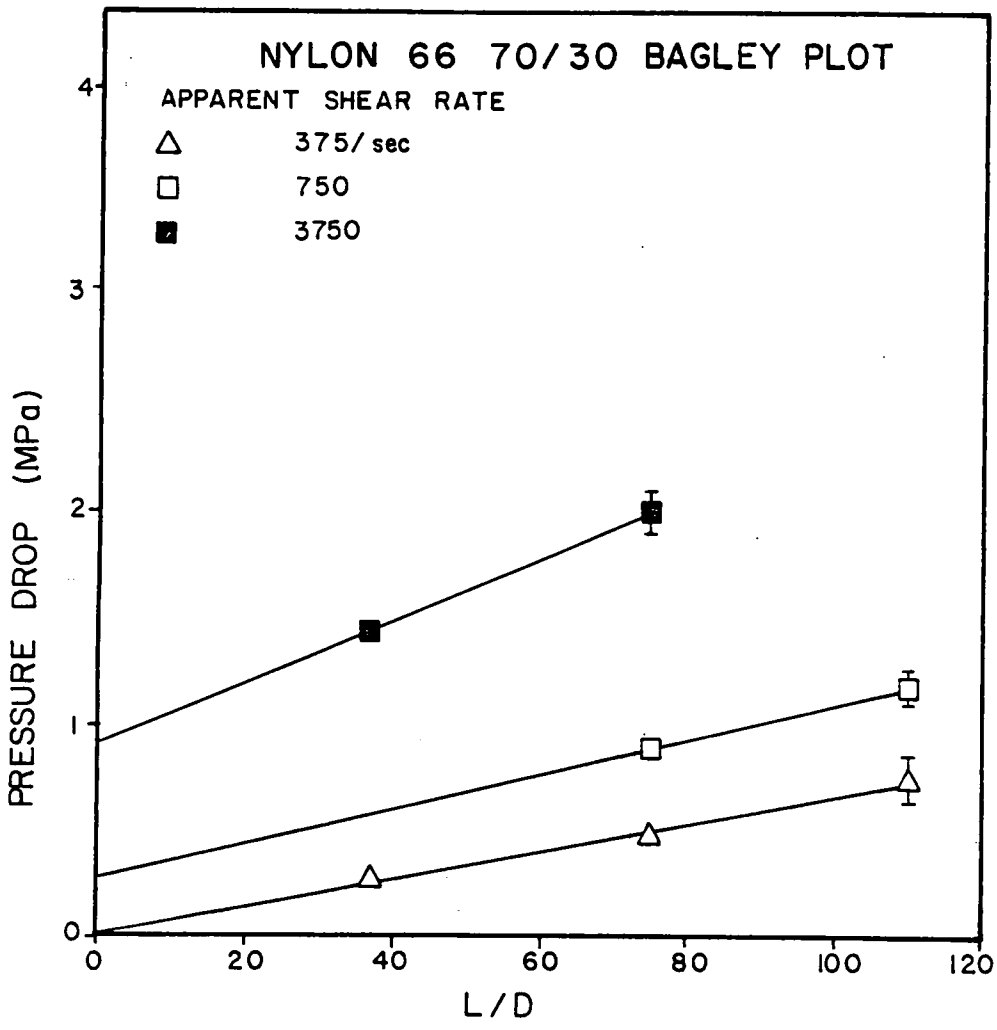

Figure B.8. Bagley Plot for 70/30 N66/LCP at 275°C. Capillary Diameter = 0.0686 cm.

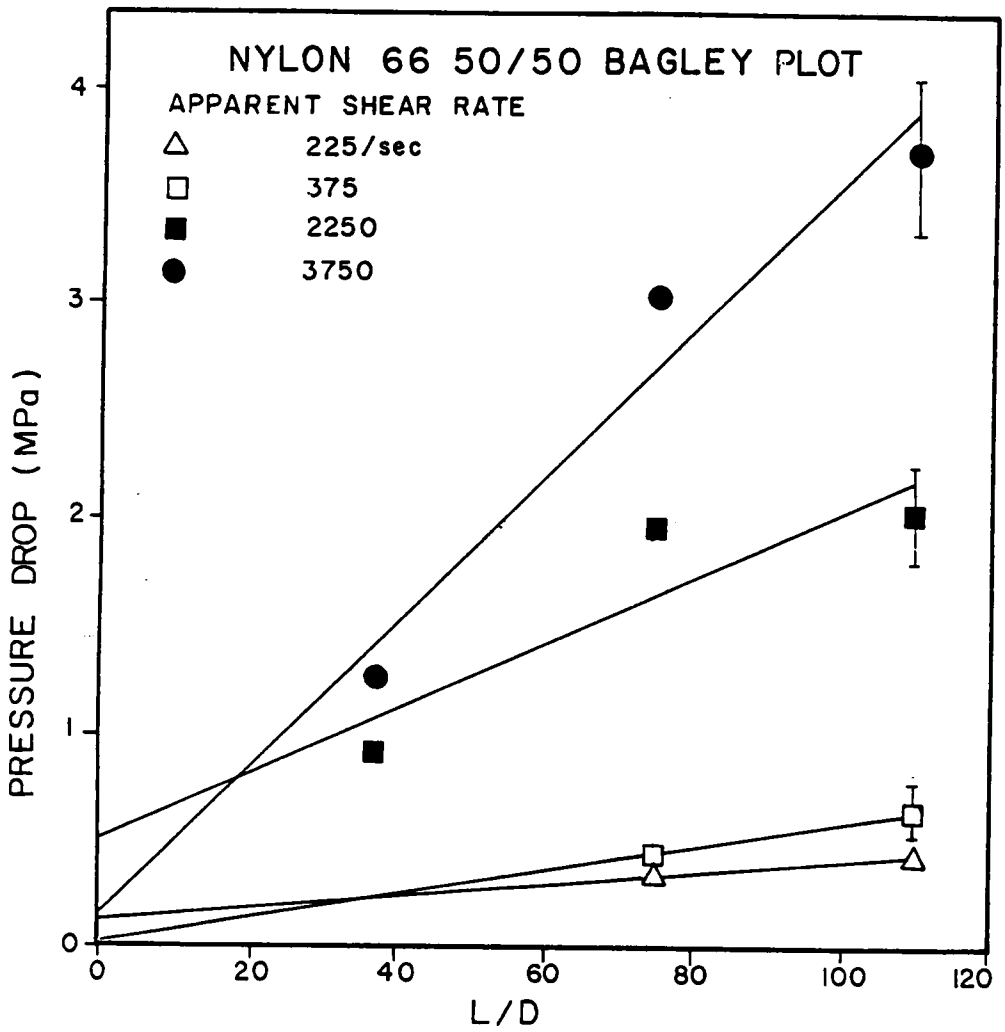

Figure B.9. Bagley Plot for 50/50 N66/LCP at 275°C. Capillary Diameter = 0.0686 cm.

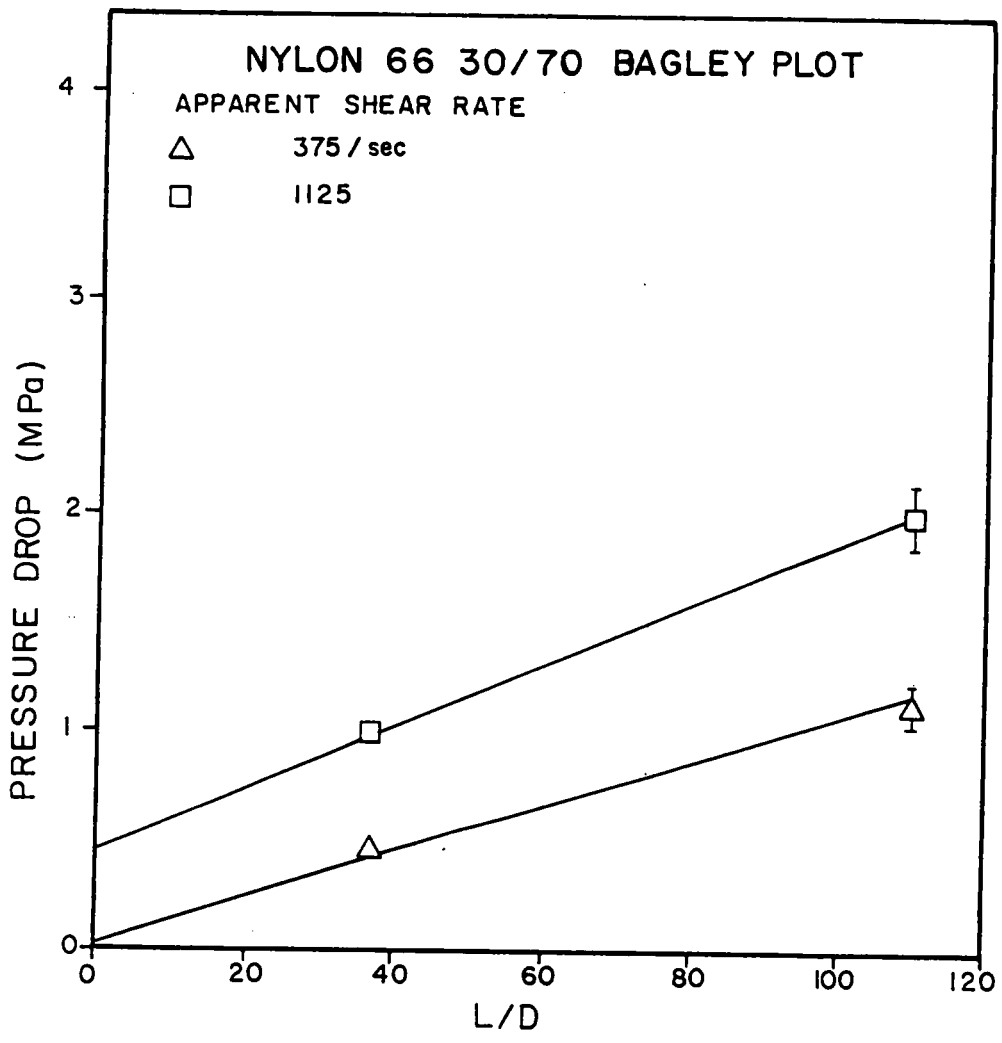

Figure B.10. Bagley Plot for 30/70 N66/LCP at 275°C. Capillary Diameter = 0.0686 cm.

The vita has been removed from the scanned document